

POLITECNICO DI TORINO

SCUOLA INTERPOLITECNICA DI DOTTORATO

Doctoral Program in Information and Communication Technology

Final Dissertation

High-Speed Interconnect Models with Stochastic Parameter Variability



Paolo Manfredi

Tutor
prof. Flavio Canavero

Co-ordinator of the Research Doctorate Course
prof. Ivo Montrosset

28 febbraio 2013

Acknowledgments

This is the conclusion of an exciting and stimulating adventure, which has been challenging but also very rewarding. Therefore, I would like to thank *in primis* my advisor, Prof. Flavio Canavero, for offering me this great opportunity and convincing me to join the EMC Group and undertake this activity. Then, I thank Prof. Igor Stievano, with whom I co-worked on the development of this project, for the continuous and fruitful discussions. I also acknowledge my colleagues, who are part of an enjoyable work environment. Special thanks to Elisabetta for her help and patience with the administrative things.

Also, many thanks to Prof. Michael H. Azarian and his wife Patty for kindly hosting me during my visit at the University of Maryland, and to all the people I met there. Thanks to Prof. Daniël De Zutter and Prof. Dries Vande Ginste and all the people at Ghent University for their very kind hospitality. They were very motivating and the visit has been very important and stimulating for both this work and my personal life.

Finally, many thanks to my girlfriend Claudia, who has been patient and encouraging during the busiest and most difficult periods. And of course, thanks to my family, to my parents for their constant support in my life. To them I dedicate this thesis.

Contents

Abstract	v
Sommario	vii
List of Acronyms	ix
1 Introduction	1
1.1 Stochastic Simulation	1
1.2 Goal of the Thesis	3
1.3 State of the Art	3
1.4 Organization of the Text	4
2 Analysis of Transmission Lines	5
2.1 The Multiconductor Transmission-Line Equations	5
2.1.1 The Quasi-TEM Assumption	6
2.1.2 The Per-Unit-Length Parameters	6
2.1.3 Dispersive Lines	8
2.2 Solution of the Multiconductor Transmission-Line Equations	9
2.2.1 Frequency-Domain Equations	10
2.2.2 General Solution	10
2.2.3 Incorporation of the Terminal Conditions	11
2.2.4 Time-Domain Solution	12
2.3 Numerical Examples	13
3 Stochastic Analysis	17
3.1 Statistical Background	17
3.1.1 Probabilistic Framework	18
3.1.2 Random Variable Transformation	19
3.2 The Monte Carlo Method	20
3.2.1 Monte Carlo Estimator of the Mean Value	21
3.2.2 Monte Carlo Estimator of the Variance	22
3.2.3 Estimation of the Distribution by Means of Monte Carlo Simulations	22
3.2.4 Example of Monte Carlo Simulation	23
3.3 Stochastic Analysis of Transmission Lines	24

4	The Polynomial Chaos Theory	29
4.1	Polynomial Chaos Overview	29
4.1.1	The Polynomial Chaos Expansion	30
4.1.2	Statistical Information	32
4.1.3	Projection	32
4.2	Gaussian and Uniform Distributions	33
4.2.1	Hermite Polynomials	33
4.2.2	Legendre Polynomials	34
4.2.3	Analytical Example	36
4.3	Gaussian Quadratures	37
4.3.1	Gauss-Hermite Quadrature	37
4.3.2	Gauss-Legendre Quadrature	38
5	Application of Polynomial Chaos to Transmission-Line Equations	39
5.1	Stochastic Multiconductor Transmission-Line Equations	39
5.2	The Stochastic Galerkin Method	40
5.3	Tutorial Example — Single Line and One Random Variable	43
5.3.1	Projection via Gaussian Quadratures	44
5.3.2	The Augmented Per-Unit-Length Matrices	46
5.4	Tutorial Example — Multiconductor Line and Multiple Random Variables	47
5.5	Augmented Terminal Conditions	50
5.5.1	Stochastic Terminations	50
5.5.2	Deterministic Terminations	51
5.6	Polynomial Chaos-Based Stochastic Simulation	51
6	Applications	59
6.1	Example #1 — Flex Cable	59
6.2	Example #2 — Microstrip Line with Temperature Variations	61
6.3	Example #3 — Transient Analysis of a Microstrip Line	62
6.4	Example #4 — Time-Domain Simulation of a Cascaded Structure	67
7	SPICE Implementation	71
7.1	A Topological Rule for the Integration of Transmission Lines	71
7.2	Inclusion of Linear Lumped Elements	73
7.3	Description of the Augmented Transmission Lines	74
7.4	Application Examples	75
7.4.1	Example of HSPICE Netlist for the Polynomial Chaos-Based Simulation	75
7.4.2	Transmission-Line Network with Single Microstrip Lines	77
7.4.3	Transmission-Line Network with Coupled Microstrip Lines	78
8	Random Field Incidence	81
8.1	Transmission-Line Equations for Incident Field Excitation	81
8.1.1	Solution of the Forced Transmission-Line Equations	82
8.1.2	Uniform Plane-Wave Incidence	82
8.2	Application of Polynomial Chaos	84

8.3	Application Example	85
8.3.1	Random Field Amplitude and Polarization	86
8.3.2	Random Direction of Incidence (Colatitude and Azimuth)	88
	Conclusions	91
	Bibliography	93
	List of Publications	101
	Biography	105

Abstract

In the process of design and fabrication of electronic products, numerical simulation plays a fundamental role for a preliminary electromagnetic compatibility (EMC) assessment of devices in the early design phase. Direct EMC measurements impact both cost and time-to-market as they require purchase and/or hiring of facilities and instruments, as well as fabrication of prototype devices, and need therefore to be minimized. Nowadays, designers can rely on several sophisticated modeling tools, helping them to perform right-the-first-time designs. Nonetheless, these simulation models are accurate as long as we are able to assign accurate values to each system parameter. In modern high-speed and high-density designs, process variations and uncertainties in operating conditions result in parameters which are hard to control or partially unavailable. The device response is thus no longer regarded as deterministic, but is more suitably interpreted as a random process. In this framework, the assessment of signal integrity requires a statistical analysis, which is traditionally based on the so-called Monte Carlo or other sampling-based methods. Yet, for practical applications, these approaches are often too time-consuming, as they are known to require a large number of samples to converge. In this thesis, we extend available literature results to the efficient analysis of high-speed interconnects, such as avionic and industrial cables or printed circuit board traces, affected by uncertainties, like process variations or unavailable operating conditions. Specifically, the framework of polynomial chaos theory is adopted to create stochastic models for transmission lines which are faster to be simulated compared to repeated Monte Carlo simulations. Such methodology is based on the expansion of random quantities in series of orthogonal polynomials, and has been already and successfully applied to the analysis of lumped circuits. In this work, the modeling of distributed components, which are key elements for modern high-frequency designs, is addressed. The advocated approach is general and overcomes the limitations of available literature models for the statistical analysis of the signal propagation over interconnects, which are based on simplified structures and approximate assumptions. Also, a SPICE-compatible implementation is presented, thus allowing the convenient use of SPICE-like circuit analysis tools for the simulation of complex stochastic network topologies, avoiding the creation of customized, ad hoc implementations. This thesis provides a comprehensive theoretical discussion together with several tutorial application examples, thus complementing the published material.

Sommario

La simulazione numerica riveste un ruolo fondamentale nel processo di progetto e fabbricazione di prodotti elettronici, per avere nelle prime fasi del progetto un riscontro preliminare circa la compatibilità elettromagnetica. Le misure dirette di compatibilità hanno impatto sia sul costo che sulle tempistiche di lancio sul mercato, dato che richiedono l'acquisto o il noleggio di strutture e strumenti, così come la fabbricazione di prototipi, e devono quindi essere minimizzate. Al giorno d'oggi, i progettisti dispongono di svariati e sofisticati strumenti di modellazione, che li aiutano a creare fin da subito progetti correttamente funzionanti. Tuttavia, questi modelli di simulazione sono accurati solo nel momento in cui siamo in grado di assegnare valori accurati ad ogni parametro del sistema. Nei moderni progetti ad elevata velocità e densità, le variazioni dovute al processo di fabbricazione e le incertezze riguardanti le reali condizioni di funzionamento comportano la presenza di parametri difficili da controllare o parzialmente sconosciuti. La risposta di un dispositivo non è più quindi considerata come deterministica, ma è più propriamente descritta come un processo casuale. In questo contesto, l'analisi dell'integrità dei segnali richiede un approccio statistico, il quale è tradizionalmente basato sul cosiddetto metodo Monte Carlo o altri metodi basati sul campionamento. Tuttavia, per applicazioni pratiche, questi approcci sono spesso eccessivamente dispendiosi in termini di tempo di simulazione, in quanto è noto che richiedono un numero elevato di campioni per convergere. In questa tesi, estendiamo dei risultati disponibili in letteratura all'analisi efficiente di interconnessioni ad alta velocità, come ad esempio cavi di utilizzo avionico o industriale, o circuiti stampati affetti da incertezze come tolleranze di fabbricazione o condizioni di funzionamento non note a priori. Nello specifico, viene adottata la teoria del caos polinomiale al fine di creare modelli stocastici per linee di trasmissione, che siano più veloci da simulare rispetto ad un ripetuto campionamento con tecnica Monte Carlo. Questa metodologia si basa sull'espansione di grandezze stocastiche in serie di polinomi ortogonali, ed è già stata applicata con successo all'analisi di circuiti concentrati. Questo lavoro si occupa della modellazione di componenti distribuiti, che sono elementi fondamentali dei moderni progetti ad alta frequenza. L'approccio proposto è generale e supera le limitazioni dei modelli disponibili in letteratura per l'analisi statistica della propagazione dei segnali sulle interconnessioni, i quali sono basati su strutture semplificate e ipotesi approssimate. Inoltre, viene presentata un'implementazione compatibile con SPICE, che permette quindi, per la simulazione di reti stocastiche con topologie complesse, il conveniente utilizzo di strumenti di analisi circuitale di tipo SPICE, senza richiedere quindi lo sviluppo di implementazioni specifiche e personalizzate. Questa tesi fornisce una discussione completa e teorica combinata con esempi illustrativi, in modo da complementare il materiale pubblicato.

List of Acronyms

CPM	chain-parameter matrix
DC	direct current
EMC	electromagnetic compatibility
LTI	linear time-invariant
MC	Monte Carlo
MNA	modified nodal analysis
MTL	multiconductor transmission line
PC	polynomial chaos
PCB	printed circuit board
PDF	probability density function
p.u.l.	per-unit-length
SGM	stochastic Galerkin method
TEM	transverse electromagnetic

Chapter 1

Introduction

The numerical simulation of electromagnetic systems [1] is commonly adopted by engineers in the early design phase of a product. As national and international laws require strict electromagnetic compatibility (EMC) compliance tests prior to marketing [2], simulations allow to perform right-the-first-time designs, thus limiting the need for expensive measurements and/or refabrications of prototype devices. This speeds up the design process and improves its economical impact on the whole production flow. So far, accurate models and reliable tools have been developed for the circuit simulation at system level, provided that accurate numerical values are assigned to each system parameter, and this is a still very active research topic. Nevertheless, the growing demand for large-scale integration, miniaturization and stringent design specifications, are making the impact of variability inside circuits and their interconnections increasingly relevant and hard to control [3]–[9]. Specifically, designers have to cope with complex electronic circuits that involve parameters that are partially unknown, uncontrolled or unavailable, and therefore more suitably described in terms of random variables with proper distributions. Signal integrity, electromagnetic interference or immunity issues may be significantly affected by random variations of the system parameters. In order to set realistic design margins, their correct assessment is unavoidably bound to the availability of accurate models that also account for possible uncertainties [10], [11].

Different sources of variability are usually present. Perhaps the major cause of randomness are the tolerances that unavoidably characterize the fabrication process. This means that different produced devices, which are designed to nominally be the same, differ from one to another as a result of the manufacturing process. Other sources are represented by routing or layout uncertainties, as well as the unpredictability of the operating conditions (e.g., chip temperature or loading). Besides these, inherent variations, the source of uncertainty may be external. A relevant example is provided by an electromagnetic structure illuminated by a random impinging field, acting as a noise source.

1.1 Stochastic Simulation

In this framework, the EMC community has recently faced a growing demand for stochastic simulation tools allowing for an efficient, uncertainty-aware analysis of electronic systems (see, e.g., [12] and [13]). The common tools, typically exploited to extract statistical information, are

based on the design of experiments [14], like the Latin hypercube sampling [15], or blind and brute-force random sampling methods such as Monte Carlo (MC) [16] or its enhanced variants, like the quasi-Monte Carlo method [17]. However, these methods suffer from several limitations, arising from the large computational time they require and/or the restrictions in their applicability. Other kinds of non-statistical analysis, also known as “what-if scenarios”, are sometimes performed, like the estimation of the worst-case behavior or the corner analysis, which considers the responses corresponding to the extreme values that the parameters can assume [18]. However, such approaches do not benefit of the advantage of having a statistical knowledge, as they might provide unnecessarily strict margins, which are very unlikely to occur.

On the other hand, there exist techniques which take advantage of a possible smoothness of the random parameters. In the recent literature, the polynomial chaos (PC) approach [19]–[21], turned out to be extremely appealing and has been used for the stochastic simulation of systems in many domains of physics and engineering, such as mechanics [22]–[24], fluid dynamics [25], [26], aerodynamics [27], acoustics [28]–[30], control theory [31], bioelectromagnetics [32], [33], and computational electromagnetics [34]–[39], with the inclusion of the simulation of electrical networks and electronic circuits affected by random variability [40]. Briefly speaking, the technique is based on the expansion of stochastic processes in terms of suitable orthogonal polynomials [41] and is therefore effective as long as the random parameters can be well approximated in terms of polynomial functions. Moreover, it often results to significantly outperform other traditional methods in terms of computational speed.

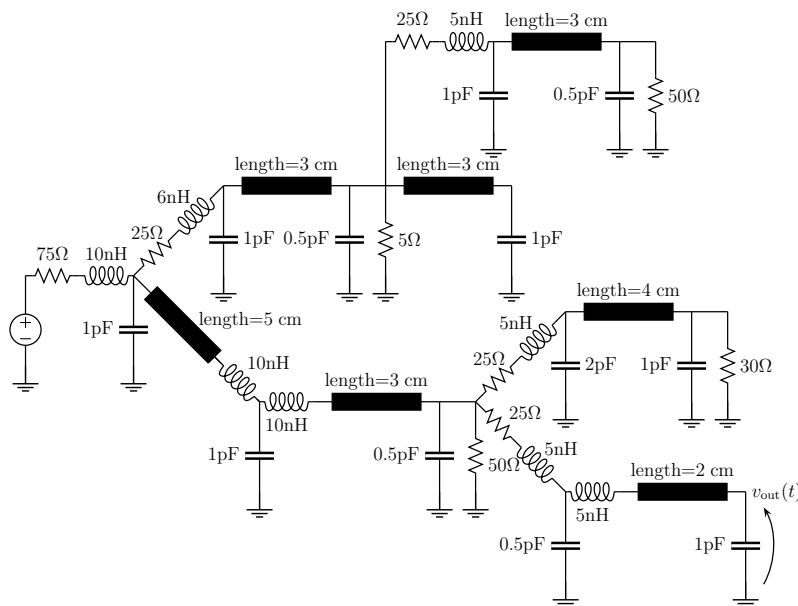


Figure 1.1. Example of an interconnect network.

1.2 Goal of the Thesis

This thesis focuses in particular on the efficient stochastic simulation of high-speed interconnects, composed by a combination of lumped and distributed transmission-line elements, like the one illustrated in Fig. 1.1 and inspired by [42]. Briefly speaking, in this context the word “distributed” means that the behavior of the interconnect strongly depends on its *electrical length*, i.e. the ratio between the conductor length and the signal wavelength. This is especially true for high-speed links, where the high frequencies give rise to unwanted and detrimental phenomena such as delay, slow-wave and skin effects, reflections, ringing and *crosstalk* (i.e., the interference between adjacent conductors).

Many parameters affect the response of an interconnect structure. First of all, any inherent interconnect property, i.e. its geometrical dimensions and the characteristics of the embedding material. Second, properties which are external to the interconnect but internal to the transmission structure, like operating temperature or loading condition. Finally, external causes like incident fields also impact of the interconnect behavior. Depending on the specific application, any of these parameters can be somehow unknown or uncontrollable, therefore needing a probabilistic description in terms of random variables. The impact of such variations becomes critical, especially in high-speed applications, where the influence of each parameter is enhanced.

The goal is then to develop probabilistic models for the electrical output quantities (typically, voltages and currents) in a circuit affected by random variations of its parameters. The main contribution in this thesis is to provide a comprehensive and general framework for the stochastic simulation of arbitrary interconnect structures by extending the PC approach to multiconductor lines governed by transmission-line equations. A SPICE implementation is also proposed, in order to facilitate the analysis of more complex circuit topologies. A complete tool for the analysis of transmission links consisting of a combination of many lumped and distributed elements is therefore provided.

1.3 State of the Art

The traditional approach that is used for stochastic analyses is based on MC simulations, and this feature is included in many circuit simulation tools (e.g., PSPICE, HSPICE or Agilent’s ADS). A MC-based statistical modeling of signal propagation on transmission lines has been addressed for instance in [43]–[47]. However, the accuracy of the MC prediction is known to have a low convergence rate with respect to the number of simulations considered, thus making it unfeasible whenever the computational cost of a single simulation is large. In [48]–[50], analytical probabilistic models were developed, but limited to low-frequency approximations as well as basic and simplified structures.

On the other hand, the PC approach has been successfully applied to the simulation of electrical networks consisting of lumped circuit elements and described by modified nodal analysis (MNA) equations [51], [52]. The methodology was applied to the statistical analysis of RC/RLC interconnects and power grid networks, respectively. However, ad hoc MATLAB implementations or customized software needed to be developed for the analysis. To improve design flexibility and facilitate the analysis of arbitrary circuit topologies, an integration into standard circuit analysis

tools, such as SPICE, is imperative. In this regard, a SPICE-like code for the stochastic analysis of lumped circuit elements was developed in [53], although still based on the creation of a customized solution engine.

Nevertheless, all the above applications lacked of the inclusion of a key component in the modeling of high-performance and high-speed links: the *distributed interconnect*, intended as a structure that conveys electric signals from a component to a distance apart and whose behavior is governed by the so-called transmission-line or *telegrapher's equations* [54]. Although a stochastic line can be in principle analyzed as a cascade of equivalent lumped sections (see, e.g., [51], [55] and [56]), this approach is not suitable to accurately model such high-frequency effects. Examples of distributed interconnects include cable bundles inside avionic equipment or industrial plants, power lines, and printed circuit board (PCB) traces inside microwave components or integrated circuits.

1.4 Organization of the Text

This text aims at providing a self-contained discussion about the application of the PC technique to the stochastic analysis of interconnect structures. In the first part, theoretical sections are combined with a tutorial approach, thus giving the reader all the information required to fully understand the general methodology, as well as its specific application and implementation. In the remaining of the text, the main applications and achievements are summarized. Therefore, this thesis is organized as follows: in Chapter 2, the simulation procedure for deterministic transmission lines is presented. In Chapter 3, the basic idea of stochastic analysis is introduced, together with the illustration of the traditional MC method. Chapter 4 introduces the PC framework, while Chapter 5 provides a tutorial description of its application to transmission-line structures. Chapter 6 provides more realistic application examples, thus highlighting the strength of the proposed methodology. Then, in Chapter 7, a SPICE implementation is presented together with the analysis of more complex interconnect topologies. Finally, in Chapter 8, the technique is extended to the analysis of a random field incidence.

Chapter 2

Analysis of Transmission Lines

This chapter represents the starting point of the work proposed in this thesis, i.e. the governing equations for the signal propagation along a multiconductor transmission line (MTL), which is the basic element for high-speed interconnects, in their deterministic formulation.

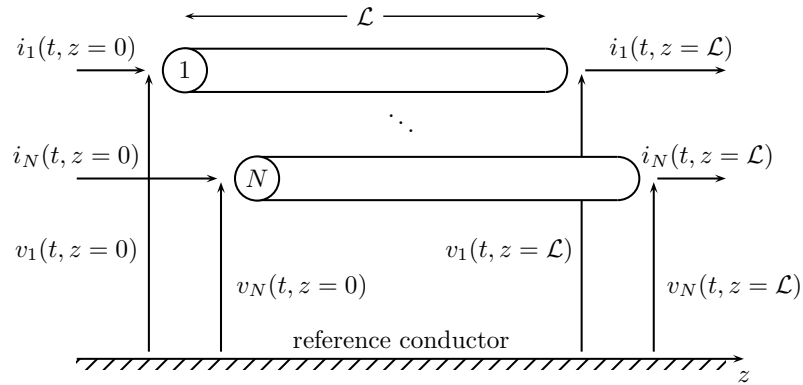


Figure 2.1. Illustration of a uniform multiconductor transmission line with N conductors of length \mathcal{L} . The definition of voltages and currents is also shown.

2.1 The Multiconductor Transmission-Line Equations

Under suitable assumptions, the signal propagation along N coupled conductors plus one reference conductor (see Fig. 2.1), all uniform along the direction z , is described by the MTL or telegrapher's equations [54]:

$$\frac{\partial}{\partial z} \mathbf{v}(z, t) = -\mathbf{R}\mathbf{i}(z, t) - \mathbf{L} \frac{\partial}{\partial t} \mathbf{i}(z, t), \quad (2.1a)$$

$$\frac{\partial}{\partial z} \mathbf{i}(z, t) = -\mathbf{G}\mathbf{v}(z, t) - \mathbf{C} \frac{\partial}{\partial t} \mathbf{v}(z, t), \quad (2.1b)$$

where $\mathbf{v} = [v_1, \dots, v_N]^T$ and $\mathbf{i} = [i_1, \dots, i_N]^T$ are vectors of size N , collecting the voltages between each signal conductor and the reference as well as the currents flowing into them, respectively. The $N \times N$ matrices \mathbf{R} (resistance), \mathbf{L} (inductance), \mathbf{G} (conductance), \mathbf{C} (capacitance) are the per-unit-length (p.u.l.) parameters and contain all the information on the electromagnetic field and the coupling among the conductors. The knowledge of such parameters is the key point in the solution of the MTL equations.

2.1.1 The Quasi-TEM Assumption

According to the above transmission-line formulation, the structure is assumed to be distributed along the direction of propagation z but lumped, i.e., electrically small, in its cross-section. As such, the validity of the above equations is restricted to the case of transverse electromagnetic (TEM) field propagation, which means that both the electric and magnetic fields surrounding the conductors are perpendicular to the line axis z . Electrically large cross-sectional dimensions give rise to additional modes of propagation, thus invalidating the TEM assumption. Another circumstance that invalidates the TEM assumption is the presence of lossy conductors and inhomogeneous surrounding media. However, as long as such violations are not extreme, the transmission-line formulation can still be considered as representative, although approximated. This situation is referred to as the *quasi-TEM* assumption. Finally, the transmission-line formulation inherently assumes that all the currents sum to zero at any cross-section. In other words, the reference conductor is the return for all the other N currents. But this might not be true, for instance in presence of nearby metallic structures that are not included in the analysis. In order to obtain a complete solution, also accounting for other modes of propagation, one has to carry-out a *full-wave* solution of Maxwell's equations.

2.1.2 The Per-Unit-Length Parameters

As already remarked, the p.u.l. parameters \mathbf{R} , \mathbf{L} , \mathbf{G} , \mathbf{C} contain all the key information about the propagation along each conductor as well as the coupling among different conductors. Specifically,

- the p.u.l. inductance matrix \mathbf{L} relates the currents flowing into the conductors to the p.u.l. magnetic fluxes penetrating the paths defined between each signal conductor and the reference. It has the following shape:

$$\mathbf{L} = \begin{bmatrix} l_{11} & l_{12} & \cdots & l_{1N} \\ l_{21} & l_{22} & \cdots & l_{2N} \\ \vdots & \vdots & \ddots & \vdots \\ l_{N1} & l_{N2} & \cdots & l_{NN} \end{bmatrix}, \quad (2.2)$$

where l_{ii} is the p.u.l. self-inductance of conductor i and l_{ij} is the p.u.l. mutual inductance between conductors i and j .

- The p.u.l. capacitance matrix \mathbf{C} relates the total p.u.l. charges on the conductors to the line

voltages producing them. Its entries are defined as

$$\mathbf{C} = \begin{bmatrix} \sum_{k=1}^N c_{1k} & -c_{12} & \cdots & -c_{1N} \\ -c_{21} & \sum_{k=1}^N c_{2k} & \cdots & -c_{2N} \\ \vdots & \vdots & \ddots & \vdots \\ -c_{N1} & -c_{N2} & \cdots & \sum_{k=1}^N c_{Nk} \end{bmatrix}, \quad (2.3)$$

with c_{ii} the p.u.l. capacitance between the i th conductor and the reference and c_{ij} the p.u.l. capacitance between conductors i and j .

- The p.u.l. conductance matrix \mathbf{G} relates the total p.u.l. transverse conduction currents passing between the conductors to the line voltages producing them. Its elements are organized similarly to those of the capacitance matrix:

$$\mathbf{G} = \begin{bmatrix} \sum_{k=1}^N g_{1k} & -g_{12} & \cdots & -g_{1N} \\ -g_{21} & \sum_{k=1}^N g_{2k} & \cdots & -g_{2N} \\ \vdots & \vdots & \ddots & \vdots \\ -g_{N1} & -g_{N2} & \cdots & \sum_{k=1}^N g_{Nk} \end{bmatrix}, \quad (2.4)$$

with g_{ii} and g_{ij} the p.u.l. conductances between the different conductors or the reference, respectively.

- The entries of the p.u.l. resistance matrix \mathbf{R} can be related to the p.u.l. resistance of the isolated conductors to a reasonable degree of accuracy, although in general one should account for the fact that the fields exterior and interior to the imperfect conductors interact. It has therefore the following shape

$$\mathbf{R} = \begin{bmatrix} r_1 + r_0 & r_0 & \cdots & r_0 \\ r_0 & r_2 + r_0 & \cdots & r_0 \\ \vdots & \vdots & \ddots & \vdots \\ r_0 & r_0 & \cdots & r_N + r_0 \end{bmatrix}, \quad (2.5)$$

where r_i is the p.u.l. resistance of the i th conductor ($i = 0$ denoting the reference conductor).

One important property of the p.u.l. matrices is that they are symmetric (in presence of reciprocal materials). Under the TEM assumption, the entries of the p.u.l. inductance matrix \mathbf{L} , conductance

matrix \mathbf{G} and of the capacitance matrix \mathbf{C} are related to the fields external to the conductors and are determined as the *static* field solutions in the transverse plane assuming perfect conductors. The entries of the p.u.l. resistance matrix \mathbf{R} are instead governed by the fields interior to the imperfect conductors.

The ease of determination of the p.u.l. parameters is related to the cross-sectional structure. For cylindrical conductors in a homogeneous medium, closed-form analytical formulas for the entries of the p.u.l. inductance are available. We limit ourselves to mention those for wires above a perfectly-conducting ground plane:

$$l_{ii} = \frac{\mu}{2\pi} \cosh^{-1} \left(\frac{h_i}{r_{w_i}} \right), \quad (2.6a)$$

$$l_{ij} = \frac{\mu}{4\pi} \ln \left(1 + 4 \frac{h_i h_j}{d_{ij}^2} \right), \quad (2.6b)$$

where h_i and r_{w_i} are the height and the radius of wire i , respectively, d_{ij} is the distance between wire i and wire j , and μ is the permeability of the embedding medium. The capacitance and inductance matrices can be obtained through the following relations, valid for homogeneous media:

$$\mathbf{C} = \mu\epsilon\mathbf{L}^{-1} \quad (2.7)$$

and

$$\mathbf{G} = \frac{\sigma_d}{\epsilon} \mathbf{C} = \sigma_d \mu \mathbf{L}^{-1}, \quad (2.8)$$

where μ , ϵ and σ_d are the permeability, permittivity and conductivity of the embedding material, respectively. When the conductors have different shapes and/or the surrounding medium is inhomogeneous, numerical computations are required [57].

2.1.3 Dispersive Lines

The material properties, as well as the distribution of the currents inside the imperfect conductors, depend on the frequency of the excitation signals. Hence, the p.u.l. parameters are generally *dispersive* (i.e., frequency dependent), and therefore more correctly indicated as $\mathbf{R}(\omega)$, $\mathbf{L}(\omega)$, $\mathbf{G}(\omega)$ and $\mathbf{C}(\omega)$, with $\omega = 2\pi f$ the angular frequency. As we will see, the dispersive behavior is hard to characterize directly in time domain, but can be readily incorporated by writing the MTL equations in the frequency domain. In particular, because of the *skin effect*, the currents flowing into the imperfect conductors migrate towards the conductor surfaces and, as a result, their p.u.l. resistances increase proportionally to \sqrt{f} . Also, these internal currents give rise to internal magnetic fluxes, that in turn yield an additional component to the p.u.l. inductance matrix, with entries decreasing as $1/\sqrt{f}$. The p.u.l. conductance matrix increases with frequency because of the loss due to the incomplete alignment of the bound charges. Finally, the p.u.l. capacitance matrix (mildly) depends on frequency because the relative permittivity of dielectrics is (mildly) frequency dependent.

Approximate relations exist for the total p.u.l. internal impedance of imperfect conductors [54]:

$$z_i(\omega) = r_i(\omega) + j\omega l_i(\omega) = \begin{cases} r_{dc}(1 + j\omega/\omega_c) & \omega \leq \omega_c, \\ r_{dc}\sqrt{\omega/\omega_c}(1 + j) & \omega \geq \omega_c, \end{cases} \quad (2.9)$$

where r_i is the p.u.l. resistance, l_i the p.u.l. internal inductance, and r_{dc} the p.u.l. DC resistance, given by the Ohm's law

$$r_{dc} = \frac{1}{\sigma_c S}, \quad (2.10)$$

with σ_c the metal conductivity and S the conductor section. Moreover, $\omega_c = 2\pi f_c$ is a transition angular frequency, that for wires corresponds to the frequency at which the wire radius equals two *skin depths*, i.e.

$$f_c = \frac{4}{\pi \sigma_c \mu_0 r_w^2}, \quad (2.11)$$

r_w denoting the wire radius. With the above definitions, the total p.u.l. impedance matrix is given by

$$\mathbf{Z}(\omega) = \mathbf{R}(\omega) + j\omega\mathbf{L}(\omega) = \begin{bmatrix} z_1(\omega) + z_0(\omega) & z_0(\omega) & \cdots & z_0(\omega) \\ z_0(\omega) & z_2(\omega) + z_0(\omega) & \cdots & z_0(\omega) \\ \vdots & \vdots & \ddots & \vdots \\ z_0(\omega) & z_0(\omega) & \cdots & z_N(\omega) + z_0(\omega) \end{bmatrix} + j\omega\mathbf{L}_e, \quad (2.12)$$

where \mathbf{L}_e is the classical “external” p.u.l. inductance, defined by (2.2).

Sometimes, the lines can be assumed as lossless, i.e. with $\mathbf{R} = \mathbf{G} = \mathbf{0}$, and/or dispersion-free, whereas in the most general case, the accurate computation of the frequency-dependent p.u.l. parameters is highly nontrivial and requires complex numerical calculations [58].

2.2 Solution of the Multiconductor Transmission-Line Equations

The system (2.1) describes the behavior of the signals in the MTL. Its solution allows the analysis of the signal propagation along the line as well as of the unintentional interaction (crosstalk) due to the electromagnetic coupling among different conductors. The solution of the MTL equations usually follows the following three-step procedure [54]:

1. Determination, either analytically or numerically, of the p.u.l. parameters for the given line geometry.
2. Computation of the general solution of the line, consisting of N forward- and N backward-traveling waves, with $2N$ unknown coefficients.
3. Incorporation of the terminal (boundary) conditions to determine the unknown coefficients.

The final step allows to fully characterize the system and to solve a given line for a given configuration of its terminations (that typically include independent sources, lumped elements, diodes, etc.). Nevertheless, the time-domain computation of the general solution is challenging whenever the line is lossy and/or the p.u.l. parameters are frequency dependent, as these behaviors are more suitably characterized in the frequency domain. Because of this, we will mainly consider and present first the frequency-domain solution of the MTL equations. However, such a solution can take only linear terminations into account.

2.2.1 Frequency-Domain Equations

When considering the frequency domain, the excitations sources are supposed to be sinusoids which have been applied for a sufficiently long time so that all transients have decayed to zero, i.e. the line is in *steady state*. Therefore, the line voltages and currents are also sinusoids. Using the *phasor* notation, we have

$$\mathbf{v}(z, t) = \Re \{ \mathbf{V}(z) e^{j\omega t} \}, \quad (2.13a)$$

$$\mathbf{i}(z, t) = \Re \{ \mathbf{I}(z) e^{j\omega t} \}, \quad (2.13b)$$

where $\Re \{ \cdot \}$ denotes the real part of the enclosed complex quantity. From now on, capital letters will denote frequency-domain voltages and currents, while the corresponding time-domain quantities will be expressed with small letters. According to Fourier theory, the time derivatives are replaced by $j\omega$. Therefore, the frequency-domain MTL equations become

$$\frac{d}{dz} \mathbf{V}(z, \omega) = -\mathbf{Z}(\omega) \mathbf{I}(z, \omega), \quad (2.14a)$$

$$\frac{d}{dz} \mathbf{I}(z, \omega) = -\mathbf{Y}(\omega) \mathbf{V}(z, \omega), \quad (2.14b)$$

with

$$\mathbf{Z}(\omega) = \mathbf{R}(\omega) + j\omega \mathbf{L}(\omega), \quad (2.15a)$$

$$\mathbf{Y}(\omega) = \mathbf{G}(\omega) + j\omega \mathbf{C}(\omega). \quad (2.15b)$$

As already remarked, in this case there is no limitation about the p.u.l. parameters being frequency dependent.

2.2.2 General Solution

The second step in the solution procedure consists in the computation of the general solution of the MTL for a given frequency and length, the latter denoted with \mathcal{L} . This is given by the *chain parameter matrix* (CPM) [54], i.e.

$$\Phi(\mathcal{L}) = \expm \left(\begin{bmatrix} \mathbf{0} & -\mathbf{Z} \\ -\mathbf{Y} & \mathbf{0} \end{bmatrix} \mathcal{L} \right), \quad (2.16)$$

where \expm denotes the matrix exponential and the frequency dependence has been dropped for notational convenience. The CPM relates the line voltages and currents at the left ($z = 0$, or near-end) termination to those at the right ($z = \mathcal{L}$, or far-end) termination, i.e.

$$\begin{bmatrix} \mathbf{V}(z = \mathcal{L}) \\ \mathbf{I}(z = \mathcal{L}) \end{bmatrix} = \begin{bmatrix} \Phi_{11}(\mathcal{L}) & \Phi_{12}(\mathcal{L}) \\ \Phi_{21}(\mathcal{L}) & \Phi_{22}(\mathcal{L}) \end{bmatrix} \begin{bmatrix} \mathbf{V}(z = 0) \\ \mathbf{I}(z = 0) \end{bmatrix}. \quad (2.17)$$

Besides the use of the matrix exponential, the entries of the CPM can be computed as

$$\Phi_{11} = \frac{1}{2} \mathbf{Y}^{-1} \mathbf{T} (\mathbf{e}^{\gamma \mathcal{L}} + \mathbf{e}^{-\gamma \mathcal{L}}) \mathbf{T}^{-1} \mathbf{Y}, \quad (2.18a)$$

$$\Phi_{12} = -\frac{1}{2} \mathbf{Y}^{-1} \mathbf{T} \gamma (\mathbf{e}^{\gamma \mathcal{L}} - \mathbf{e}^{-\gamma \mathcal{L}}) \mathbf{T}^{-1}, \quad (2.18b)$$

$$\Phi_{21} = -\frac{1}{2} \mathbf{T} (\mathbf{e}^{\gamma \mathcal{L}} - \mathbf{e}^{-\gamma \mathcal{L}}) \gamma^{-1} \mathbf{T}^{-1} \mathbf{Y}, \quad (2.18c)$$

$$\Phi_{22} = \frac{1}{2} \mathbf{T} (\mathbf{e}^{\gamma \mathcal{L}} + \mathbf{e}^{-\gamma \mathcal{L}}) \mathbf{T}^{-1}, \quad (2.18d)$$

where \mathbf{T} and γ are such that diagonalize the product \mathbf{YZ} , i.e.

$$\mathbf{T}^{-1} \mathbf{YZT} = \gamma^2. \quad (2.19)$$

Clearly, this solution is general in the sense that the information about the specific excitations and terminations is still missing and must be included in order to fully determine the signals along the line.

2.2.3 Incorporation of the Terminal Conditions

The CPM does not explicitly determine the N voltages and N currents at the line terminations. Therefore, we need $2N$ relations to determine such voltages and currents from the CPM relation. We suppose that the terminal constraints are given in terms of Thévenin or Norton equivalents, which for linear networks always exist (at least one of the two) [59].

In the case in which both the near-end (source) and far-end (load) configurations are given as Thévenin equivalents, we have

$$\mathbf{V}(z=0) = \mathbf{V}_S - \mathbf{Z}_S \mathbf{I}(z=0), \quad (2.20a)$$

$$\mathbf{V}(z=\mathcal{L}) = \mathbf{V}_L + \mathbf{Z}_L \mathbf{I}(z=\mathcal{L}), \quad (2.20b)$$

where the \mathbf{V}_S and \mathbf{V}_L are vectors of size N and contain the effects of the independent voltage and current sources in the near- and far-end termination networks, respectively, while the $N \times N$ matrices \mathbf{Z}_S and \mathbf{Z}_L contain the effects of the impedances and controlled sources. Given the CPM and the Thévenin representation, the terminal currents can be computed as follows

$$\mathbf{I}(z=0) = [\Phi_{12} - \Phi_{11} \mathbf{Z}_S - \mathbf{Z}_L \Phi_{22} + \mathbf{Z}_L \Phi_{21} \mathbf{Z}_S]^{-1} [\mathbf{V}_L - (\Phi_{11} - \mathbf{Z}_L \Phi_{21}) \mathbf{V}_S], \quad (2.21a)$$

$$\mathbf{I}(z=\mathcal{L}) = \Phi_{21} \mathbf{V}_S + (\Phi_{22} - \Phi_{21} \mathbf{Z}_S) \mathbf{I}(z=0), \quad (2.21b)$$

whereas the terminal voltages are obtained from (2.20).

When Norton representations are used, the terminal conditions are expressed as

$$\mathbf{I}(z=0) = \mathbf{I}_S - \mathbf{Y}_S \mathbf{V}(z=0), \quad (2.22a)$$

$$\mathbf{I}(z=\mathcal{L}) = -\mathbf{I}_L + \mathbf{Y}_L \mathbf{V}(z=\mathcal{L}), \quad (2.22b)$$

where, with respect to (2.20), equivalent current sources $\mathbf{I}_{S,L}$ replace the voltage sources and equivalent admittance matrices $\mathbf{Y}_{S,L}$ replace the impedance matrices. With these new definitions, the terminal voltages are given by

$$\mathbf{V}(z=0) = [\Phi_{21} - \Phi_{22}\mathbf{Y}_S - \mathbf{Y}_L\Phi_{11} + \mathbf{Y}_L\Phi_{12}\mathbf{Y}_S]^{-1} [-\mathbf{I}_L - (\Phi_{22} - \mathbf{Y}_L\Phi_{12})\mathbf{I}_S], \quad (2.23a)$$

$$\mathbf{V}(z=\mathcal{L}) = \Phi_{12}\mathbf{I}_S + (\Phi_{11} - \Phi_{12}\mathbf{Y}_S)\mathbf{V}(z=0). \quad (2.23b)$$

Other ways can be used to relate voltages and currents at the terminals of a N -port linear network, such as mixed representations. For instance, when the near-end constraint is given in terms of a Thévenin equivalent and the far-end termination is described with a Norton equivalent, we have

$$\mathbf{V}(z=0) = \mathbf{V}_S - \mathbf{Z}_S\mathbf{I}(z=0), \quad (2.24a)$$

$$\mathbf{I}(z=\mathcal{L}) = -\mathbf{I}_L + \mathbf{Y}_L\mathbf{V}(z=\mathcal{L}), \quad (2.24b)$$

The current at the near-end termination and the voltage at the far-end termination are obtainable as

$$\mathbf{I}(z=0) = [\Phi_{22} - \Phi_{21}\mathbf{Z}_S - \mathbf{Y}_L\Phi_{12} + \mathbf{Y}_L\Phi_{11}\mathbf{Z}_S]^{-1} [-\mathbf{I}_L - (\Phi_{21} - \mathbf{Y}_L\Phi_{11})\mathbf{V}_S], \quad (2.25a)$$

$$\mathbf{V}(z=\mathcal{L}) = \Phi_{11}\mathbf{V}_S + (\Phi_{12} - \Phi_{11}\mathbf{Z}_S)\mathbf{I}(z=0). \quad (2.25b)$$

This last representation is useful when the source contains voltage generators, possibly with zero internal impedance, whereas the loads are better described in terms of admittances, like in the case of open circuits or capacitors.

Clearly, the solution at each frequency is independent from the others. If the behavior at more than one frequency is desired, one simply needs to repeat the computations outlined in this section for every frequency point, starting from the corresponding values of the p.u.l. parameters. Moreover, numerical solution can be easily carried out by means of, e.g., MATLAB, since it only involves standard matrix operations.

2.2.4 Time-Domain Solution

The frequency-domain solution of a MTL is a straightforward process, as one simply needs to iterate for every frequency of interest a solution procedure which can be easily implemented numerically. This is not readily the case for time-domain simulations, as in general the inclusion of losses and/or dispersive parameters is a challenging task. A possible approach, which exploits the convenient frequency-domain solution procedure, is the Fourier analysis. The basic idea is to decompose a time-domain waveform into sinusoidal components (*harmonics*), which define its *spectrum*. Thanks to the superposition principle, the overall effect is the sum of the responses due to each harmonic. If the signal is periodic, the harmonics appear only at discrete points, which are multiples of the fundamental repetition frequency $f_0 = 1/T$, with T the period of the waveform. In the case of non-periodic waveforms, the spectrum appears as a continuum, but in practice it is

usually discretized by suitably periodizing the waveform. This can be done by choosing a sufficiently long period to guarantee that, for each pulse, the response reaches its steady-state before the onset of the next pulse. This criterion applies also to the output waveform, which is longer, and not only to the inputs. Of course this method, being based on the frequency domain solution, only allows to deal with linear terminations. Examples of time-domain simulations via Fourier analysis will be given in Chapter 6. The description of other available techniques for time-domain analysis is out of the scope of this work, and the reader is referred to [54].

2.3 Numerical Examples

We consider a single bare wire of radius $r_w = 0.5$ mm, placed at a height $h = 5$ cm above a perfectly-conducting ground plane, as illustrated in Fig. 2.2. According to (2.6a) and (2.7), the p.u.l. inductance and capacitance are

$$L = \frac{\mu_0}{2\pi} \cosh^{-1} \left(\frac{5 \times 10^{-2}}{5 \times 10^{-4}} \right) = 1.1 \mu\text{H}/\text{m}$$

and

$$C = \frac{2\pi\epsilon_0}{\cosh^{-1} \left(\frac{5 \times 10^{-2}}{5 \times 10^{-4}} \right)} = 10.5 \text{ pF}/\text{m}$$

respectively. The surrounding medium is vacuum, with permeability $\mu_0 = 400\pi$ nH/m and permittivity $\epsilon_0 = 8.854$ pF/m. Vacuum can be regarded to be lossless, thus the p.u.l. conductance is $G = 0$ and the p.u.l. capacitance is frequency-independent. Moreover, in contrast to on-board structures, for these wire structures the effect of conductor losses is usually negligible, i.e. it can be assumed $R = 0$ and a frequency-independent L as well (this assumption is justified next). The wire is $\mathcal{L} = 80$ -cm long and is driven at the near-end side by a voltage source of amplitude

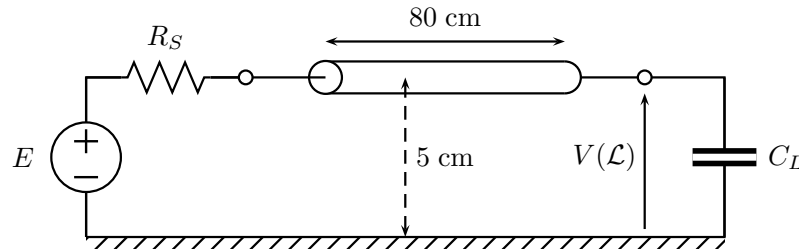


Figure 2.2. Transmission line consisting of a single wire above a ground plane, driven by a voltage source and terminated by a capacitor.

$E = 1$ V (constant with frequency) and with an internal impedance of $R_S = 75 \Omega$, whereas the far-end side is terminated by a capacitance of $C_L = 5$ pF. The terminal conditions can be expressed by a mixed representation having the following parameters:

$$\begin{aligned} V_S &= E, & Z_S &= R_S, \\ I_L &= 0, & Y_L &= j\omega C_L. \end{aligned} \quad (2.26)$$

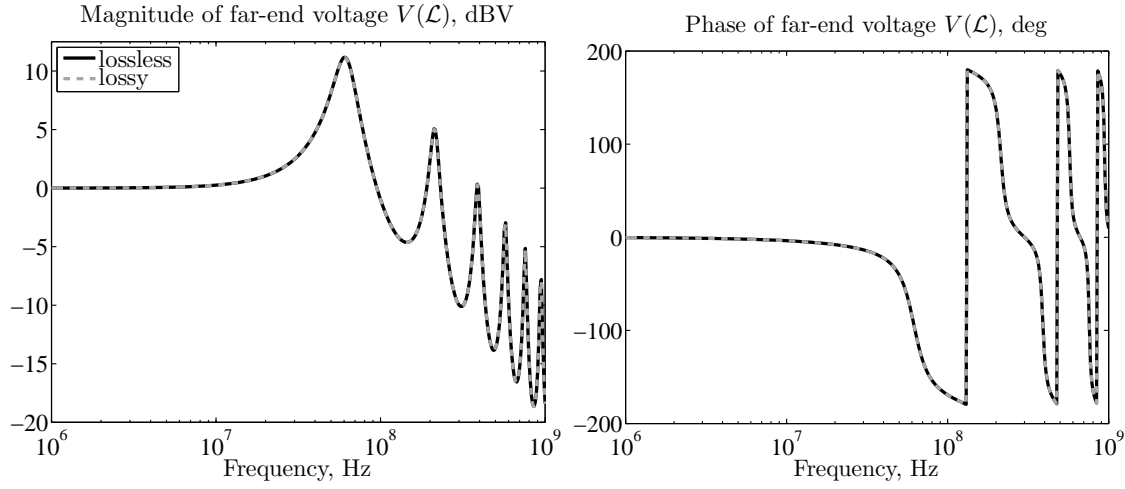


Figure 2.3. Magnitude (left panel) and phase (right panel) of the far-end transmitted voltage.

Fig. 2.3 shows the magnitude and phase of the voltage transmitted to the far-end termination, i.e. $V(z = \mathcal{L})$, computed at 401 frequency points from 6 GHz to 9 GHz. The black line has been computed with the lossless assumption, whereas the dashed gray line is obtained by including losses according to (2.9) and (2.12), considering a wire conductivity of 58 MS/m (copper). The perfect agreement between the two curves justifies the neglect of losses.

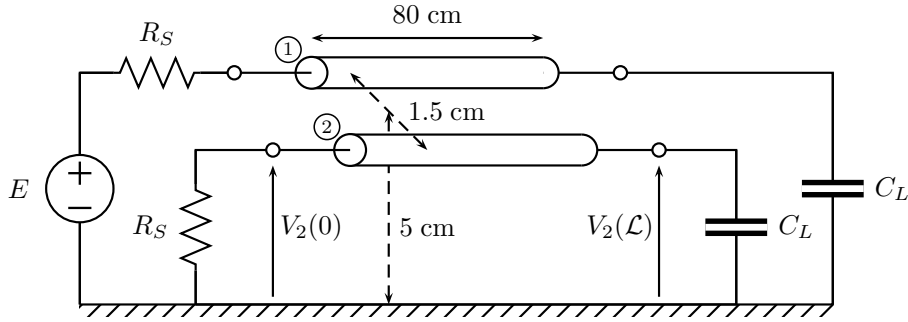


Figure 2.4. Multiconductor transmission line consisting of two coupled wires above a ground plane. One wire is active and driven by a voltage source.

We consider next the coupled line depicted in Fig. 2.4. The wire radii and height above ground are again $r_{w1} = r_{w2} = 0.5$ mm and $h_1 = h_2 = 5$ cm, respectively, whilst their separation is $d = 1.5$ cm. We now have the following p.u.l. inductance and capacitance matrices:

$$\mathbf{L} = \begin{bmatrix} 1059.7 & 381.6 \\ 381.6 & 1059.7 \end{bmatrix} \text{ nH/m}$$

and

$$\mathbf{C} = \mu_0 \varepsilon_0 \mathbf{L}^{-1} = \begin{bmatrix} 12.06 & -4.35 \\ -4.35 & 12.06 \end{bmatrix} \text{ pF/m.}$$

The source-line-load configuration is also shown in Fig. 2.4, with one active line fed by a voltage generator having an amplitude of $V_S = E = 1$ V, constant with frequency, and a quiet line terminated by a $75\text{-}\Omega$ impedance at its near-end. Both conductors are terminated with 5-pF capacitances at the far-end side. The Thévenin and Norton equivalents of such terminations are

$$\mathbf{V}_S = \begin{bmatrix} E \\ 0 \end{bmatrix}, \quad \mathbf{Z}_S = \begin{bmatrix} R_S & 0 \\ 0 & R_S \end{bmatrix},$$

$$\mathbf{I}_L = \begin{bmatrix} 0 \\ 0 \end{bmatrix}, \quad \mathbf{Y}_L = j\omega \begin{bmatrix} C_L & 0 \\ 0 & C_L \end{bmatrix},$$

respectively. Fig. 2.5 shows the magnitudes of the near- and far-end crosstalk voltages, i.e. $V_2(z = 0)$ and $V_2(z = \mathcal{L})$, respectively, computed by considering again a length of $\mathcal{L} = 80$ cm.

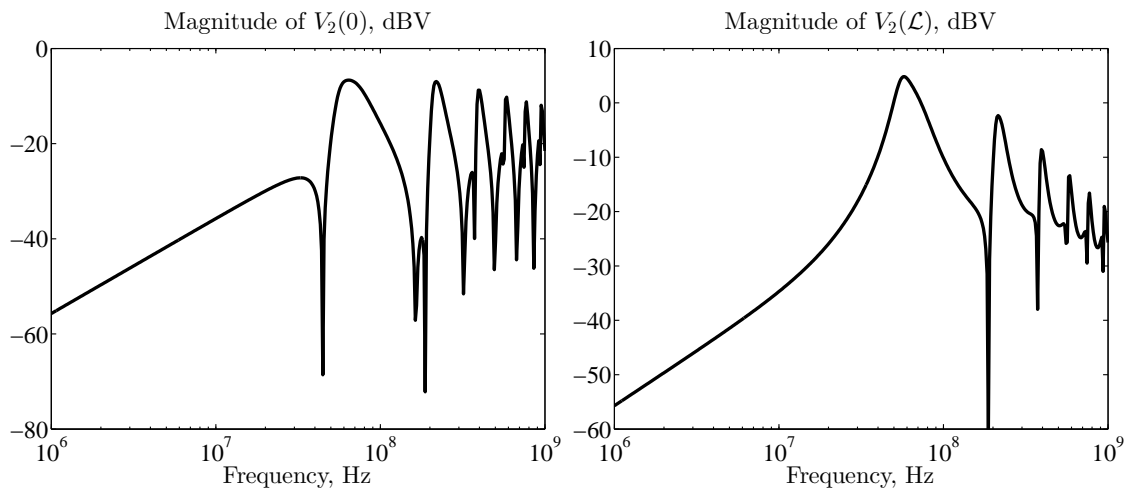


Figure 2.5. Magnitude of the near-end (left panel) and far-end (right panel) crosstalk voltage.

Chapter 3

Stochastic Analysis

The previous chapter introduced the equations which govern the signal propagation along a MTL system. With the outlined solution procedure, it is possible to carry out the full analysis of a MTL whose cross-section and termination networks are *deterministically* known: one simply needs to determine the corresponding p.u.l. parameters and solve the pertinent MTL equations. Nonetheless, there exist many situations in which some parameters are unknown or hard to control and, therefore, more appropriately represented in terms of random variables with suitable distributions. This is the case, for instance, of the outcomes of a fabrication process, where the manufacturing tolerances introduce differences in each produced device, although they should nominally be the same. Such tolerances are usually indicated in the datasheet provided by the vendors to their customers, but sometimes they are hard to quantify. In the case of high-speed interconnects, a relevant example is provided by the random trapezoidal shape of PCB trace cross-sections resulting from the etching process [60]. Also, the positioning of cables within large bundles is unavoidably random [46]. Another example is that of a single device, whose characteristics are well-known, but which is subject to uncertain operating conditions, like temperature fluctuations or variable loading conditions [18]. As a result, the system response becomes a stochastic process itself and needs to be characterized from a statistical standpoint. Such a statistical analysis allows to predict, for instance, the confidence bounds for the behavior of the majority of devices or the probability that a single device meets the design specifications, thus working correctly in the environment it is placed (yield analysis). Typical characterizations of such random quantities include the estimation of their expected (average) value, standard deviation and probability density function (PDF). This chapter introduces the basic concepts of stochastic analysis and illustrates the so-called MC method, perhaps the most widely adopted for statistical assessments in the design phase. This will be used as a reference tool throughout this text. Its computational limitations will be also highlighted, thus emphasizing the need for alternative approaches.

3.1 Statistical Background

This section introduces the basic statistical concepts that will be used in this text.

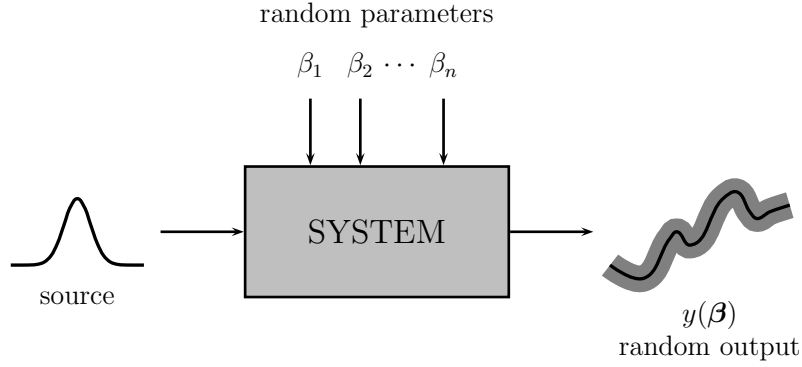


Figure 3.1. Pictorial illustration of the response of a system affected by uncertain parameters. In presence of random variations, the response to a deterministic stimulus becomes a random variable. The black line denotes the nominal response, whilst the gray area indicates its spread or fluctuation.

3.1.1 Probabilistic Framework

First of all, we adopt a probabilistic framework and introduce a n -variate random vector $\boldsymbol{\beta} = [\beta_1, \dots, \beta_n]$, with statistically independent components. Specifically, in our applications, $\boldsymbol{\beta}$ will collect all the random input parameters affecting the system behavior. Fig. 3.1 illustrates the situation: the system has multiple parameters $\boldsymbol{\beta}$, which are possibly random. The output response y depends on these system parameters and, as a result, is a random quantity itself. Thence, it is more appropriately described in statistical terms, e.g. with an associated confidence bound.

Let us define $f_{\beta_i}(\beta) : \Gamma_i \rightarrow \mathbb{R}^+$ as the PDF of the random variable β_i . Then

$$f_{\boldsymbol{\beta}}(\boldsymbol{\beta}) = \prod_{i=1}^N f_{\beta_i}(\beta_i) \quad (3.1)$$

is the joint PDF of the random vector $\boldsymbol{\beta}$ with the support

$$\Gamma = \prod_{i=1}^n \Gamma_i \subset \mathbb{R}^n. \quad (3.2)$$

Typically, the random variables in $\boldsymbol{\beta}$ are assumed to have standard distributions with well-known properties, such as the Gaussian or uniform distribution.

It should be remarked that this parameterization of the variability into a finite set of independent random variables $\boldsymbol{\beta}$ is a fundamental step to be accomplished before carrying out numerical simulations of stochastic systems. The task is relatively easy when the random inputs are the physical parameters of the system, as it is quite straightforward to identify the independent parameters to be modeled as random variables, based on experiments or reasonable and intuitive assumptions. When a random process is continuous, or correlation among several random parameters exists, techniques for the decomposition into a finite set of uncorrelated variables, like the Karhunen-Loève (KL) expansion, can be used [61]. The KL expansion consists on the spectral expansion of

the covariance matrix of a n -variate random process β and takes the following form

$$\beta = \mu + \sum_{k=1}^n \sqrt{\lambda_k} \Upsilon_k \xi_k, \quad (3.3)$$

where μ is a vector of size n collecting the mean values of β , λ_k are the eigenvalues of the covariance matrix, Υ_k the corresponding eigenvectors, and ξ_k are normalized and independent random variables. The variables ξ_k become the fundamental building blocks which parameterize the variations via (3.3)¹. In presence of a continuous random process $\beta(x)$,² characterized by a covariance function $\zeta(x_1, x_2)$, the KL expansion become an infinite series [62]

$$\beta(x) = \mu(x) + \sum_{k=1}^{\infty} \sqrt{\lambda_k} \Upsilon_k(x) \xi_k \quad (3.4)$$

with decaying coefficients λ_k , which is thus in practice truncated to n terms. In the above expression, $\Upsilon_k(x)$ are the eigenfunctions associated to the eigenvalues λ_k , i.e., satisfying the integral relation

$$\int \zeta(x_1, x_2) \Upsilon_k(x_2) dx_2 = \lambda_k \Upsilon_k(x_1). \quad (3.5)$$

Nevertheless, a through discussion about the existing techniques for such decomposition is out of the scope of this work. For the sake of simplicity, we will consider only random system parameters which are already mutually independent.

3.1.2 Random Variable Transformation

It is useful to recall here some rules for the transformation of random variables, which can be applied for instance when there is a known and explicit relationship between the output and the random input parameters [63]. The PDF of any function $y = g(\beta)$ of a single random variable β , having known distribution $f_\beta(\beta)$, is given by

$$f_y(y) = \sum_{k=1}^K \frac{f_\beta(\beta_k)}{|g'(\beta_k)|}, \quad (3.6)$$

where, for a specific value y , the β_k are the K real roots of $y = g(\beta)$, while $g'(\beta)$ denotes the derivative of $g(\beta)$. The above expression allows to readily obtain the distribution of an arbitrary random variable, provided it has an analytical relationship with another random variable of known distribution. When the inverse of $g(\beta)$ is not available in closed form, the roots of $y = g(\beta)$ can be determined numerically.

The derivation of the PDF for a function of more than one random variable is less trivial. Nonetheless, the mean value of a generic multivariate function $g(\beta)$ is obtainable as

$$\mathbb{E}\{g(\beta)\} = \int_{\Gamma} g(\beta) f_\beta(\beta) d\beta, \quad (3.7)$$

¹Although there exist random number generators for correlated random variables, they are usually based on such decorrelation methods, which are therefore simply hidden to the user.

²The process $\beta(x)$ could be, for instance, a coefficient with a given spatial dependence and a decaying correlation between values at more distant points.

while its variance is given by

$$\text{Var}\{g(\beta)\} = \int_{\Gamma} g^2(\beta) f_{\beta}(\beta) d\beta - \text{E}^2\{g(\beta)\}. \quad (3.8)$$

To provide an example, we select a Gaussian random variable β with mean $\mu = 3$ and standard deviation $\sigma = 0.6$ (we denote it as $\beta \sim \mathcal{N}(3, 0.6)$, where \mathcal{N} indicates the normal distribution). We now define a random variable y such that

$$y = g(\beta) = 3\beta^2 - 2\beta - 1. \quad (3.9)$$

The inverse and derivative of g are

$$\beta = g^{-1}(y) = \frac{1 \pm \sqrt{4 + 3y}}{3} \quad (3.10)$$

and

$$g'(\beta) = 6\beta - 2, \quad (3.11)$$

respectively. We can observe that there are two real roots when $y > -4/3$. Then, from (3.6),

$$\begin{aligned} f_y(y) = & -\frac{1}{2\sqrt{4+3y}} \frac{1}{\sqrt{2\pi}\sigma} \exp\left(-\frac{((1-\sqrt{4+3y})/3-\mu)^2}{2\sigma^2}\right) + \\ & + \frac{1}{2\sqrt{4+3y}} \frac{1}{\sqrt{2\pi}\sigma} \exp\left(-\frac{((1+\sqrt{4+3y})/3-\mu)^2}{2\sigma^2}\right). \end{aligned} \quad (3.12)$$

The mean value and variance of y can be computed by numerically integrating (3.7) and (3.8) and are $\mu = 21.08$ and $\sigma^2 = 94.49$, respectively.

3.2 The Monte Carlo Method

The MC method is perhaps the most common algorithm employed for the stochastic simulation of arbitrary systems affected by random variations, due to its robustness, as well as the relative simplicity, intuitiveness and versatility. Because of this, MC is very often used for design purposes and in this text will play the role of a reference tool for the generation of results against which to compare and validate the proposed methodology. In this section, we limit ourselves to briefly introduce the algorithm and highlight its main features. A comprehensive and thorough discussion about the MC method and its properties is out of the scope of this work.

Although an unambiguous definition does not exist, we consider the MC method as a computational algorithm that relies on repeated random sampling to obtain statistical information. It can be summarized by the following four-step procedure:

1. Determine the random parameters of interest and their distribution.
2. Generate a set of (pseudo-)random samples of such parameters according to their distribution (note that each sample can be a vector of values in case of multiple random variables).

3. Perform a deterministic computation for each sample. This means repeatedly solving the problem for the scenarios associated to the different samples.
4. Aggregate and analyze the results to obtain statistical information.³

The generation of the random samples is actually a key point in the application of a MC analysis [64]. However, truly random numbers are not always required for this method to be useful. Deterministic, *pseudorandom* sequences are adopted instead. In this work, we will rely on the samples generated by some software such as MATLAB or SPICE, and we assume that these samples are good (random) enough to our purpose. The following sections address the issue of the estimation of the statistical parameters by means of MC simulations and, when possible, the associated error.

3.2.1 Monte Carlo Estimator of the Mean Value

Suppose to run a MC simulation consisting of M simulations and producing a corresponding set $\{y_k\}_{k=1}^M$ of samples of the output quantity y . The mean value of y can be estimated as the expected value of the discrete set of random variables $\{y_k\}$, i.e.

$$\mu_Y = E\{y\} \approx \hat{\mu} = \frac{1}{M} \sum_{k=1}^M y_k. \quad (3.13)$$

It should be noted that $\hat{\mu}$ itself is a random variable, as different MC simulations on the same system and with the same number of samples M would produce different values of $\hat{\mu}$. The estimator (3.13) can be proven to be *unbiased*, meaning that its mean value coincides with the quantity it estimates. In fact, it is easy to show that $E\{\hat{\mu}\} \equiv E\{y\}$. The variance of the estimator (3.13) is

$$\text{Var}\{\hat{\mu}\} = \frac{\text{Var}\{y\}}{M} = \frac{\sigma_Y^2}{M}. \quad (3.14)$$

The above result implies that the variance of the estimator $\hat{\mu}$ can be made arbitrarily small by increasing the number of samples, i.e. simulations, M . In fact, using the Čebyšev inequality, the probability of having an estimation error above an arbitrary ϵ is

$$P\{|\hat{\mu} - \mu_Y| \geq \epsilon\} \leq \frac{\text{Var}\{\hat{\mu}\}}{\epsilon^2} = \frac{\sigma_Y^2}{M\epsilon^2}. \quad (3.15)$$

The Čebyšev inequality basically tells that we can get an arbitrarily small error by choosing a large enough value of M . The estimator (3.13) is then also said to be *consistent*. Furthermore, according to the central limit theorem, a linear combination of random variables, such as (3.13), approaches the Gaussian distribution. Therefore, we can conclude that, for M large, $\hat{\mu}$ has a

³It should be noted that, sometimes, the MC method is considered as the solution by probabilistic methods of non-stochastic problems, like the computation of deterministic (multidimensional) integrals by random sampling of the integrand function. In this case, the outlined procedure is then simply referred to as a computer implementation of a stochastic simulation [64].

Gaussian distribution with mean μ_Y and standard deviation σ_Y/\sqrt{M} , i.e. $\hat{\mu} \sim \mathcal{N}(\mu_Y, \sigma_Y/\sqrt{M})$. Therefore, by defining

$$P_k = p \left\{ |\hat{\mu} - \mu_Y| \leq k \frac{\sigma_Y}{\sqrt{M}} \right\}, \quad (3.16)$$

we can state that, when M is large, $P_1 = 68.3\%$, $P_2 = 95.4\%$, $P_3 = 99.7\%$. However, in general the variance of y is not a-priori known.

3.2.2 Monte Carlo Estimator of the Variance

A consistent and unbiased estimator of the variance of y is

$$\sigma_Y^2 = \text{Var}\{y\} \approx \hat{\sigma}^2 = \frac{1}{M-1} \sum_{k=1}^M (y_k - \hat{\mu})^2. \quad (3.17)$$

In this case, there is no explicit expression for the variance of the estimator (3.17), apart from some specific situations. For instance, when y is normally distributed, we have

$$\text{Var}\{\hat{\sigma}^2\} = \frac{2\sigma_Y^4\{y\}}{M-1}. \quad (3.18)$$

Nevertheless, the above expression allows to draw the general, qualitative conclusion that the convergence rate of the variance estimator is similar to the convergence rate of the mean estimator, but the fluctuation of the former will be in general larger due to the presence of the scale factor $2\sigma_Y^4$ compared to σ_Y^2 . The estimator $\hat{\sigma}^2$ can in turn be used to predict the variance of $\hat{\mu}$, i.e.

$$\widehat{\text{Var}\{\hat{\mu}\}} = \frac{1}{M(M-1)} \sum_{k=1}^M (y_k - \hat{\mu})^2. \quad (3.19)$$

This expression can be used for the estimation of P_k in (3.16).

3.2.3 Estimation of the Distribution by Means of Monte Carlo Simulations

We now want to construct the PDF $f_y(y)$ at a discrete set of points $\{y_j\}_{j=1}^B$, starting from the outcomes $\{y_k\}_{k=1}^M$ of the MC simulation. For simplicity, the points y_j are assumed to be equally spaced by $\Delta y = (y_B - y_1)/(B - 1)$. The value of the PDF at the point y_j can be estimated as

$$\hat{f}_y(y_j) = \frac{m_j}{M\Delta y} \quad (3.20)$$

where m_j is the number of samples $y_k \in [y_j - \Delta y/2, y_j + \Delta y/2]$. Therefore, the PDF of y is approximated by a staircase function, or histogram, where a bin is associated to each point y_j . Intuitively, for an accurate prediction of $f_y(y)$, we both need a large number of bins B (or, equivalently, a small Δy) and a large number of samples M . In fact, a large B ensures that $f_y(y)$ is finely discretized by the staircase function and, consequently, the corresponding values are representative, and not just an average value over the interval Δy . At the same time, a large M allows a sufficiently large and representative number of samples to fall in each bin.

3.2.4 Example of Monte Carlo Simulation

As a trivial and illustrative example, a MC simulation is performed to estimate the mean value, standard deviation and PDF for the transformed random variable (3.9), analyzed in Section 3.1.2. Assuming of course β as the random parameter, we can perform the remaining three steps of the MC approach: we generate (with MATLAB) a set of M random samples $\{\beta_k\}$; for each sample β_k , we deterministically compute the corresponding sample of y as $y_k = g(\beta_k)$; finally, we obtain statistical information by means of the introduced estimators. We recall that the exact values are 21.08 for the average value and 94.49 for the variance. Tab. 3.1 collects the results computed with an increasing number of samples and confirms that, for a given number of samples, the error of the variance estimator is larger than the error of the mean estimator. In addition, Fig. 3.2 compares the

Table 3.1. Monte Carlo estimation of the mean and variance of y in (3.9).

Number of samples M	Estimated mean $\hat{\mu}$	error	Estimated variance $\hat{\sigma}^2$	error
10	29.46	39.8%	402.20	325.7%
100	21.95	4.1%	109.58	16.0%
1000	20.66	2.0%	92.19	2.4%
10000	21.10	0.1%	92.56	2.0%
100000	21.08	< 0.1%	94.30	0.2%

exact PDF of y computed at 100 points with (3.12) (solid line) and by means of MC method using 10^7 samples (circles). This simple example shows that an accurate estimation of the statistical

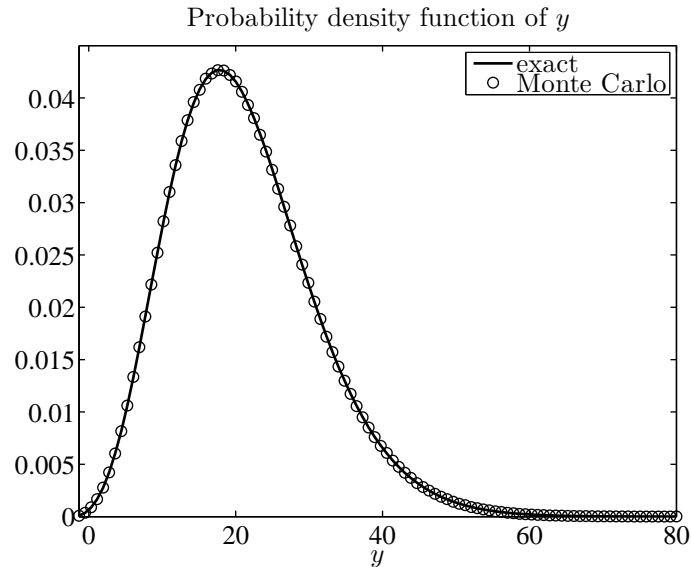


Figure 3.2. Probability density function of y . Solid line: exact analytical result; circles (\circ): MC estimation from 10^7 samples.

information and, in particular, an accurate reproduction of the PDF are possible only upon the consideration of a very large number of simulations. Whenever the simulation involves numerical solutions, the computational burden of MC rapidly becomes prohibitive.

3.3 Stochastic Analysis of Transmission Lines

In this section, we apply the concepts of MC simulations to the stochastic analysis of the two line structures introduced in Section 2.3. For this purpose, we consider first the line of Fig. 2.2, where

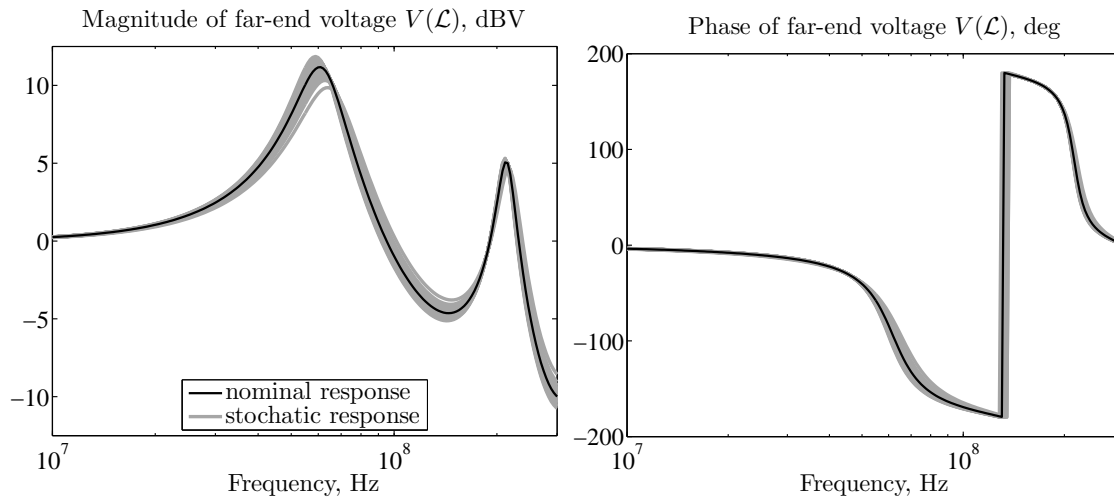


Figure 3.3. Stochastic simulation of the far-end voltage $V(\mathcal{L})$ in the line of Fig. 2.2, in presence of random variations in the conductor height above ground. Black line: nominal response; gray lines: 100 samples of the random response.

now the wire height above ground is a normally distributed random variable with mean 5 cm and standard deviation 1 cm, i.e. $h \sim \mathcal{N}(5, 1)$ cm. All the remaining parameters are left unchanged. A MC simulation is performed within MATLAB, by generating random samples for the height above ground and repeating the solution procedure for each sample. Fig. 3.3 shows a close-up of the resulting stochastic behavior of the far-end voltage $V(\mathcal{L})$. Specifically, the gray area results from the superposition of 100 samples of the response while, for comparison, the black line is the deterministic response already shown in Fig. 2.3. Indeed, the variability in the height above ground causes a random spread in the response.

In order to statistically quantify such fluctuations, Fig. 3.4 shows the average response (black line) and the standard deviation (gray line), which have been estimated with (3.13) and (3.17), respectively, based on 10000 runs. It should be noted that the average response is different, although often similar, from the nominal response, which is the response computed by considering the nominal value of the random parameters. The local maxima of the standard deviation indicate points in which the spread is larger, and this fluctuation vanishes at low frequencies. Concerning the phase, the variability is larger where the angle has rapid transitions. However, although the random input parameter is normally distributed, the distribution of the resulting response is

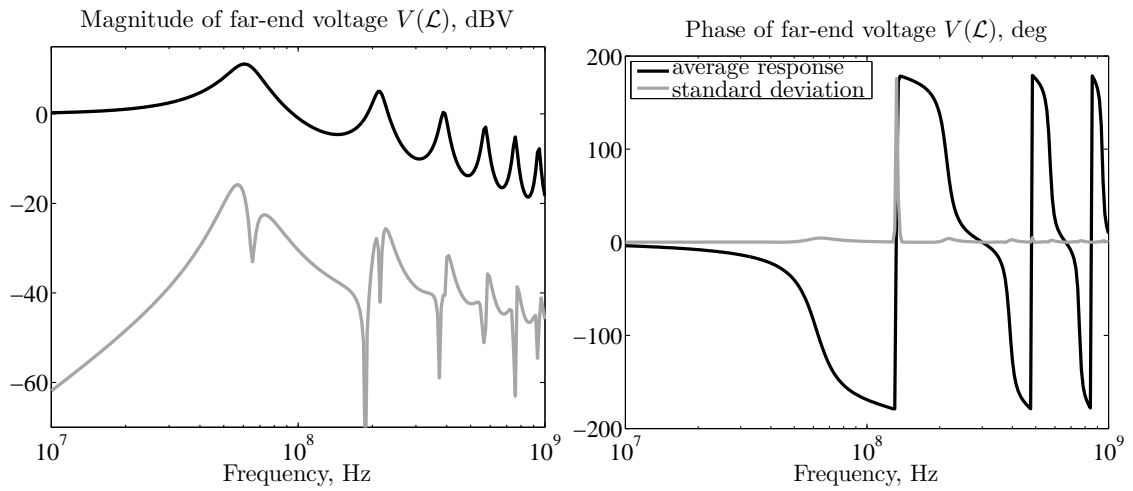


Figure 3.4. Statistical description of the far-end voltage $V(\mathcal{L})$. Black line: average response; gray line: standard deviation. Both quantities are computed after 10000 MC simulations.

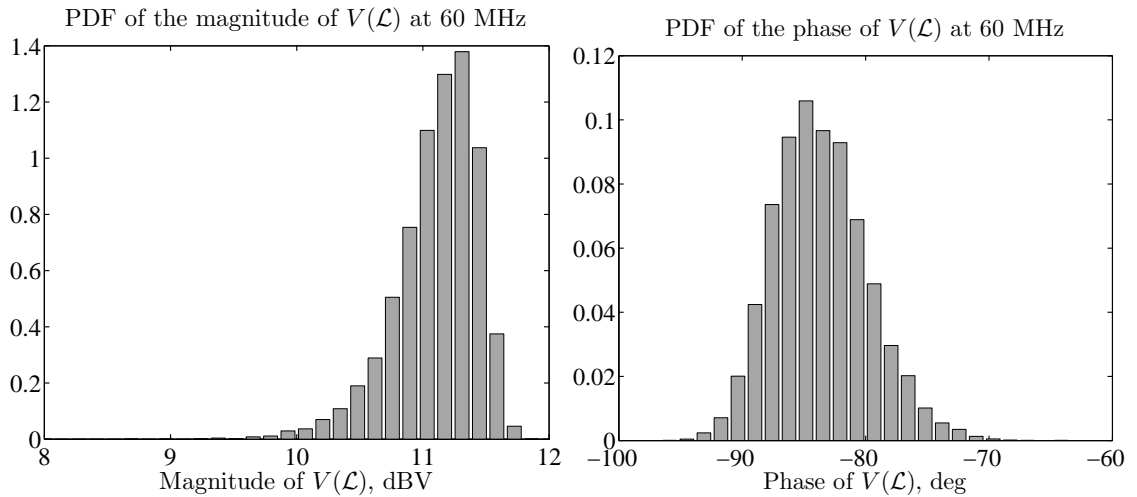


Figure 3.5. Probability density functions of the magnitude and phase of $V(\mathcal{L})$, computed at 60 MHz after 10000 MC simulations.

not necessarily Gaussian. Therefore, mean value and standard deviation are not sufficient to completely characterize it and its distribution needs to be numerically calculated. For instance, Fig. 3.5 displays the distributions of the magnitude and phase of the far-end voltage $V(\mathcal{L})$, computed at 60 MHz. This frequency corresponds to the first resonance in the response. The 10000 samples are sorted into 30 bins. The PDF of the magnitude is rather asymmetric and then differs from a Gaussian distribution.

As far as the simulation time is concerned, the MC simulation over the entire frequency range required 5 min and 6 s. This computational time is expected to significantly grow when deal-

ing with multiconductor lines having a large number of conductors and/or requiring numerical calculations for the computation of their p.u.l. parameters.

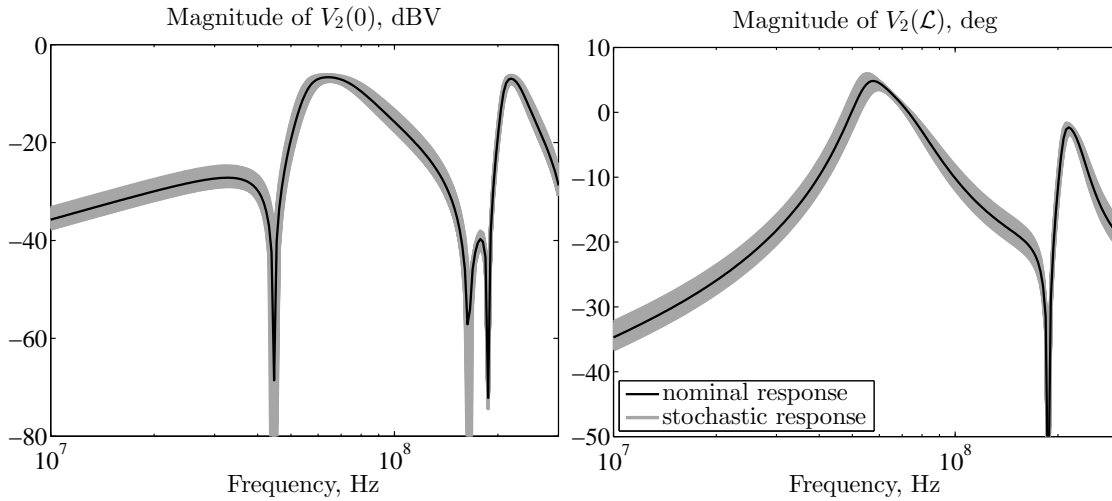


Figure 3.6. Stochastic simulation of the near-end (left panel) and far-end (right panel) crosstalk voltages in the line of Fig. 2.4, in presence of random variations in the height above ground and wire-to-wire separation. Black line: nominal response; gray lines: 100 samples of the random response.

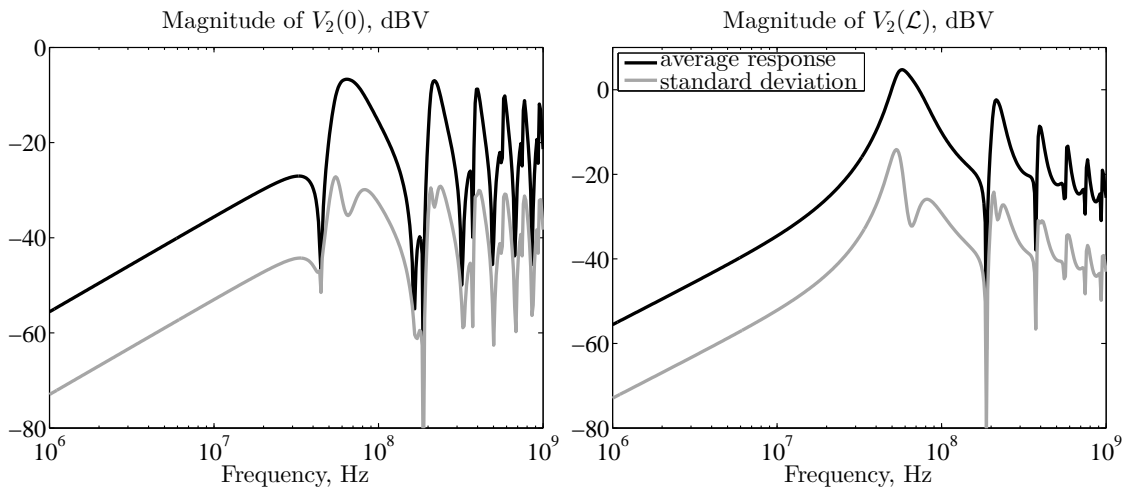


Figure 3.7. Statistical description of the near-end (left panel) and far-end (right panel) crosstalk voltages. Black line: average response; gray line: standard deviation. Both quantities are computed from 10000 MC simulations.

Analogously, for the second example in Fig. 2.4, we consider variations in the height above ground and wire-to-wire separation. This time we assume that the height is uniformly distributed in the range $[4, 6]$ cm ($h \sim \mathcal{U}(4, 6)$ cm), whilst the distance is uniformly distributed within

[1, 2] cm ($d \sim \mathcal{U}(1, 2)$ cm). Again, a MC analysis is run within MATLAB by generating independent samples for the height and separation and iterating the solution. Fig. 3.6 shows the effect of these variations on the near- and far-end crosstalk voltages, i.e. $V_2(0)$ and $V_2(\mathcal{L})$, respectively. Fig. 3.7 illustrates the average (black line) and the standard deviation (gray line) of the magnitudes of the two crosstalk voltages, computed after 10000 MC runs. The total amount of time required by these frequency sweeps is 12 min and 12 s. Also, the probability distribution of these stochastic responses is computed at two different frequencies and is displayed in Fig. 3.8. This example again demonstrates how the resulting distributions can greatly differ from the uniform distribution of the original input parameters.

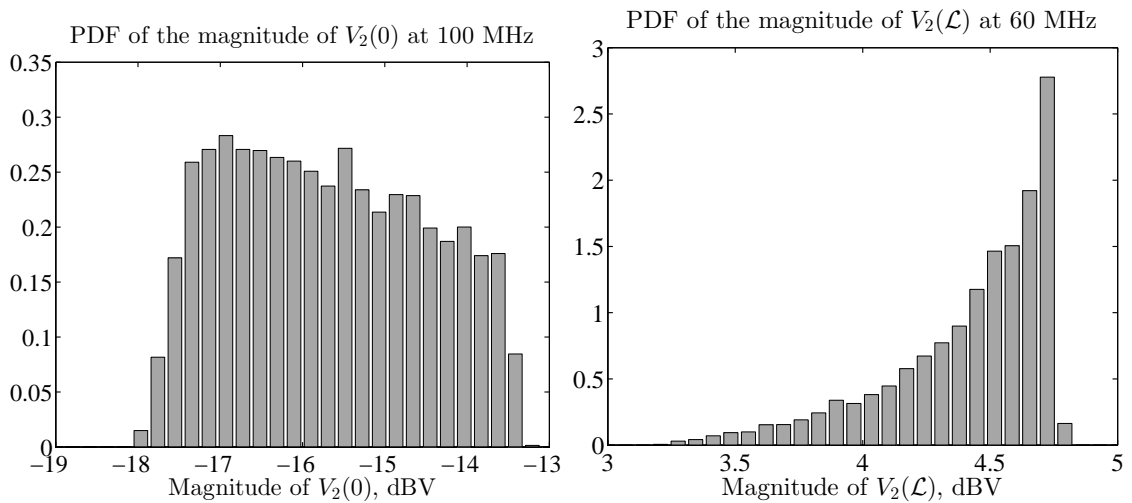


Figure 3.8. Probability density function of $V_0(\mathcal{L})$ (left panel) and $V_2(\mathcal{L})$ (right panel) computed at 100 and 60 MHz, respectively, by means of 10000 MC simulations.

Finally, we consider a third example, in which a 10% relative (Gaussian) standard deviation ($= 0.5$ pF) is ascribed to the load capacitance of the line in Fig. 2.2, in addition to the height variation. Fig. 3.9 shows the magnitude of the resulting stochastic far-end voltage as well as its average value and standard deviation.

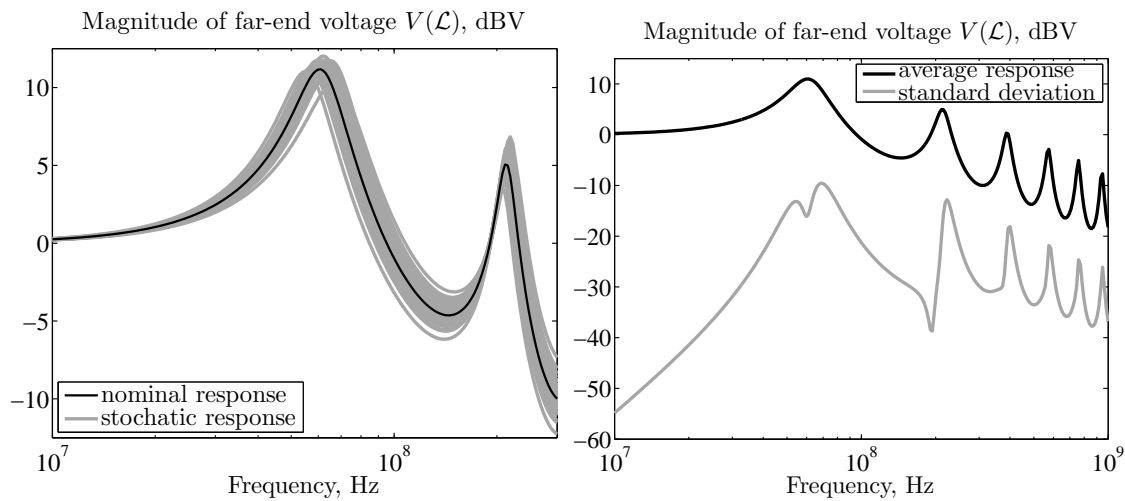


Figure 3.9. Stochastic simulation of the far-end transmitted voltage $V(\mathcal{L})$ in the line of Fig. 2.2, in presence of variations in the conductor height above ground and load capacitance. Left panel: nominal response (black line) and samples of the random response (gray lines); right panel: average response (black line) and standard deviation (gray line).

Chapter 4

The Polynomial Chaos Theory

The previous chapter discussed the main statistical tools as well as the concept of MC analysis. The main drawback of MC is that it requires a large number of samples to converge, and this number generally increases when looking at higher statistical *moments* or distribution functions. Therefore, this approach becomes unfeasible when the time required by a single simulation is large, like in the case of lines with many conductors and/or more complex circuit topologies, such as interconnect networks. Hence, the goal of this thesis is to provide an alternative and more efficient strategy for this kind of analysis. When the solution of the transmission-line equations is analytically known, one may attempt to apply rules of random variable transformation in order to retrieve the statistical information pertaining to the random response. This has been done, via approximate analytical relations valid under low-frequency and weak-coupling assumptions, for the case of crosstalk between two wires with random positioning [48], [49]. However, these closed-form results only apply to pre-determined and simplified (e.g., lossless, non-dispersive and homogeneous) wire structures with one or two signal conductors. In many practical applications involving high-speed interconnects, none of the above assumptions is usually met. First of all, high-speed interconnects are inherently “high-frequency”, thus invalidating any low-frequency approximation. Moreover, cable bundles in avionic applications as well as PCB interconnects have complex multiconductor geometries which also contain dielectric materials, being therefore inhomogeneous. Also, in the case of PCB lines, losses and dispersion play a fundamental role [65]. A more general approach is then mandatory and can be achieved by means of the PC technique, which is outlined in this chapter. Its application to the development of a general framework for the stochastic simulation of multiconductor transmission lines is provided in the next chapter instead.

4.1 Polynomial Chaos Overview

The underlying idea of PC¹ is to represent stochastic solutions in terms of orthogonal polynomial expansions of the random input parameters. In the first applications of PC [19], Hermite polynomials were employed as an orthogonal basis to represent random processes [66], [67]. However, for

¹The word “chaos” is here used in the sense originally defined by Wiener [66], i.e. as an approximation of a Gaussian random process by means of Hermite polynomials.

non-Gaussian problems, more suitable polynomial bases can be chosen, according to the probability distribution of the random inputs [20]. The choice, yielding optimal convergence, follows the so-called Askey scheme [68], and defines the *generalized* polynomial chaos framework. Tab. 4.1 illustrates the optimal polynomial bases corresponding to the most common distributions. The applications in this work will only consider Gaussian or uniform variations, and therefore will make exclusively use of Hermite and Legendre polynomials. However, the procedure is general and can be readily extended to other distributions, including non-standard ones, for which customized polynomial bases can be constructed [69]. For the discussion, we will again refer to a n -variate

Table 4.1. Wiener-Askey Polynomial Chaos.

Distribution of ξ	Class of orthogonal polynomials	Support Γ
Gaussian	Hermite	$(-\infty, +\infty)$
gamma	Laguerre	$[0, +\infty)$
beta	Jacobi	$[-1, 1]$
uniform	Legendre	$[-1, 1]$

random variable, but with the additional assumption that its components are “standard”, i.e. normalized by proper translation and scaling. Therefore, we denote it as ξ , in order to distinguish it from the non-normalized variable β . Also, we will denote the normalized joint PDF of ξ as $w(\xi)$.

4.1.1 The Polynomial Chaos Expansion

The PC seeks to approximate a random system output variable $y(\xi)$, like the situation depicted in Fig. 3.1, in terms of the following truncated expansion of the random inputs ξ :

$$y(\xi) \approx \hat{y}(\xi) = \sum_{k=0}^P c_k \phi_k(\xi), \quad (4.1)$$

where $\{\phi_k\}$ is a suitable multivariate basis of polynomial functions, orthogonal with respect to the following inner product in the Hilbert space of the variables ξ :

$$\langle f, g \rangle = \int_{\Gamma} f(\xi)g(\xi)w(\xi)d\xi. \quad (4.2)$$

Specifically, the univariate basis $\{\phi_k(\xi)\}$ is represented by the space of the polynomials orthogonal to the measure $w(\xi)d\xi$ in Γ , i.e. satisfying the orthogonality condition

$$\langle \phi_k, \phi_j \rangle = \int_{\Gamma} \phi_k(\xi)\phi_j(\xi)w(\xi)d\xi = \alpha_k^2 \delta_{kj}, \quad (4.3)$$

where δ_{kj} denotes the Kronecker’s delta function and

$$\alpha_k^2 = \langle \phi_k, \phi_k \rangle = \int_{\Gamma} \phi_k^2(\xi)w(\xi)d\xi \quad (4.4)$$

is a normalization factor. Although not necessarily useful, one can always normalize the polynomials such that $\alpha_k^2 \equiv 1, \forall k$. The degree of the polynomials is

$$\deg(\phi_k) = k. \quad (4.5)$$

It should be noted that $w(\xi)$ in (4.3) corresponds to the PDF of ξ and plays the role of a weighting function for the integration. As such, it defines the type of polynomials that must be used in (4.1).

Chosen a maximum degree p , the elements of the multivariate basis $\{\phi_k(\boldsymbol{\xi})\}$ can be readily obtained as products of a sequence of univariate polynomials in each direction $\xi_i, i = 1, \dots, n$ [70], i.e.

$$\phi_k(\boldsymbol{\xi}) = \prod_{i=1}^n \phi_{k_i}(\xi_i), \quad \sum_{i=1}^n k_i \leq p, \quad (4.6)$$

where there is a one-to-one correspondence between the index k and the multidimensional index $\mathbf{k} = [k_1, \dots, k_n]$, k_i being the degree of the univariate polynomial in the direction ξ_i . This basis defines the space of the n -variate orthogonal polynomials of total degree at most p . For example, the bivariate basis is given by the following series of functions

$$\begin{aligned} & \phi_0(\xi_1)\phi_0(\xi_2) \\ & \phi_1(\xi_1)\phi_0(\xi_2) \quad \phi_0(\xi_1)\phi_1(\xi_2) \\ & \phi_2(\xi_1)\phi_0(\xi_2) \quad \phi_1(\xi_1)\phi_1(\xi_2) \quad \phi_0(\xi_1)\phi_2(\xi_2) \\ & \phi_3(\xi_1)\phi_0(\xi_2) \quad \phi_2(\xi_1)\phi_1(\xi_2) \quad \phi_1(\xi_1)\phi_2(\xi_2) \quad \phi_0(\xi_1)\phi_3(\xi_2) \\ & \phi_4(\xi_1)\phi_0(\xi_2) \quad \phi_3(\xi_1)\phi_1(\xi_2) \quad \phi_2(\xi_1)\phi_2(\xi_2) \quad \phi_1(\xi_1)\phi_3(\xi_2) \quad \phi_0(\xi_1)\phi_4(\xi_2) \\ & \dots \end{aligned}$$

Recalling (4.5), it is readily shown that the *total degree* of the bivariate polynomials in each row of the above scheme is constant, and is incremented row by row. In practice, the series is truncated by taking a finite number of $p + 1$ rows into consideration, and the total number of terms in the expansion (4.1), for a generic number n of random variables, results to be $[70]^2$

$$P + 1 = \binom{n + p}{p} = \frac{(p + n)!}{p!n!}. \quad (4.7)$$

Owing to its definition, the orthogonality condition (4.3) readily extends to the multivariate basis. In fact, we have

$$\langle \phi_k, \phi_j \rangle = \int_{\Gamma} \phi_k(\boldsymbol{\xi})\phi_j(\boldsymbol{\xi})w(\boldsymbol{\xi})d\boldsymbol{\xi} = \prod_{i=1}^n \int_{\Gamma} \phi_{k_i}(\xi_i)\phi_{j_i}(\xi_i)w(\xi_i)d\xi_i = \prod_{i=1}^n \langle \phi_{k_i}, \phi_{j_i} \rangle, \quad (4.8)$$

where we used (4.6), (3.2), and we exploited the separation of variables. The above expression differs from zero only if $k_i = j_i \forall i = 1, \dots, n$, which in turn only happens when the two multivariate polynomials are identical.

²Alternatively to this “total degree” choice, the full tensor product combination of univariate polynomials is sometimes used, where each index k_i in (4.6) can be less or equal to p [71]. This choice is usually avoided as it involves a much larger number of terms, i.e. $(p + 1)^n$.

Since the polynomials from the Wiener-Askey scheme form a complete basis in the Hilbert space determined by the corresponding support Γ , the expansion is the best approximation in the linear polynomial space spanned by $\{\phi_k\}$, and converges in the L_2 sense as p is increased. In other words,

$$\lim_{p \rightarrow \infty} \|y(\boldsymbol{\xi}) - \hat{y}(\boldsymbol{\xi})\|_{L_2} = \lim_{p \rightarrow \infty} \sqrt{\int_{\Gamma} (y(\boldsymbol{\xi}) - \hat{y}(\boldsymbol{\xi}))^2 w(\boldsymbol{\xi}) d\boldsymbol{\xi}} \equiv \sqrt{\mathbb{E}\{(y(\boldsymbol{\xi}) - \hat{y}(\boldsymbol{\xi}))^2\}} = 0 \quad (4.9)$$

i.e. the root-mean-square error tends to zero when the number of functions in the expansion is increased. The convergence is then defined in a statistical sense [72].

4.1.2 Statistical Information

The expansion (4.1) provides a convenient, analytical relationship between the random output y and the random system parameters $\boldsymbol{\xi}$. As such, when the expansion is sufficiently accurate, statistical information on the random variable $y(\boldsymbol{\xi})$ can be readily obtained from $\hat{y}(\boldsymbol{\xi})$. For instance, the expected value of $y(\boldsymbol{\xi})$ is estimated as

$$\mathbb{E}\{y(\boldsymbol{\xi})\} \approx \mathbb{E}\{\hat{y}(\boldsymbol{\xi})\} = \int_{\Gamma} \hat{y}(\boldsymbol{\xi}) w(\boldsymbol{\xi}) d\boldsymbol{\xi} = \sum_{k=0}^P c_k \int_{\Gamma} \phi_k(\boldsymbol{\xi}) w(\boldsymbol{\xi}) d\boldsymbol{\xi} \equiv \sum_{k=0}^P c_k \frac{1}{\alpha_0} \langle \phi_k, \phi_0 \rangle = c_0 \alpha_0. \quad (4.10)$$

Moreover, the variance is given by

$$\begin{aligned} \text{Var}\{y(\boldsymbol{\xi})\} &\approx \text{Var}\{\hat{y}(\boldsymbol{\xi})\} = \int_{\Gamma} \hat{y}^2(\boldsymbol{\xi}) w(\boldsymbol{\xi}) d\boldsymbol{\xi} - \mathbb{E}\{\hat{y}(\boldsymbol{\xi})\}^2 = \sum_{k=0}^P \sum_{j=0}^P c_k c_j \int_{\Gamma} \phi_k(\boldsymbol{\xi}) \phi_j(\boldsymbol{\xi}) w(\boldsymbol{\xi}) d\boldsymbol{\xi} \\ &- c_0^2 \alpha_0^2 = \sum_{k=0}^P \sum_{j=0}^P c_k c_j \langle \phi_k, \phi_j \rangle - c_0^2 \alpha_0^2 = \sum_{k=0}^P c_k^2 \alpha_k^2 - c_0^2 \alpha_0^2 = \sum_{k=1}^P c_k^2 \alpha_k^2. \end{aligned} \quad (4.11)$$

For the calculation of the PDF of $y(\boldsymbol{\xi})$, one can rely on the rule of random variable transformation (3.6) or, in the multivariate case, on a MC sampling of (4.1), as described in Section 3.2. We stress here that this is not detrimental for the PC technique, as the evaluation of a polynomial function like (4.1) is usually orders of magnitude faster than the computation of an actual sample of the system output $y(\boldsymbol{\xi})$.

4.1.3 Projection

The key point in the use of PC expansions (4.1) is then the calculation of the coefficients c_k . With the definitions introduced, the coefficients c_k can be readily computed by means of the classical projection theorem, i.e. as an orthogonal projection onto the polynomial basis:

$$c_k = \frac{\langle y, \phi_k \rangle}{\langle \phi_k, \phi_k \rangle} = \frac{\int_{\Gamma} y(\boldsymbol{\xi}) \phi_k(\boldsymbol{\xi}) w(\boldsymbol{\xi}) d\boldsymbol{\xi}}{\alpha_k^2} \quad (4.12)$$

However, the above definition is of little use, as it involves the unknown output quantity $y(\boldsymbol{\xi})$. In practice, the strategy is to approximate the integral in (4.12) by means of either collocation or Galerkin methods [70]. In the former case, the integral is numerically evaluated by using a limited, discrete set of samples of the variable y [73]. In principle, the MC integration [64] is itself a collocation method, but requires again a large number of samples. More clever approaches take again advantage of polynomials and of the smoothness of the integrand, and define the class of stochastic collocation methods.

Nevertheless, when the governing equations that describe the behavior of y are relatively simple to manipulate, a Galerkin approach can be used. The result is a set of coupled and *deterministic* equations, whose solution provides the sought-for expansion coefficients. This strategy is called stochastic Galerkin method (SGM) and will be adopted in this work. However, when the governing equations take complicated forms, the derivation of Galerkin equations can become highly nontrivial.

4.2 Gaussian and Uniform Distributions

So far, we introduced the general concepts of the PC framework, which are common to every polynomial basis. From now on, we focus on problems that involve Gaussian or uniform random variables and, therefore, Hermite and Legendre bases [74] are introduced in this section.

4.2.1 Hermite Polynomials

The Hermite polynomials are a class of polynomial functions orthogonal to the weighting function

$$w(\xi) = \frac{1}{\sqrt{2\pi}} e^{-\xi^2/2}, \quad (4.13)$$

which corresponds to the PDF of a standard normal random variable $\mathcal{N}(0, 1)$.³ Therefore, they can be proven to form the optimal basis to represent a random process in terms of (4.1) when $\boldsymbol{\xi}$ is normally distributed [20]. The Hermite polynomials can be obtained by using the following generating function

$$H_k(\xi) = (-1)^k e^{\xi^2/2} \frac{d^k}{d\xi^k} e^{-\xi^2/2} \quad (4.14)$$

or, alternatively, the three-term recurrence relation

$$H_{k+1}(\xi) = \xi H_k(\xi) - k H_{k-1}(\xi) \quad (4.15)$$

with $k > 1$, given, from (4.14), that $H_0 = 1$ and $H_1 = \xi$. It is easy to show that the Hermite polynomials satisfy

$$\langle H_k, H_j \rangle = \frac{1}{\sqrt{2\pi}} \int_{-\infty}^{+\infty} H_k(\xi) H_j(\xi) e^{-\xi^2/2} = \alpha_k^2 \delta_{kj} \quad (4.16)$$

³These polynomials are sometimes called the “probabilists’ Hermite polynomials”, to distinguish them from the “physicists’ Hermite polynomials”, which are orthogonal with respect to $w(\xi) = e^{-\xi^2}$.

Table 4.2. Hermite polynomials.

Index k	Hermite polynomials	$\langle H_k, H_k \rangle$
0	$H_0(\xi) = 1$	1
1	$H_1(\xi) = \xi$	1
2	$H_2(\xi) = \xi^2 - 1$	2
3	$H_3(\xi) = \xi^3 - 3\xi$	6
4	$H_4(\xi) = \xi^4 - 6\xi^2 + 3$	24
5	$H_5(\xi) = \xi^5 - 10\xi^3 + 15\xi$	120

with

$$\alpha_k^2 = \langle H_k, H_k \rangle = k!. \quad (4.17)$$

Tab. 4.2 lists the first six Hermite polynomials. Also, a useful property is [75]

$$\langle H_k H_j, H_i \rangle = \frac{1}{\sqrt{2\pi}} \int_{-\infty}^{+\infty} H_k(\xi) H_j(\xi) H_i(\xi) e^{-\xi^2/2} d\xi = \frac{k!j!i!}{(m-k)!(m-j)!(m-i)!} \quad (4.18)$$

with $2m = k + j + i$. The above equation holds when m is integer and the argument of the factorials is non-negative, being zero otherwise.

The multivariate basis can be constructed according to (4.6), i.e. using product combinations of univariate polynomials. For illustration purposes, Tab. 4.3 lists the polynomials forming the bivariate basis ($n = 2$) with total degree $p = 3$. According to (4.8) and (4.17), the norm of each multivariate function can be straightforwardly computed:

$$\alpha_k^2 = \langle \phi_k, \phi_k \rangle = \prod_{i=1}^n \langle H_{k_i}, H_{k_i} \rangle = \prod_{i=1}^n k_i!. \quad (4.19)$$

Also, the result in (4.18) can be analogously generalized.

4.2.2 Legendre Polynomials

The discussion for Legendre polynomials parallels the one for Hermite polynomials. The Legendre polynomials are orthogonal to a weighting function coinciding with the PDF of $\mathcal{U}(-1, 1)$, i.e. a uniform random variable normalized into the support $\Gamma = [-1, 1]$:

$$w(\xi) = \begin{cases} \frac{1}{2} & -1 \leq \xi \leq 1 \\ 0 & \text{otherwise} \end{cases}. \quad (4.20)$$

Table 4.3. Bivariate Hermite basis ($\xi = [\xi_1, \xi_2]$).

Index k	Total degree	Index k	Basis function $\phi_k(\xi) = H_{k_1}(\xi_1)H_{k_2}(\xi_2)$	$\langle \phi_k, \phi_k \rangle$
0	0	[0,0]	$\phi_0(\xi) = H_0(\xi_1)H_0(\xi_2) = 1$	1
1	1	[1,0]	$\phi_1(\xi) = H_1(\xi_1)H_0(\xi_2) = \xi_1$	1
2		[0,1]	$\phi_2(\xi) = H_0(\xi_1)H_1(\xi_2) = \xi_2$	1
3	2	[2,0]	$\phi_3(\xi) = H_2(\xi_1)H_0(\xi_2) = \xi_1^2 - 1$	2
4		[1,1]	$\phi_4(\xi) = H_1(\xi_1)H_1(\xi_2) = \xi_1\xi_2$	1
5		[0,2]	$\phi_5(\xi) = H_0(\xi_1)H_2(\xi_2) = \xi_2^2 - 1$	2
6	3	[3,0]	$\phi_6(\xi) = H_3(\xi_1)H_0(\xi_2) = \xi_1^3 - 3\xi_1$	6
7		[2,1]	$\phi_7(\xi) = H_2(\xi_1)H_1(\xi_2) = \xi_1^2\xi_2 - \xi_2$	2
8		[1,2]	$\phi_8(\xi) = H_1(\xi_1)H_2(\xi_2) = \xi_1\xi_2^2 - \xi_1$	2
9		[0,3]	$\phi_9(\xi) = H_0(\xi_1)H_3(\xi_2) = \xi_2^3 - 3\xi_2$	6

The generating function for Legendre polynomials is

$$P_k(\xi) = \frac{1}{2^k k!} \frac{d^k}{d\xi^k} (\xi^2 - 1)^k, \quad (4.21)$$

while the three-term recurrence relation is

$$P_{k+1}(\xi) = \frac{2k+1}{k+1} \xi P_k(\xi) - \frac{k}{k+1} P_{k-1}(\xi) \quad (4.22)$$

with $k > 1$, $P_0 = 1$ and $P_1 = \xi$. The Legendre polynomials are orthogonal with respect to the following inner product:

$$\langle P_k, P_j \rangle = \frac{1}{2} \int_{-1}^1 P_k(\xi) P_j(\xi) d\xi = \alpha_k^2 \delta_{kj}, \quad (4.23)$$

where

$$\alpha_k^2 = \frac{1}{2} \int_{-1}^1 P_k^2(\xi) d\xi = \frac{1}{2k+1}. \quad (4.24)$$

Table 4.4. Legendre polynomials.

Index k	Legendre polynomials	$\langle P_k, P_k \rangle$
0	$P_0(\xi) = 1$	1
1	$P_1(\xi) = \xi$	$\frac{1}{3}$
2	$P_2(\xi) = \frac{3}{2}\xi^2 - \frac{1}{2}$	$\frac{1}{5}$
3	$P_3(\xi) = \frac{5}{2}\xi^3 - \frac{3}{2}\xi$	$\frac{1}{7}$
4	$P_4(\xi) = \frac{35}{8}\xi^4 - \frac{30}{8}\xi^2 + \frac{3}{8}$	$\frac{1}{9}$
5	$P_5(\xi) = \frac{63}{8}\xi^5 - \frac{70}{8}\xi^3 + \frac{15}{8}\xi$	$\frac{1}{11}$

Tab. 4.4 lists the first six Legendre polynomials. Like for the case of Hermite polynomials, it is useful to provide the following relation, derived from the Gaunt's formula [76]:

$$\langle P_k P_j, P_i \rangle = \frac{1}{2} \int_{-1}^1 P_k(\xi) P_j(\xi) P_i(\xi) d\xi =$$

$$(-1)^{s-j} \frac{i!(2s-2i)!s!}{(s-k)!(s-j)!(s-i)!(2s+1)!} \sum_{t=p}^q (-1)^t \frac{(k+t)!(j+i-t)!}{t!(k-t)!(j-i+t)!(i-t)!} \quad (4.25)$$

with $s = (k+j+i)/2$, $p = \max(0, i-j)$, and $q = \min(j+i, k, i)$. The above expression holds when s is even and the arguments of the factorials are non-negative, being null otherwise. The multivariate Legendre basis is once again constructed using product combinations of univariate Legendre polynomials. As a result,

$$\alpha_k^2 = \langle \phi_k, \phi_k \rangle = \prod_{i=1}^n \frac{1}{2k_i + 1}. \quad (4.26)$$

4.2.3 Analytical Example

For a simple illustration of the PC properties, we recall the function (3.9):

$$y(\beta) = 3\beta^2 - 2\beta - 1,$$

where $\beta \sim \mathcal{N}(3, 0.6)$. We can express β in terms of the normalized random variable $\xi \sim \mathcal{N}(0, 1)$ as follows:

$$\beta = 3 + 0.6\xi. \quad (4.27)$$

Using the above expression and recasting the polynomials, we can rewrite (3.9) as

$$y(\xi) = 1.08\xi^2 + 9.6\xi + 20. \quad (4.28)$$

The above function being already polynomial, it can be *exactly* written as a second-order Hermite expansion:

$$y(\xi) = 21.08H_0(\xi) + 9.60H_1(\xi) + 1.08H_2(\xi). \quad (4.29)$$

Using (4.10) and (4.11), we have $E\{y\} = 0! \times 21.08 = 21.08$ and $\text{Var}\{y\} = 1! \times 9.6^2 + 2! \times 1.08^2 = 94.49$, coinciding with the results already obtained in Section 3.1.2.

4.3 Gaussian Quadratures

Gaussian quadratures are rules providing an approximation of a weighted integral of a function $F(\xi)$ and are tightly related to orthogonal polynomials [77]. As such, they provide a simple and expedite tool for the evaluation of the inner product (4.2). The approximation is in terms of a weighted sum of function values computed at specific points (nodes) within the domain of integration. The general form is

$$\int_{\Gamma} F(\xi)w(\xi)d\xi \approx \sum_{k=0}^p F(\xi^{(k)})w_k, \quad (4.30)$$

where $w(\xi)$ is a weighting function and w_k are corresponding discrete weights. The above integral is *exact* when $F(\xi)$ is a polynomial of degree $2p+1$ or lower. With a direct analogy to the Wiener-Askey scheme, the nodes $\xi^{(k)}$ correspond to the roots of the $(p+1)$ th polynomial orthogonal to the weighting function $w(\xi)$ [77]. The quadrature rules can be readily extended to multidimensional integrals via tensor product summations along each dimension, i.e.

$$\int_{\Gamma} F(\boldsymbol{\xi})w(\boldsymbol{\xi})d\boldsymbol{\xi} \approx \sum_{k=0}^K F(\boldsymbol{\xi}^{(k)})\hat{w}_k \quad (4.31)$$

with $K+1 = (p+1)^n$, the nodes $\boldsymbol{\xi}^{(k)}$ the tensor product combination of the univariate nodes $\xi^{(k)}$ and the weights \hat{w}_k the product of the tensor product combinations of weights w_k . In the following, we will indicate p as the “order” of the quadrature. The above integral is indeed similar to the inner product (4.2), with $F(\boldsymbol{\xi}) = f(\boldsymbol{\xi})g(\boldsymbol{\xi})$, and the quadrature rule can be used for its convenient evaluation.

4.3.1 Gauss-Hermite Quadrature

Specifically, the Gauss-Hermite quadrature provides the following approximation

$$\int_{-\infty}^{+\infty} f(\xi) \frac{e^{-\xi^2/2}}{\sqrt{2\pi}} d\xi \approx \sum_{k=0}^p f(\xi^{(k)})w_k, \quad (4.32)$$

where the nodes $\xi^{(k)}$ are the roots of the $(p+1)$ th Hermite polynomial. Since the Hermite polynomials are *monic* (i.e., the highest degree coefficient is equal to one), the nodes and weights

can be obtained by means of the Golub-Welsch algorithm [78], i.e. as a solution of an eigenvalue problem:

$$\mathbf{W}^{-1}\mathbf{J}\mathbf{W} = \mathbf{\Lambda}, \quad (4.33)$$

where, for this specific case, \mathbf{J} is a $(p+1) \times (p+1)$ triangular matrix with entries $J_{ii} = 0$, $i = 0, \dots, p$ and $J_{i,i-1} = J_{i-1,i} = \sqrt{i}$, $i = 1, \dots, p$.⁴ The nodes $\xi^{(k)}$ coincide with the eigenvalues of \mathbf{J} , i.e. $\xi^{(k)} = \Lambda_{kk}$, while the corresponding weights are the squares of the first element of each eigenvector, i.e. $w_k = W_{0k}^2$.

4.3.2 Gauss-Legendre Quadrature

The Gauss-Legendre quadrature is an approximation of the integral of a function $f(\xi)$ over the interval $[-1, 1]$:

$$\frac{1}{2} \int_{-1}^1 f(\xi) d\xi \approx \sum_{k=0}^p f(\xi^{(k)}) w_k. \quad (4.34)$$

In this case, the nodes $\xi^{(k)}$ are the roots of the $(p+1)$ th Legendre polynomial. The corresponding weights can be obtained as [74]

$$w_k = \frac{1}{[1 - (\xi^{(k)})^2][P'_{p+1}(\xi^{(k)})]^2}, \quad (4.35)$$

where P'_{p+1} is the derivative of the $(p+1)$ th Legendre polynomial.

⁴We here point out that, for notation convenience, the indexing of matrices and vectors is sometimes considered as zero-based. However, it will always be clear from the context whether zero- or one-based indexes are used.

Chapter 5

Application of Polynomial Chaos to Transmission-Line Equations

This chapter outlines the procedure for the application of PC and the SGM to the stochastic analysis of MTLs, and represents therefore the core of this thesis. As we will see, thanks to the SGM, the original stochastic problem is rewritten in terms of a larger but deterministic one [79]–[81]. Its solution provides the PC coefficients, which allow to retrieve the statistical information pertinent to the random response, and is generally much faster than running a large number of MC simulations, like it was done in Chapter 3.

5.1 Stochastic Multiconductor Transmission-Line Equations

In Chapter 2, we introduced the MTL equations and highlighted the relationship between the p.u.l. parameters and the geometric and material properties of the line. In presence of uncertainty in the cross-sectional characteristics, the p.u.l. parameters become random variables and, consequently, the voltages and currents along the line are also stochastic. We can therefore define $\boldsymbol{\xi}$ as the random vector that collects all the random parameters affecting the interconnect properties and rewrite the pertinent frequency-domain MTL equations in a stochastic fashion:

$$\frac{d}{dz}\mathbf{V}(z, \omega, \boldsymbol{\xi}) = -\mathbf{Z}(\omega, \boldsymbol{\xi})\mathbf{I}(z, \omega, \boldsymbol{\xi}), \quad (5.1a)$$

$$\frac{d}{dz}\mathbf{I}(z, \omega, \boldsymbol{\xi}) = -\mathbf{Y}(\omega, \boldsymbol{\xi})\mathbf{V}(z, \omega, \boldsymbol{\xi}), \quad (5.1b)$$

with

$$\mathbf{Z}(\omega, \boldsymbol{\xi}) = \mathbf{R}(\omega, \boldsymbol{\xi}) + j\omega\mathbf{L}(\omega, \boldsymbol{\xi}), \quad (5.2a)$$

$$\mathbf{Y}(\omega, \boldsymbol{\xi}) = \mathbf{G}(\omega, \boldsymbol{\xi}) + j\omega\mathbf{C}(\omega, \boldsymbol{\xi}). \quad (5.2b)$$

The dependence on $\boldsymbol{\xi}$ is emphasized to highlight the quantities that exhibit variability.

5.2 The Stochastic Galerkin Method

The stochastic p.u.l. parameters are functions of the random input parameters $\boldsymbol{\xi}$. As such, they can be expanded according to (4.1)

$$\mathbf{Z}(\omega, \boldsymbol{\xi}) \approx \hat{\mathbf{Z}}(\omega, \boldsymbol{\xi}) = \sum_{k=0}^P \mathbf{Z}_k(\omega) \phi_k(\boldsymbol{\xi}), \quad (5.3a)$$

$$\mathbf{Y}(\omega, \boldsymbol{\xi}) \approx \hat{\mathbf{Y}}(\omega, \boldsymbol{\xi}) = \sum_{k=0}^P \mathbf{Y}_k(\omega) \phi_k(\boldsymbol{\xi}), \quad (5.3b)$$

with

$$\mathbf{Z}_k(\omega) = \mathbf{R}_k(\omega) + j\omega \mathbf{L}_k(\omega), \quad (5.4a)$$

$$\mathbf{Y}_k(\omega) = \mathbf{G}_k(\omega) + j\omega \mathbf{C}_k(\omega). \quad (5.4b)$$

In the above expansions, the coefficients are obtained according to the projection theorem (4.12), i.e.

$$\mathbf{Z}_k(\omega) = \frac{\langle \mathbf{Z}, \phi_k \rangle}{\langle \phi_k, \phi_k \rangle} = \frac{\int_{\Gamma} \mathbf{Z}(\omega, \boldsymbol{\xi}) \phi_k(\boldsymbol{\xi}) w(\boldsymbol{\xi}) d\boldsymbol{\xi}}{\int_{\Gamma} \phi_k^2(\boldsymbol{\xi}) w(\boldsymbol{\xi}) d\boldsymbol{\xi}}, \quad (5.5a)$$

$$\mathbf{Y}_k(\omega) = \frac{\langle \mathbf{Y}, \phi_k \rangle}{\langle \phi_k, \phi_k \rangle} = \frac{\int_{\Gamma} \mathbf{Y}(\omega, \boldsymbol{\xi}) \phi_k(\boldsymbol{\xi}) w(\boldsymbol{\xi}) d\boldsymbol{\xi}}{\int_{\Gamma} \phi_k^2(\boldsymbol{\xi}) w(\boldsymbol{\xi}) d\boldsymbol{\xi}}, \quad (5.5b)$$

which are computed via analytical or numerical integration. If necessary, the real and imaginary parts appearing in (5.4) can be obtained through the separate projection of the corresponding stochastic p.u.l. parameter. The unknown voltages and currents can also be expanded in a similar fashion:

$$\mathbf{V}(z, \omega, \boldsymbol{\xi}) \approx \hat{\mathbf{V}}(z, \omega, \boldsymbol{\xi}) = \sum_{k=0}^P \mathbf{V}_k(z, \omega) \phi_k(\boldsymbol{\xi}), \quad (5.6a)$$

$$\mathbf{I}(z, \omega, \boldsymbol{\xi}) \approx \hat{\mathbf{I}}(z, \omega, \boldsymbol{\xi}) = \sum_{k=0}^P \mathbf{I}_k(z, \omega) \phi_k(\boldsymbol{\xi}). \quad (5.6b)$$

However, the computation of \mathbf{V}_k and \mathbf{I}_k by means of projection would imply the knowledge of unknown line responses \mathbf{V} and \mathbf{I} . Here, the coefficients \mathbf{V}_k and \mathbf{I}_k become the new unknowns of the problem. Substitution of (5.3) and (5.6) into (5.1) yields

$$\frac{d}{dz} \sum_{k=0}^P \mathbf{V}_k(z, \omega) \phi_k(\boldsymbol{\xi}) = - \sum_{k=0}^P \sum_{j=0}^P \mathbf{Z}_k(\omega) \mathbf{I}_j(z, \omega) \phi_k(\boldsymbol{\xi}) \phi_j(\boldsymbol{\xi}), \quad (5.7a)$$

$$\frac{d}{dz} \sum_{k=0}^P \mathbf{I}_k(z, \omega) \phi_k(\boldsymbol{\xi}) = - \sum_{k=0}^P \sum_{j=0}^P \mathbf{Y}_k(\omega) \mathbf{V}_j(z, \omega) \phi_k(\boldsymbol{\xi}) \phi_j(\boldsymbol{\xi}). \quad (5.7b)$$

It should be observed that (5.7), like (5.1), is still a stochastic problem, albeit approximated in terms of (5.3) and (5.6). Furthermore, the dependence on the random vector ξ has been confined into the polynomial basis functions. The second step involves the application of Galerkin projection, i.e. (5.7) is weighted with the same set of polynomials $\{\phi_i\}$, $i = 0, \dots, P$, using the inner product (4.2):

$$\left\langle \frac{d}{dz} \sum_{k=0}^P \mathbf{V}_k \phi_k, \phi_i \right\rangle = - \left\langle \sum_{k=0}^P \sum_{j=0}^P \mathbf{Z}_k \mathbf{I}_j \phi_k \phi_j, \phi_i \right\rangle, \quad (5.8a)$$

$$\left\langle \frac{d}{dz} \sum_{k=0}^P \mathbf{I}_k \phi_k, \phi_i \right\rangle = - \left\langle \sum_{k=0}^P \sum_{j=0}^P \mathbf{Y}_k \mathbf{V}_j \phi_k \phi_j, \phi_i \right\rangle. \quad (5.8b)$$

Thanks to the linearity of the inner product, the above system reduces to

$$\frac{d}{dz} \sum_{k=0}^P \mathbf{V}_k \underbrace{\langle \phi_k, \phi_i \rangle}_{=0 \ \forall k \neq i} = \frac{d}{dz} \mathbf{V}_i \langle \phi_i, \phi_i \rangle = - \sum_{k=0}^P \sum_{j=0}^P \mathbf{Z}_k \mathbf{I}_j \langle \phi_k \phi_j, \phi_i \rangle, \quad (5.9a)$$

$$\frac{d}{dz} \sum_{k=0}^P \mathbf{I}_k \underbrace{\langle \phi_k, \phi_i \rangle}_{=0 \ \forall k \neq i} = \frac{d}{dz} \mathbf{I}_i \langle \phi_i, \phi_i \rangle = - \sum_{k=0}^P \sum_{j=0}^P \mathbf{Y}_k \mathbf{V}_j \langle \phi_k \phi_j, \phi_i \rangle, \quad (5.9b)$$

for $i = 0, \dots, P$, where the orthogonality condition has been used to simplify the left-hand side. It is worthwhile to note that the remaining terms $\langle \phi_i, \phi_i \rangle$ and $\langle \phi_k \phi_j, \phi_i \rangle$ in the left- and right-hand sides, respectively, are mere real numbers, for which there usually exist specific analytical expressions, at least for the most common classes of orthogonal polynomials.

The above result defines $2(P+1)$ equations relating the coefficients of the voltage and current variables through the coefficients of the p.u.l. parameters. By dividing both sides by $\langle \phi_i, \phi_i \rangle$, the equations can be recast in order to still resemble telegrapher's equations:

$$\begin{array}{c} \vdots \\ \frac{d}{dz} \mathbf{V}_i \\ \vdots \end{array} = - \left[\dots \sum_{k=0}^P \mathbf{Z}_k \frac{\langle \phi_k \phi_j, \phi_i \rangle}{\langle \phi_i, \phi_i \rangle} \dots \right] \begin{bmatrix} \vdots \\ \mathbf{I}_j \\ \vdots \end{bmatrix}, \quad (5.10a)$$

$$\begin{array}{c} \vdots \\ \frac{d}{dz} \mathbf{I}_i \\ \vdots \end{array} = - \left[\dots \sum_{k=0}^P \mathbf{Y}_k \frac{\langle \phi_k \phi_j, \phi_i \rangle}{\langle \phi_i, \phi_i \rangle} \dots \right] \begin{bmatrix} \vdots \\ \mathbf{V}_j \\ \vdots \end{bmatrix}. \quad (5.10b)$$

After defining

$$\alpha_{kji} = \frac{\langle \phi_k \phi_j, \phi_i \rangle}{\langle \phi_i, \phi_i \rangle}, \quad (5.11)$$

as well as $\tilde{\mathbf{V}} = [\mathbf{V}_0, \dots, \mathbf{V}_P]^T$ and $\tilde{\mathbf{I}} = [\mathbf{I}_0, \dots, \mathbf{I}_P]^T$, the above equations can be written in a

single and larger matrix form, thus leading to the following augmented set of MTL-like equations

$$\frac{d}{dz} \tilde{\mathbf{V}}(z, \omega) = -\tilde{\mathbf{Z}}(\omega) \tilde{\mathbf{I}}(z, \omega), \quad (5.12a)$$

$$\frac{d}{dz} \tilde{\mathbf{I}}(z, \omega) = -\tilde{\mathbf{Y}}(\omega) \tilde{\mathbf{V}}(z, \omega), \quad (5.12b)$$

where $\tilde{\mathbf{Z}}$ and $\tilde{\mathbf{Y}}$ are $N(P+1) \times N(P+1)$ p.u.l. matrices, organized into $(P+1) \times (P+1)$ blocks, each block given by

$$\tilde{\mathbf{Z}}_{ij}(\omega) = \sum_{k=0}^P \mathbf{Z}_k(\omega) \alpha_{kji}, \quad (5.13a)$$

$$\tilde{\mathbf{Y}}_{ij}(\omega) = \sum_{k=0}^P \mathbf{Y}_k(\omega) \alpha_{kji}, \quad (5.13b)$$

$i, j = 0, \dots, P$. Such matrices can be still split into their real and imaginary parts

$$\tilde{\mathbf{Z}}(\omega) = \tilde{\mathbf{R}}(\omega) + j\omega \tilde{\mathbf{L}}(\omega), \quad (5.14a)$$

$$\tilde{\mathbf{Y}}(\omega) = \tilde{\mathbf{G}}(\omega) + j\omega \tilde{\mathbf{C}}(\omega), \quad (5.14b)$$

where each augmented component is constructed from the corresponding expansion coefficients as in (5.13).

It is important noting that (5.12) amounts to a *deterministic* system of differential equations, thanks to the Galerkin projection that eliminates the functions $\{\phi_k\}$ and, consequently, the random vector $\boldsymbol{\xi}$ from (5.7). Thus, (5.12) requires a single solution, which is generally much faster than running a large number of MC simulations. The unique solution of the augmented problem (5.12) provides the sought-for coefficients for the voltage and current variables, to be used in (5.6) and which are now collected into the new unknowns $\tilde{\mathbf{V}}$ and $\tilde{\mathbf{I}}$. The knowledge of the coefficients for the voltage and current variables allows to quickly extract their statistical information from (5.6), by using the relations in Section 4.1.2, as well as by means of rules of random variable transformation (cfr. Section 3.1.2) or numerical techniques.

From a practical point of view, the application of the PC approach to the MTL equations can be summarized as follows:

1. Project the p.u.l. matrices \mathbf{Z} and \mathbf{Y} onto a basis of orthogonal polynomials according to (5.3), thus finding the expansion coefficients \mathbf{Z}_k and \mathbf{Y}_k .
2. Use the above coefficients to build the augmented MTL system matrices $\tilde{\mathbf{Z}}$ and $\tilde{\mathbf{Y}}$ via (5.13). Fig. 5.1 visualizes this procedure in the case $N = 2$ and $P = 2$: the original, stochastic line, described by the p.u.l. matrices \mathbf{Z} and \mathbf{Y} , is “expanded” into a deterministic one, having a larger number of terminals, and described by equivalent p.u.l. matrices $\tilde{\mathbf{Z}}$ and $\tilde{\mathbf{Y}}$. Of course, the augmented line has no physical description.

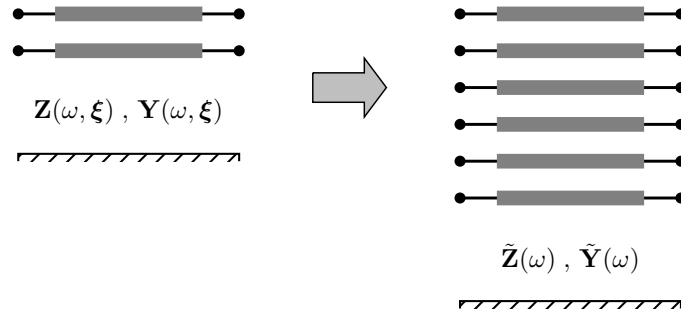


Figure 5.1. Pictorial illustration of the augmentation procedure: the original, stochastic line is replaced by a deterministic line having a larger number of conductors.

3. Solve (once, then faster) the obtained deterministic system (5.12) for a specific source-load configuration, thus finding the coefficients \mathbf{V}_k and \mathbf{I}_k . In order to solve (5.12), augmented terminal constraints for this new deterministic problem must be imposed, and this point will be addressed in Section 5.5.
4. Use the PC expansion (5.6) in place of the actual \mathbf{V} and \mathbf{I} to extract statistical information.

It is relevant to point out that the PC model, generated after steps 1 and 2, does not need to be re-computed when the same transmission line with the given variations is to be simulated in a different circuit. The examples in the following sections clarify the above procedure, which can be easily automated in a computer code.

5.3 Tutorial Example — Single Line and One Random Variable

The PC-SGM is here applied to generate augmented models for the single line of Fig. 2.2. In this case, the variability considered for the MC analysis in Chapter 3 was provided by the height above the ground plane, which was a Gaussian random variable with mean 5 cm and standard deviation 1 cm. Therefore, the height can be expressed in terms of a standard normal random variable ξ as follows:

$$h(\xi) = 0.05 + 0.01\xi \quad [\text{m}].$$

The p.u.l. inductance and capacitance can then be written as

$$L(\xi) = \frac{\mu_0}{2\pi} \cosh^{-1} \left(\frac{0.05+0.01\xi}{0.0005} \right) \quad (5.15)$$

and

$$C(\xi) = \frac{2\pi\epsilon_0}{\cosh^{-1} \left(\frac{0.05+0.01\xi}{0.0005} \right)}, \quad (5.16)$$

respectively. As already discussed, losses and dispersion are in this case negligible and for illustration purposes they are not considered. Since the random variable ξ has a Gaussian distribution, the

above parameters can be expressed in terms of Hermite expansions. For instance, the expression for the p.u.l. inductance with order $p = 2$ writes

$$L(\xi) \approx L_0 + L_1 \cdot \xi + L_2 \cdot (\xi^2 - 1), \quad (5.17)$$

with

$$L_0 = \frac{1}{0!} \int_{-\infty}^{+\infty} L(\xi) \cdot 1 \cdot w(\xi) d\xi = \frac{\mu_0}{2\pi} \int_{-\infty}^{+\infty} \cosh^{-1} \left(\frac{0.05+0.01\xi}{0.0005} \right) \frac{e^{-\xi^2/2}}{\sqrt{2\pi}} d\xi, \quad (5.18a)$$

$$L_1 = \frac{1}{1!} \int_{-\infty}^{+\infty} L(\xi) \cdot \xi \cdot w(\xi) d\xi = \frac{\mu_0}{2\pi} \int_{-\infty}^{+\infty} \cosh^{-1} \left(\frac{0.05+0.01\xi}{0.0005} \right) \cdot \xi \cdot \frac{e^{-\xi^2/2}}{\sqrt{2\pi}} d\xi, \quad (5.18b)$$

$$L_2 = \frac{1}{2!} \int_{-\infty}^{+\infty} L(\xi) \cdot (\xi^2 - 1) \cdot w(\xi) d\xi = \frac{\mu_0}{4\pi} \int_{-\infty}^{+\infty} \cosh^{-1} \left(\frac{0.05+0.01\xi}{0.0005} \right) \cdot (\xi^2 - 1) \cdot \frac{e^{-\xi^2/2}}{\sqrt{2\pi}} d\xi. \quad (5.18c)$$

It is possible to numerically compute the above integrals with the MATLAB function `quadgk`. The results are $L_0 = 1055.4$ nH/m, $L_1 = 41.9$ nH/m, and $L_2 = -4.6$ nH/m. The coefficients decrease thanks to the convergence properties of the PC expansions. Similarly, the PC-expansion coefficients for the p.u.l. capacitance can be computed as

$$C_0 = \int_{-\infty}^{+\infty} \frac{2\pi\epsilon_0}{\cosh^{-1} \left(\frac{0.05+0.01\xi}{0.0005} \right)} \frac{e^{-\xi^2/2}}{\sqrt{2\pi}} d\xi, \quad (5.19a)$$

$$C_1 = \int_{-\infty}^{+\infty} \frac{2\pi\epsilon_0}{\cosh^{-1} \left(\frac{0.05+0.01\xi}{0.0005} \right)} \cdot \xi \cdot \frac{e^{-\xi^2/2}}{\sqrt{2\pi}} d\xi, \quad (5.19b)$$

$$C_2 = \frac{1}{2} \int_{-\infty}^{+\infty} \frac{2\pi\epsilon_0}{\cosh^{-1} \left(\frac{0.05+0.01\xi}{0.0005} \right)} \cdot (\xi^2 - 1) \cdot \frac{e^{-\xi^2/2}}{\sqrt{2\pi}} d\xi, \quad (5.19c)$$

yielding $C_0 = 10.560$ pF/m, $C_1 = -0.429$ pF/m, and $C_2 = 0.068$ pF/m.

Fig. 5.2 visualizes the projection procedure. The solid black lines in the top left panels are the p.u.l. inductance and the p.u.l. capacitance plotted as deterministic functions of ξ , while the dashed gray lines are the corresponding approximations given by the PC expansions. The bottom panels depict the PDF of ξ , whereas the right panels show the resulting PDF of the p.u.l. parameter, both for the exact case and for the expansion. It is worth noting one key step in the PC approach: the expansions become less accurate when $|\xi|$ assumes larger values, which however have a lower probability to occur (cfr. the PDF of ξ in the bottom panels). Therefore, the expansions are overall accurate from a statistical standpoint, as confirmed by their capability of reproducing (see the dashed gray lines in the right panel) the actual probability distributions of $L(\xi)$ and $C(\xi)$ (solid black lines).

5.3.1 Projection via Gaussian Quadratures

An alternative and convenient way to compute the projection integrals (5.18) and (5.19) is to use a Gauss-Hermite quadrature with 3 nodes. In fact, such a quadrature is accurate for integrands

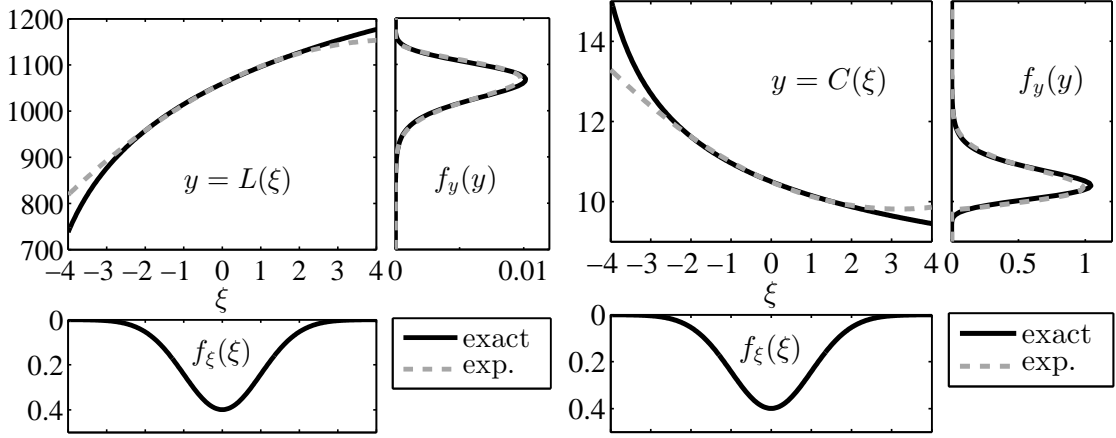


Figure 5.2. Illustration of the projection of the p.u.l. inductance (left plot) and capacitance (right plot). In each plot, the top left panel shows the p.u.l. parameter as a function of ξ . The bottom panel is the (standard normal) distribution of ξ , whilst the right panel is the resulting distribution of the p.u.l. parameter. The exact result (solid black line) is compared with the approximation given by the PC expansion (dashed gray line).

which are similar to polynomials of degree 5. In our case, the integrand is the product of $L(\xi)$ (or $C(\xi)$) and $\phi_k(\xi)$. Recalling (4.5), with k here at most 2, the use of Gaussian quadratures provides accurate values as long as $L(\xi)$ (or $C(\xi)$) is well-approximated by a polynomial of degree 3. Also, the accuracy is expected to decrease for the computation of higher-order coefficients, as the integrand include a polynomial of increasing order. It is worth noting that the use of a second-order polynomial expansion inherently implies that the function is well-approximated by a polynomial of degree 2, thus corroborating the idea of using Gaussian quadratures. In general, for a p -order expansion, a quadrature of order p can be used.

The nodes and weights for a Gauss-Hermite quadrature with 3 nodes are $\xi = \{-1.732, 0, 1.732\}$ and $w = \{0.167, 0.667, 0.167\}$, respectively. Therefore, the PC coefficients for the p.u.l. inductance can be computed as

$$L_0 \approx L(-1.732) \cdot 0.167 + L(0) \cdot 0.667 + L(1.732) \cdot 0.167, \quad (5.20)$$

$$L_1 \approx L(-1.732) \cdot (-1.732) \cdot 0.167 + L(0) \cdot 0 \cdot 0.667 + L(1.732) \cdot 1.732 \cdot 0.167, \quad (5.21)$$

$$L_2 \approx L(-1.732) \cdot 2 \cdot 0.167 + L(0) \cdot (-1) \cdot 0.667 + L(1.732) \cdot 2 \cdot 0.167, \quad (5.22)$$

yielding $L_0 \approx 1055.4$ nH/m, $L_1 \approx 41.7$ nH/m, and $L_2 \approx -4.3$ nH/m. The PC-expansion coefficients for the p.u.l. capacitance can be analogously computed to be $C_0 \approx 10.560$ pF/m, $C_1 \approx -0.426$ pF/m, and $C_2 \approx 0.060$ pF/m. These new results confirm that the accuracy of the quadrature decreases with the computation of higher-order coefficients. Clearly, the use of Gaussian quadratures for the integration introduces an additional error in the PC expansions, besides the truncation error, since now the coefficients are computed via approximate numerical rules. However, this approach turns out to be particularly convenient, as we will explain with the next example.

5.3.2 The Augmented Per-Unit-Length Matrices

According to (5.13), the augmented p.u.l. inductance matrix $\tilde{\mathbf{L}}$ is given by

$$\tilde{\mathbf{L}} = \begin{bmatrix} L_0 & L_1 & 2L_2 \\ L_1 & L_0 + 2L_2 & 2L_1 \\ L_2 & L_1 & L_0 + 4L_2 \end{bmatrix} = \begin{bmatrix} 1055.4 & 41.7 & -8.5 \\ 41.7 & 1046.9 & 83.5 \\ -4.3 & 41.7 & 1038.3 \end{bmatrix} \text{ nH/m} \quad (5.23)$$

and, similarly,

$$\tilde{\mathbf{C}} = \begin{bmatrix} C_0 & C_1 & 2C_2 \\ C_1 & C_0 + 2C_2 & 2C_1 \\ C_2 & C_1 & C_0 + 4C_2 \end{bmatrix} = \begin{bmatrix} 10.560 & -0.426 & 0.119 \\ -0.426 & 10.679 & -0.851 \\ 0.060 & -0.426 & 10.798 \end{bmatrix} \text{ pF/m}, \quad (5.24)$$

where the coefficients computed via the Gauss-Hermite quadrature have been used. The formula (4.18) is used to compute the terms $\langle \phi_k \phi_j, \phi_i \rangle$ in (5.11).

It should be noted that the PC-augmented p.u.l. matrices are no longer symmetric. This is due to the fact that classical orthogonal polynomials [74] are not *orthonormal*, i.e. they do not have unitary L_2 norm $\|\phi_k\|_{L_2} = \langle \phi_k, \phi_k \rangle$, which appears at the denominator of (5.11). Although this does not affect numerical implementation, it is sometimes useful (see Chapter 7) to preserve the symmetry belonging to the original p.u.l. matrices. This can be achieved [82] by adopting a *normalized* polynomial basis $\{\varphi_k\}$ for the expansions, with

$$\varphi_k(\xi) = \phi_k(\xi) / \sqrt{\langle \phi_k, \phi_k \rangle}. \quad (5.25)$$

For instance, the normalized Hermite polynomials are $\varphi_k(\xi) = H_k(\xi) / \sqrt{k!}$, the first three being $\varphi_0 = 1$, $\varphi_1 = \xi$, and $\varphi_2 = (\xi^2 - 1) / \sqrt{2}$. With the above definitions, the resulting p.u.l. augmented inductance and capacitance matrices are

$$\tilde{\mathbf{L}} = \begin{bmatrix} L_0 & L_1 & L_2 \\ L_1 & L_0 + \sqrt{2}L_2 & \sqrt{2}L_1 \\ L_2 & \sqrt{2}L_1 & L_0 + 2\sqrt{2}L_2 \end{bmatrix} = \begin{bmatrix} 1055.4 & 41.7 & -6.0 \\ 41.7 & 1046.9 & 59.0 \\ -6.0 & 59.0 & 1038.3 \end{bmatrix} \text{ nH/m} \quad (5.26)$$

and

$$\tilde{\mathbf{C}} = \begin{bmatrix} C_0 & C_1 & C_2 \\ C_1 & C_0 + \sqrt{2}C_2 & \sqrt{2}C_1 \\ C_2 & \sqrt{2}C_1 & C_0 + 2\sqrt{2}C_2 \end{bmatrix} = \begin{bmatrix} 10.560 & -0.426 & 0.084 \\ -0.426 & 10.679 & -0.602 \\ 0.084 & -0.602 & 10.798 \end{bmatrix} \text{ pF/m}, \quad (5.27)$$

respectively, which are indeed symmetric. It is relevant to note that different coefficients $L_{0,1,2}$ and $C_{0,1,2}$, given by the projection onto the new normalized basis, must be used. It is easy to show that the coefficients for the normalized basis are obtainable from those of the classical, non-normalized basis as $\sqrt{\langle \phi_k, \phi_k \rangle} c_k$. The multivariate basis can be obtained as usual according to (4.6), and this preserves the orthonormality. In the following, the PC basis is always selected to be orthonormal and, consequently, the matrices are symmetric.

5.4 Tutorial Example — Multiconductor Line and Multiple Random Variables

Concerning the MC analysis of the coupled line of Fig. 2.4, the variability was provided by the height above ground, uniform within [4, 6] cm, and the wire separation, uniform within [1, 2] cm. The random parameters can be expressed in terms of two uniform random variables $\boldsymbol{\xi} = [\xi_1, \xi_2]$ in the support $[-1, 1]$, as follows:

$$\begin{aligned} h(\xi_1) &= 0.05 + 0.01\xi_1 \quad [\text{m}], \\ d(\xi_2) &= 0.015 + 0.005\xi_2 \quad [\text{m}]. \end{aligned}$$

The entries of the p.u.l. inductance matrix can be written as

$$L_{11}(\boldsymbol{\xi}) = L_{22}(\boldsymbol{\xi}) = \frac{\mu_0}{2\pi} \cosh^{-1} \left(\frac{0.05 + 0.01\xi_1}{0.0005} \right), \quad (5.28a)$$

$$L_{12}(\boldsymbol{\xi}) = L_{21}(\boldsymbol{\xi}) = \frac{\mu_0}{4\pi} \ln \left[1 + 4 \frac{(0.05 + 0.01\xi_1)^2}{(0.015 + 0.005\xi_2)^2} \right], \quad (5.28b)$$

whereas the entries of the p.u.l. capacitance matrix are

$$C_{11}(\boldsymbol{\xi}) = C_{22}(\boldsymbol{\xi}) = \mu_0 \varepsilon_0 \frac{L_{11}(\boldsymbol{\xi})}{L_{11}^2(\boldsymbol{\xi}) - L_{12}^2(\boldsymbol{\xi})}, \quad (5.29a)$$

$$C_{12}(\boldsymbol{\xi}) = C_{21}(\boldsymbol{\xi}) = \mu_0 \varepsilon_0 \frac{-L_{12}(\boldsymbol{\xi})}{L_{11}^2(\boldsymbol{\xi}) - L_{12}^2(\boldsymbol{\xi})}. \quad (5.29b)$$

The p.u.l. inductance matrix can be expanded according to a second-order, bivariate series of normalized Legendre polynomials, which are constructed using the rule (4.6) and the normalization (5.25):

$$\mathbf{L}(\boldsymbol{\xi}) \approx \mathbf{L}_0 \cdot 1 + \mathbf{L}_1 \cdot \sqrt{3}\xi_1 + \mathbf{L}_2 \cdot \sqrt{3}\xi_2 + \mathbf{L}_3 \cdot \frac{\sqrt{5}}{2}(3\xi_1^2 - 1) + \mathbf{L}_4 \cdot 3\xi_1\xi_2 + \mathbf{L}_5 \cdot \frac{\sqrt{5}}{2}(3\xi_2^2 - 1). \quad (5.30)$$

According to the projection theorem, the entries of the expansion coefficients are given by

$$L_{k,ij} = \frac{1}{4} \int_{-1}^1 \int_{-1}^1 L_{ij}(\xi_1, \xi_2) \varphi_k(\xi_1, \xi_2) d\xi_1 d\xi_2 \quad (5.31)$$

(notice that now $\langle \varphi_k, \varphi_k \rangle = 1$). Similar expressions hold of course for the p.u.l. capacitance matrix. The calculations are performed by using MATLAB `dblquad` function for double integrals and produce

$$\begin{aligned} \mathbf{L}_0 &= \begin{bmatrix} 1058.3 & 384.3 \\ 384.3 & 1058.3 \end{bmatrix}, \quad \mathbf{L}_1 = \begin{bmatrix} 23.3 & 22.7 \\ 22.7 & 23.3 \end{bmatrix}, \quad \mathbf{L}_2 = \begin{bmatrix} 0 & -38.5 \\ -38.5 & 0 \end{bmatrix}, \\ \mathbf{L}_3 &= \begin{bmatrix} -1.2 & -1.1 \\ -1.1 & -1.2 \end{bmatrix}, \quad \mathbf{L}_4 = \begin{bmatrix} 0 & -0.2 \\ -0.2 & 0 \end{bmatrix}, \quad \mathbf{L}_5 = \begin{bmatrix} 0 & 3.6 \\ 3.6 & 0 \end{bmatrix}, \end{aligned} \quad [\text{nH/m}]$$

where some diagonal elements are null since the diagonal elements of the inductance matrix do not depend on ξ_2 .

It is worth noting that the multidimensional integration becomes inefficient as the number of dimension is increased. Moreover, a separate call to the integration function must be performed for the projection of each matrix entry. This makes the standard integration approach inefficient in case of multiconductor structures having a large number of lines and/or requiring a complex and time-consuming numerical computation of the p.u.l. parameters. Again, the projection can be carried out more efficiently by means of Gaussian quadratures, which now provide a twofold advantage: 1) they can be readily generalized to arbitrary multiple dimensions by using a tensor product grid of evaluation points; 2) the integration can be vectorized, since the same nodes and weights are used for the computation of every entry of the matrix coefficients.

The nodes for a second-order Gauss-Legendre quadrature are $\xi = \{-0.775, 0, 0.775\}$, while the corresponding weights are $w = \{0.278, 0.444, 0.278\}$. The expansion coefficients for the L-matrix can be then computed as

$$\mathbf{L}_k = \sum_{i=0}^2 \sum_{j=0}^2 \mathbf{L}(\xi_1^{(i)}, \xi_2^{(j)}) \varphi_k(\xi_1^{(i)}, \xi_2^{(j)}) w_i w_j, \quad (5.32)$$

and are

$$\begin{aligned} \mathbf{L}_0 &\approx \begin{bmatrix} 1058.3 & 384.3 \\ 384.3 & 1058.3 \end{bmatrix}, \quad \mathbf{L}_1 \approx \begin{bmatrix} 23.3 & 22.7 \\ 22.7 & 23.3 \end{bmatrix}, \quad \mathbf{L}_2 \approx \begin{bmatrix} 0 & -38.5 \\ -38.5 & 0 \end{bmatrix}, \\ \mathbf{L}_3 &\approx \begin{bmatrix} -1.2 & -1.1 \\ -1.1 & -1.2 \end{bmatrix}, \quad \mathbf{L}_4 \approx \begin{bmatrix} 0 & -0.2 \\ -0.2 & 0 \end{bmatrix}, \quad \mathbf{L}_5 \approx \begin{bmatrix} 0 & 3.5 \\ 3.5 & 0 \end{bmatrix}. \end{aligned} \quad [\text{nH/m}]$$

The coefficients for the C-matrix expansion are

$$\begin{aligned} \mathbf{C}_0 &\approx \begin{bmatrix} 12.145 & -4.419 \\ -4.419 & 12.145 \end{bmatrix}, \quad \mathbf{C}_1 \approx \begin{bmatrix} -0.130 & -0.117 \\ -0.117 & -0.130 \end{bmatrix}, \quad \mathbf{C}_2 \approx \begin{bmatrix} -0.376 & 0.582 \\ 0.582 & -0.376 \end{bmatrix}, \\ \mathbf{C}_3 &\approx \begin{bmatrix} 0.011 & 0.009 \\ 0.009 & 0.011 \end{bmatrix}, \quad \mathbf{C}_4 \approx \begin{bmatrix} -0.008 & -0.004 \\ -0.004 & -0.008 \end{bmatrix}, \quad \mathbf{C}_5 \approx \begin{bmatrix} 0.060 & -0.074 \\ -0.074 & 0.060 \end{bmatrix} \end{aligned} \quad [\text{pF/m}]$$

instead. The augmented p.u.l. matrices write

$$\tilde{\mathbf{L}} = \begin{bmatrix} 1058.3 & 384.3 & 23.3 & 22.7 & 0.0 & -38.5 & -1.2 & -1.1 & 0.0 & -0.2 & 0.0 & 3.5 \\ 384.3 & 1058.3 & 22.7 & 23.3 & -38.5 & 0.0 & -1.1 & -1.2 & -0.2 & 0.0 & 3.5 & 0.0 \\ 23.3 & 22.7 & 1057.2 & 383.3 & 0.0 & -0.2 & 20.8 & 20.3 & 0.0 & -38.5 & 0.0 & 0.0 \\ 22.7 & 23.3 & 383.3 & 1057.2 & -0.2 & 0.0 & 20.3 & 20.8 & -38.5 & 0.0 & 0.0 & 0.0 \\ 0.0 & -38.5 & 0.0 & -0.2 & 1058.3 & 387.4 & 0.0 & 0.0 & 23.3 & 22.7 & 0.0 & -34.4 \\ -38.5 & 0.0 & -0.2 & 0.0 & 387.4 & 1058.3 & 0.0 & 0.0 & 22.7 & 23.3 & -34.4 & 0.0 \\ -1.2 & -1.1 & 20.8 & 20.3 & 0.0 & 0.0 & 1057.5 & 383.6 & 0.0 & -0.2 & 0.0 & 0.0 \\ -1.1 & -1.2 & 20.3 & 20.8 & 0.0 & 0.0 & 383.6 & 1057.5 & -0.2 & 0.0 & 0.0 & 0.0 \\ 0.0 & -0.2 & 0.0 & -38.5 & 23.3 & 22.7 & 0.0 & -0.2 & 1057.2 & 386.4 & 0.0 & -0.2 \\ -0.2 & 0.0 & -38.5 & 0.0 & 22.7 & 23.3 & -0.2 & 0.0 & 386.4 & 1057.2 & -0.2 & 0.0 \\ 0.0 & 3.5 & 0.0 & 0.0 & 0.0 & -34.4 & 0.0 & 0.0 & 0.0 & -0.2 & 1058.3 & 386.5 \\ 3.5 & 0.0 & 0.0 & 0.0 & -34.4 & 0.0 & 0.0 & 0.0 & -0.2 & 0.0 & 386.5 & 1058.3 \end{bmatrix} \quad (5.33)$$

[nH/m] and

$$\tilde{\mathbf{C}} = \begin{bmatrix} 12.14 & -4.42 & -0.13 & -0.12 & -0.38 & 0.58 & 0.00 & 0.00 & -0.01 & -0.00 & 0.06 & -0.07 \\ -4.42 & 12.14 & -0.12 & -0.13 & 0.58 & -0.38 & 0.00 & 0.00 & -0.00 & -0.01 & -0.07 & 0.06 \\ -0.13 & -0.12 & 12.14 & -4.42 & -0.01 & -0.00 & -0.12 & -0.10 & -0.38 & 0.58 & 0.00 & 0.00 \\ -0.12 & -0.13 & -4.42 & 12.14 & -0.00 & -0.01 & -0.10 & -0.12 & 0.58 & -0.38 & 0.00 & 0.00 \\ -0.38 & 0.58 & -0.01 & -0.00 & 12.20 & -4.49 & 0.00 & 0.00 & -0.13 & -0.12 & -0.34 & 0.52 \\ 0.58 & -0.38 & -0.00 & -0.01 & -4.49 & 12.20 & 0.00 & 0.00 & -0.12 & -0.13 & 0.52 & -0.34 \\ 0.00 & 0.00 & -0.12 & -0.10 & 0.00 & 0.00 & 12.14 & -4.42 & -0.01 & -0.00 & 0.00 & 0.00 \\ 0.00 & 0.00 & -0.10 & -0.12 & 0.00 & 0.00 & -4.42 & 12.14 & -0.00 & -0.01 & 0.00 & 0.00 \\ -0.01 & -0.00 & -0.38 & 0.58 & -0.13 & -0.12 & -0.01 & -0.00 & 12.20 & -4.49 & -0.01 & -0.00 \\ -0.00 & -0.01 & 0.58 & -0.38 & -0.12 & -0.13 & -0.00 & -0.01 & -4.49 & 12.20 & -0.00 & -0.01 \\ 0.06 & -0.07 & 0.00 & 0.00 & -0.34 & 0.52 & 0.00 & 0.00 & -0.01 & -0.00 & 12.18 & -4.47 \\ -0.07 & 0.06 & 0.00 & 0.00 & 0.52 & -0.34 & 0.00 & 0.00 & -0.00 & -0.01 & -4.47 & 12.18 \end{bmatrix} \quad (5.34)$$

[pF/m].

In this section we outlined, by means of tutorial examples, how to build the augmented, deterministic PC-based MTL models starting from the original, stochastic p.u.l. parameters. In the considered cases, $\tilde{\mathbf{Z}}(\omega) = j\omega\tilde{\mathbf{L}}$ and $\tilde{\mathbf{Y}}(\omega) = j\omega\tilde{\mathbf{C}}$. In the most general situation, in which the p.u.l. parameters are lossy and frequency-dependent, the projection and augmentation procedures must be iterated for every frequency point. However, thanks to Gaussian quadratures, the computational cost is limited. Upon interpretation of (5.12) as a classical (deterministic) transmission-line system, described by the new p.u.l. matrices $\tilde{\mathbf{Z}}$ and $\tilde{\mathbf{Y}}$, the general solution is readily given by (2.16), i.e.

$$\tilde{\Phi}(\mathcal{L}) = \expm \left(\begin{bmatrix} \mathbf{0} & -\tilde{\mathbf{Z}} \\ -\tilde{\mathbf{Y}} & \mathbf{0} \end{bmatrix} \mathcal{L} \right). \quad (5.35)$$

The last step in the development of the proposed methodology is to derive new, consistent terminal conditions for the complete solution of the augmented problem.

5.5 Augmented Terminal Conditions

The solution of the augmented transmission-line equations provides the sought-for coefficients for the unknown voltage and current variables to be used in (5.6). Nonetheless, the solution of transmission-line equations require to combine the general solution with terminal constraints. Therefore, proper terminal equations need to be derived.

5.5.1 Stochastic Terminations

We start from the most general case in which the line terminations are also random. By considering for the discussion a Thévenin representation, the equivalent voltage sources and termination impedances are also stochastic

$$\mathbf{V}(z = 0, \boldsymbol{\xi}) = \mathbf{V}_S(\boldsymbol{\xi}) - \mathbf{Z}_S(\boldsymbol{\xi})\mathbf{I}(z = 0, \boldsymbol{\xi}), \quad (5.36a)$$

$$\mathbf{V}(z = \mathcal{L}, \boldsymbol{\xi}) = \mathbf{V}_L(\boldsymbol{\xi}) + \mathbf{Z}_L(\boldsymbol{\xi})\mathbf{I}(z = \mathcal{L}, \boldsymbol{\xi}), \quad (5.36b)$$

and therefore expressible in terms of PC expansions. This leads to

$$\sum_{k=0}^P \mathbf{V}_k(0) \phi_k(\boldsymbol{\xi}) = \sum_{k=0}^P \mathbf{V}_{S,k} \phi_k(\boldsymbol{\xi}) - \sum_{k=0}^P \sum_{j=0}^P \mathbf{Z}_{S,k} \mathbf{I}_j(0) \phi_k(\boldsymbol{\xi}) \phi_j(\boldsymbol{\xi}), \quad (5.37a)$$

$$\sum_{k=0}^P \mathbf{V}_k(\mathcal{L}) \phi_k(\boldsymbol{\xi}) = \sum_{k=0}^P \mathbf{V}_{L,k} \phi_k(\boldsymbol{\xi}) + \sum_{k=0}^P \sum_{j=0}^P \mathbf{Z}_{L,k} \mathbf{I}_j(\mathcal{L}) \phi_k(\boldsymbol{\xi}) \phi_j(\boldsymbol{\xi}). \quad (5.37b)$$

Again, Galerkin projection, i.e.

$$\sum_{k=0}^P \mathbf{V}_k(0) \underbrace{\langle \phi_k, \phi_i \rangle}_{=0 \ \forall k \neq i} = \sum_{k=0}^P \mathbf{V}_{S,k} \underbrace{\langle \phi_k, \phi_i \rangle}_{=0 \ \forall k \neq i} - \sum_{k=0}^P \sum_{j=0}^P \mathbf{Z}_{S,k} \mathbf{I}_j(0) \langle \phi_k \phi_j, \phi_i \rangle, \quad (5.38a)$$

$$\sum_{k=0}^P \mathbf{V}_k(\mathcal{L}) \underbrace{\langle \phi_k, \phi_i \rangle}_{=0 \ \forall k \neq i} = \sum_{k=0}^P \mathbf{V}_{L,k} \underbrace{\langle \phi_k, \phi_i \rangle}_{=0 \ \forall k \neq i} + \sum_{k=0}^P \sum_{j=0}^P \mathbf{Z}_{L,k} \mathbf{I}_j(\mathcal{L}) \langle \phi_k \phi_j, \phi_i \rangle, \quad (5.38b)$$

is applied, thus yielding

$$\mathbf{V}_i(0) \langle \phi_i, \phi_i \rangle = \mathbf{V}_{S,i} \langle \phi_i, \phi_i \rangle - \sum_{k=0}^P \sum_{j=0}^P \mathbf{Z}_{S,k} \mathbf{I}_j(0) \langle \phi_k \phi_j, \phi_i \rangle, \quad (5.39a)$$

$$\mathbf{V}_i(\mathcal{L}) \langle \phi_i, \phi_i \rangle = \mathbf{V}_{L,i} \langle \phi_i, \phi_i \rangle + \sum_{k=0}^P \sum_{j=0}^P \mathbf{Z}_{L,k} \mathbf{I}_j(\mathcal{L}) \langle \phi_k \phi_j, \phi_i \rangle. \quad (5.39b)$$

for $i = 0, \dots, P$. In matrix form, the above equations become

$$\tilde{\mathbf{V}}(z = 0) = \tilde{\mathbf{V}}_S - \tilde{\mathbf{Z}}_S \tilde{\mathbf{I}}(z = 0), \quad (5.40a)$$

$$\tilde{\mathbf{V}}(z = \mathcal{L}) = \tilde{\mathbf{V}}_L + \tilde{\mathbf{Z}}_L \tilde{\mathbf{I}}(z = \mathcal{L}), \quad (5.40b)$$

where $\tilde{\mathbf{V}}_S = [\mathbf{V}_{S,0}, \dots, \mathbf{V}_{S,P}]^T$ collects the PC-expansion coefficients of the equivalent sources, whereas the entries of $\tilde{\mathbf{Z}}_S$ are obtained analogously to (5.13). Similar relations hold for $\tilde{\mathbf{V}}_L$ and $\tilde{\mathbf{Z}}_L$. Again, such augmented matrices are symmetric only after adoption of a normalized basis.

It relevant to here point out that, in general, the variations affecting the line are independent from those affecting its terminations, and therefore parameterized by different subsets of elements of $\boldsymbol{\xi}$. However, for consistency with the line voltages and currents, which are affected by all the random parameters, every expansion must be carried out according to the full random vector $\boldsymbol{\xi}$, and this may result in a sparse structure of the augmented matrices (cfr. the example in Section 5.6).

A similar procedure allows to obtain analogous expressions for the augmented terminal conditions given as Norton equivalents, i.e.

$$\tilde{\mathbf{I}}(z=0) = \tilde{\mathbf{I}}_S - \tilde{\mathbf{Y}}_S \tilde{\mathbf{V}}(z=0), \quad (5.41a)$$

$$\tilde{\mathbf{I}}(z=\mathcal{L}) = -\tilde{\mathbf{I}}_L + \tilde{\mathbf{Y}}_L \tilde{\mathbf{V}}(z=\mathcal{L}), \quad (5.41b)$$

where the structures of vectors $\tilde{\mathbf{I}}_{S,L}$ and matrices $\tilde{\mathbf{Y}}_{S,L}$ coincide with those in (5.40).

5.5.2 Deterministic Terminations

A specific, though relevant, case is the one in which the terminal constraints are deterministic, i.e. the equivalent voltage sources and termination impedances do not vary. It should be noted that, although the terminations are not random, terminal voltages and currents are still stochastic due to the variability affecting the line. Given that non-stochastic quantities can be represented as a zero-order expansion, the structure of (5.40) greatly simplifies, leading to

$$\tilde{\mathbf{V}}_{S,L} = [\mathbf{V}_{S,L}, 0, \dots, 0]^T, \quad (5.42a)$$

$$\tilde{\mathbf{Z}}_{S,L} = \text{blkdiag}([\mathbf{Z}_{S,L}, \dots, \mathbf{Z}_{S,L}]), \quad (5.42b)$$

where `blkdiag` operator denotes the block diagonal concatenation of matrix input arguments. Of course, a similar reasoning yields

$$\tilde{\mathbf{I}}_{S,L} = [\mathbf{I}_{S,L}, 0, \dots, 0]^T, \quad (5.43a)$$

$$\tilde{\mathbf{Y}}_{S,L} = \text{blkdiag}([\mathbf{Y}_{S,L}, \dots, \mathbf{Y}_{S,L}]). \quad (5.43b)$$

With the introduced terminal conditions, the solution of the augmented transmission-line problem (5.12) is carried out as a standard, deterministic analysis of a MTL (cfr. Section 2.2) described by larger p.u.l. matrices.

5.6 Polynomial Chaos-Based Stochastic Simulation

We now have all the ingredients to perform a full stochastic simulation of random transmission-line structures without resorting to the time-consuming MC method. For example, the augmented p.u.l. inductance and capacitance matrix for the single transmission line of Fig. 2.2, in presence of Gaussian variations in the height above ground, were given in (5.26) and (5.27), respectively. Due

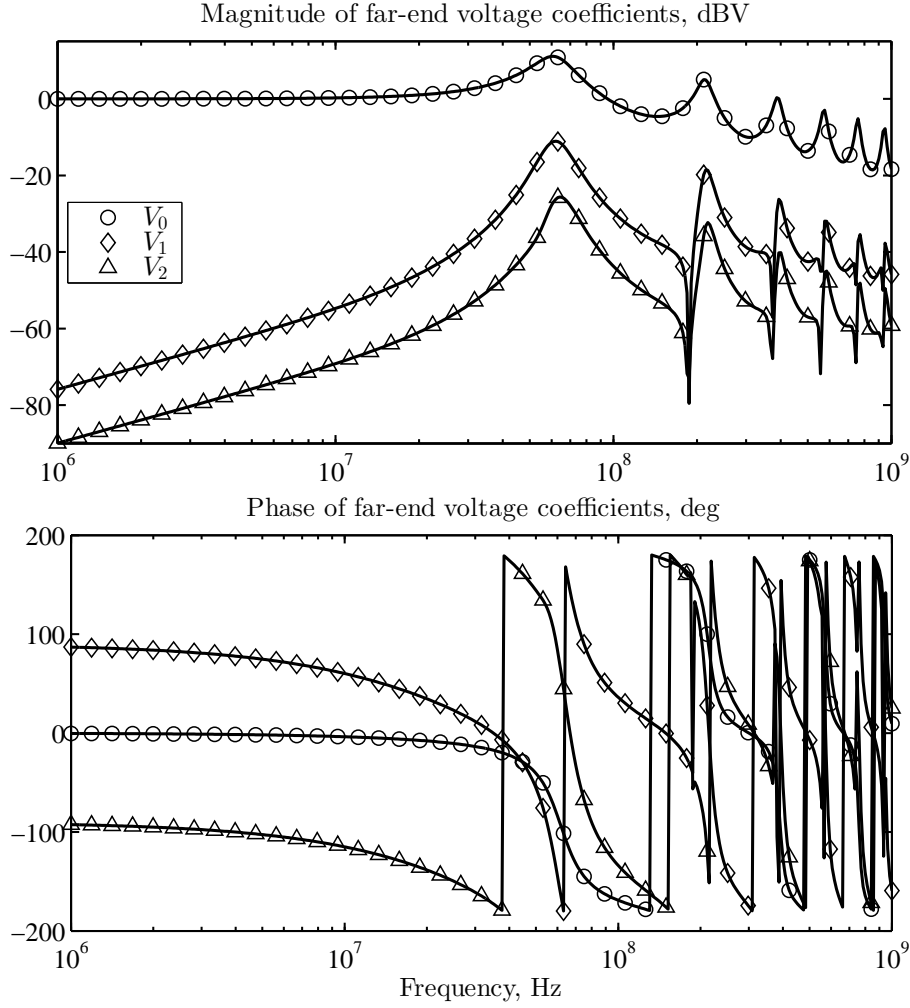


Figure 5.3. PC-expansion coefficients for the far-end transmitted voltage. Circles (\circ): V_0 ; diamonds (\diamond): V_1 ; triangles (\triangle): V_2 .

to the deterministic nature of the source and load, the augmented terminal conditions in the mixed representation are

$$\mathbf{V}_S = \begin{bmatrix} E \\ 0 \\ 0 \end{bmatrix}, \quad \mathbf{Z}_S = \begin{bmatrix} R_S & 0 & 0 \\ 0 & R_S & 0 \\ 0 & 0 & R_S \end{bmatrix}, \quad (5.44)$$

$$\mathbf{I}_L = \begin{bmatrix} 0 \\ 0 \\ 0 \end{bmatrix}, \quad \mathbf{Y}_L = j\omega \begin{bmatrix} C_L & 0 & 0 \\ 0 & C_L & 0 \\ 0 & 0 & C_L \end{bmatrix},$$

The combination of the CPM, computed via (5.35), with the above constraints allows to compute the PC-expansion coefficients for the terminal voltages and currents. Fig. 5.3 shows the three

coefficients for the voltage at the far-end termination $z = \mathcal{L} = 80$ cm, namely $V_0(\mathcal{L})$, $V_1(\mathcal{L})$ and $V_2(\mathcal{L})$. These coefficients define an explicit relation between the stochastic terminal voltage and the random input parameters in terms of a second-order expansion of normalized Hermite polynomials:

$$V(\mathcal{L}, \omega, \xi) \approx V_0(\mathcal{L}, \omega) \cdot 1 + V_1(\mathcal{L}, \omega) \cdot \xi + V_2(\mathcal{L}, \omega) \cdot (\xi^2 - 1)/\sqrt{2}. \quad (5.45)$$

A MC sampling of (5.45) allows to quickly extract the average value, standard deviation and probability distribution for the magnitude and phase of the far-end voltage, like shown in Section 3.2. This is fast thanks to the analyticity of (5.45). Furthermore, the time required by this post-processing step is independent from the complexity of the original problem. It is relevant to note that the computation of the magnitude and phase of (5.45) introduces a transformation which does not permit to use relations (4.10) and (4.11) to determine the average value and standard deviation of (5.45). Fig. 5.4 compares the average response and standard deviation obtained from the PC expansion (indicated with markers) with those previously computed by means of the MC analysis (solid lines) and already shown in Fig. 3.4. The comparison reveals excellent agreement between the two approaches. The time required to compute the solution of the augmented line over the entire frequency sweep is 0.1 s. For the estimation of the average response and standard deviation, the PC expansion (5.45) has been sampled 10000 times and this step took 0.2 s. Compared to the MC analysis, which required 5 min and 6 s, there is a $1020\times$ speed-up.

Finally, Fig. 5.5 compares the PDFs at 60 MHz, obtained after the MC analysis (see Fig. 3.5), with those extracted from the PC expansion. In order to obtain a smooth function, the PC expansion has been sampled 10^7 times and the outcomes have been collected into 200 bins. This evaluation only took 1.6 s. Nonetheless, a more accurate prediction is achieved. In conclusion to this first example, we can state that a second-order PC expansion is already accurate enough to reproduce the statistical behavior of the far-end voltage, nevertheless yielding a large speed-up in computational time.

The second example was that of the coupled line in Fig. 2.4, with uniform variations in the height above ground and wire-to-wire separation. The pertinent PC-augmented p.u.l. parameters are given in (5.33) and (5.34). Also for this case, to perform the PC-based simulation, we need the augmented terminal conditions, which assume a diagonal 12×12 structure due to the deterministic nature of the terminations. Fig. 5.6 reports the comparison on the estimation of the average and standard deviation of the near- and far-end crosstalk voltages (in Fig. 3.7), revealing again excellent agreement. For the PC simulation, the expansions have been sampled 10000 times. The computation of the PC coefficients in the entire frequency range required 0.3 s, whereas the sampling for the extraction of the statistical parameters required 0.5 s. The speed-up with respect to the MC analysis, which took 12 min and 12 s, is thus $915\times$. Fig. 5.7 displays the PDFs extracted from the PC expansions, which match very well with those in Fig. 3.5, obtained from the MC analysis. It is again possible to appreciate the smoother reproduction, made possible by the PC approach, of distribution functions, which often differ greatly from the distribution of the random input parameters (see the right panel).

The last example is the simulation of the single line with variations in both the height above ground and load capacitance. In addition to the random variable parameterizing the height variation, now denoted with ξ_1 , we introduce another random variable ξ_2 , associated to the uncertainty

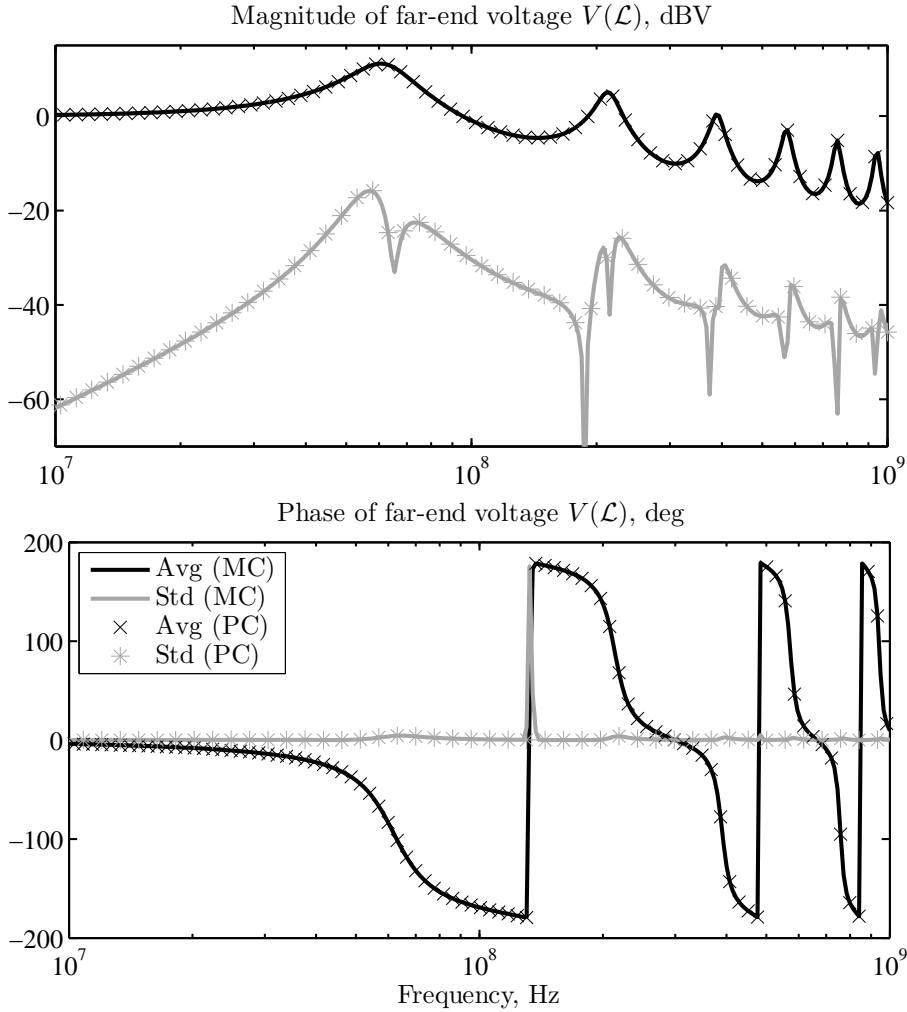


Figure 5.4. Comparison between the statistical information obtained by means of PC expansions (denoted with crosses \times and asterisks $*$) and MC (solid lines). Black curves: average response; gray curves: standard deviation.

of the load capacitance. Since the cross-sectional characteristics are not affected by the variations of the load, i.e. they do not depend on ξ_2 , we can re-use for the expansions of the p.u.l. parameters the coefficients computed in the previous example. However, we have to keep in mind that, for a consistent representation, all the PC expansions must now include the new random variable as well. For instance, the expansion of the p.u.l. inductance becomes a bivariate series of normalized Hermite polynomials:

$$L(\boldsymbol{\xi}) \approx L_0 \cdot 1 + L_1 \cdot \xi_1 + L_2 \cdot \xi_2 + L_3 \cdot \frac{1}{\sqrt{2}}(\xi_1^2 - 1) + L_4 \cdot \xi_1 \xi_2 + L_5 \cdot \frac{1}{\sqrt{2}}(\xi_2^2 - 1), \quad (5.46)$$

where $L_0 = 1055.4$ nH/m, $L_1 = 41.7$ nH/m and $L_3 = -6.0$ nH/m, whilst L_2 , L_4 and L_5 are

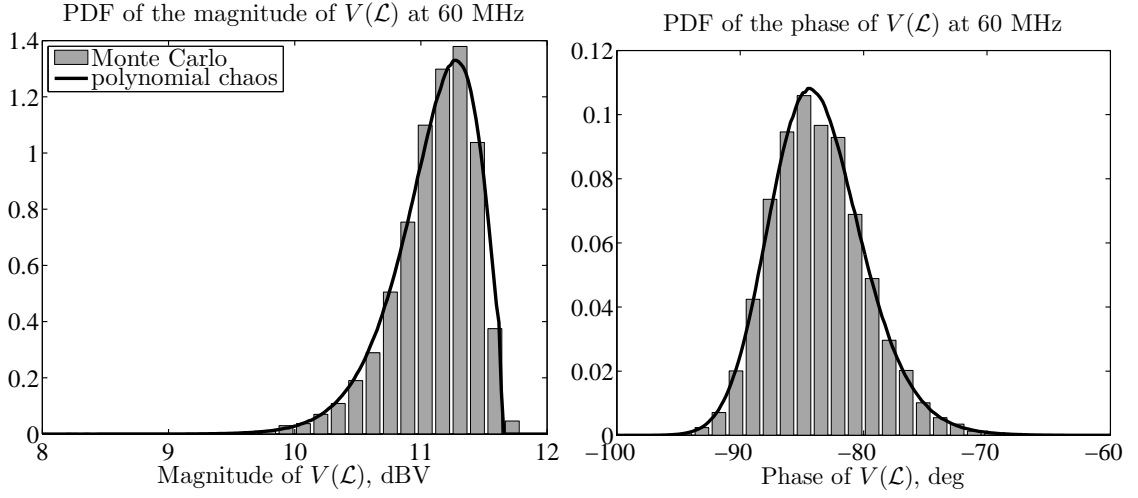


Figure 5.5. Comparison between the probability density functions of the magnitude and phase of $V(\mathcal{L})$, computed at 60 MHz by means of MC simulations and PC.

null because they are related to the load variable ξ_2 . A similar expression holds for the p.u.l. capacitance expansion, with $C_0 = 10.560$ pF/m, $C_1 = -0.426$ pF/m and $C_3 = 0.084$ pF/m. As to the load admittance, the expansion is merely

$$Y_L(\boldsymbol{\xi}) = j\omega C_L(\boldsymbol{\xi}) = j\omega C_L(1 + 0.1\xi_2). \quad (5.47)$$

Thence, $C_{L,0} = j\omega \cdot 5 \times 10^{-12} \Omega$, $C_{L,2} = j\omega \cdot 0.5 \times 10^{-12} \Omega$, and the remaining terms are null because related to ξ_1 , i.e. to the cross-sectional variation. The corresponding augmented matrices are

$$\tilde{\mathbf{L}} = \begin{bmatrix} 1055.4 & 41.7 & 0.0 & -6.0 & 0.0 & 0.0 \\ 41.7 & 1046.9 & 0.0 & 59.0 & 0.0 & 0.0 \\ 0.0 & 0.0 & 1055.4 & 0.0 & 41.7 & 0.0 \\ -6.0 & 59.0 & 0.0 & 1038.3 & 0.0 & 0.0 \\ 0.0 & 0.0 & 41.7 & 0.0 & 1046.9 & 0.0 \\ 0.0 & 0.0 & 0.0 & 0.0 & 0.0 & 1055.4 \end{bmatrix} \text{ nH/m}, \quad (5.48)$$

$$\tilde{\mathbf{C}} = \begin{bmatrix} 10.560 & -0.426 & 0.0 & 0.084 & 0.0 & 0.0 \\ -0.426 & 10.679 & 0.0 & -0.602 & 0.0 & 0.0 \\ 0.0 & 0.0 & 10.560 & 0.0 & -0.426 & 0.0 \\ 0.084 & -0.602 & 0.0 & 10.798 & 0.0 & 0.0 \\ 0.0 & 0.0 & -0.426 & 0.0 & 10.679 & 0.0 \\ 0.0 & 0.0 & 0.0 & 0.0 & 0.0 & 10.560 \end{bmatrix} \text{ pF/m}, \quad (5.49)$$

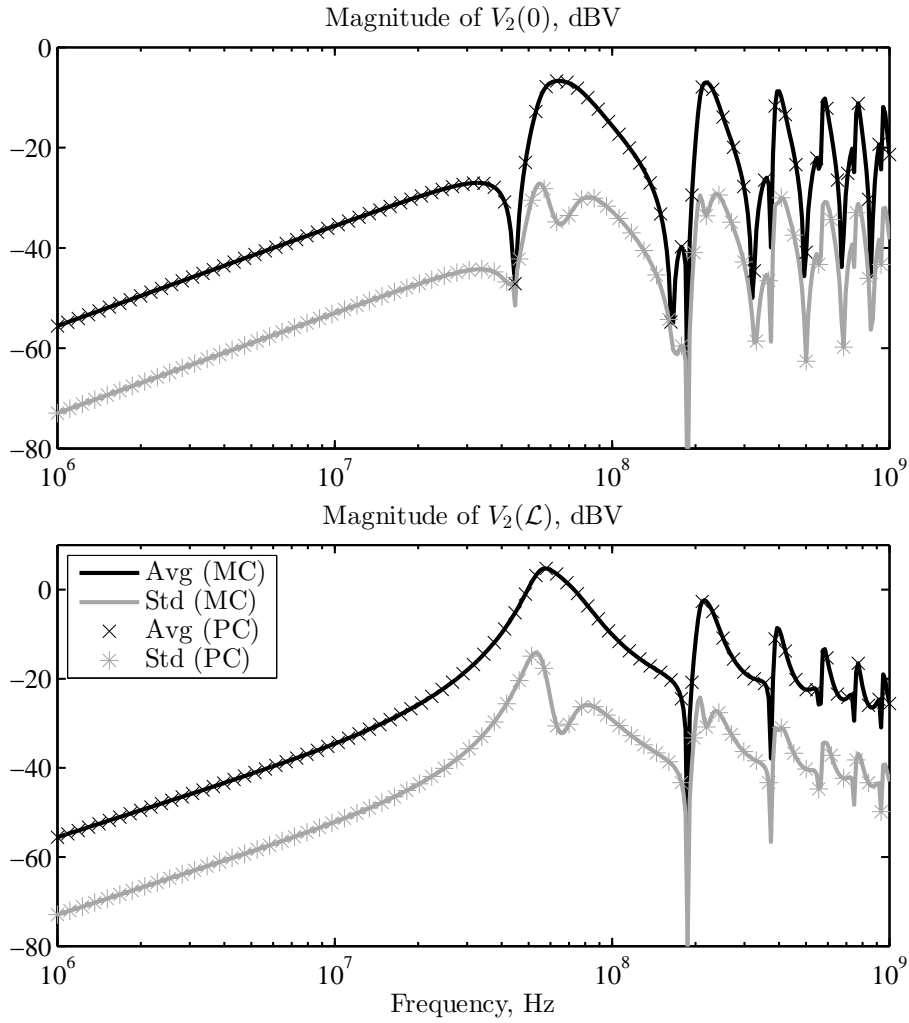


Figure 5.6. Comparison between the statistical information obtained by means of PC expansions (denoted with crosses \times and asterisks $*$) and MC (solid lines). Black curves: average response; gray curves: standard deviation.

and

$$\tilde{\mathbf{Y}}_L = j\omega \begin{bmatrix} 5.0 & 0.5 & 0 & 0 & 0 & 0 \\ 0 & 5.0 & 0 & 0 & 0.5 & 0 \\ 0.5 & 0 & 5.0 & 0 & 0 & \sqrt{2}/2 \\ 0 & 0 & 0 & 5.0 & 0 & 0 \\ 0 & 0.5 & 0 & 0 & 5.0 & 0 \\ 0 & 0 & \sqrt{2}/2 & 0 & 0 & 5.0 \end{bmatrix} \times 10^{-12} \Omega. \quad (5.50)$$

The above augmented matrices have a sparse structure because their stochastic counterparts only depend on one of the two random variables. Finally, the augmented impedance matrix for the

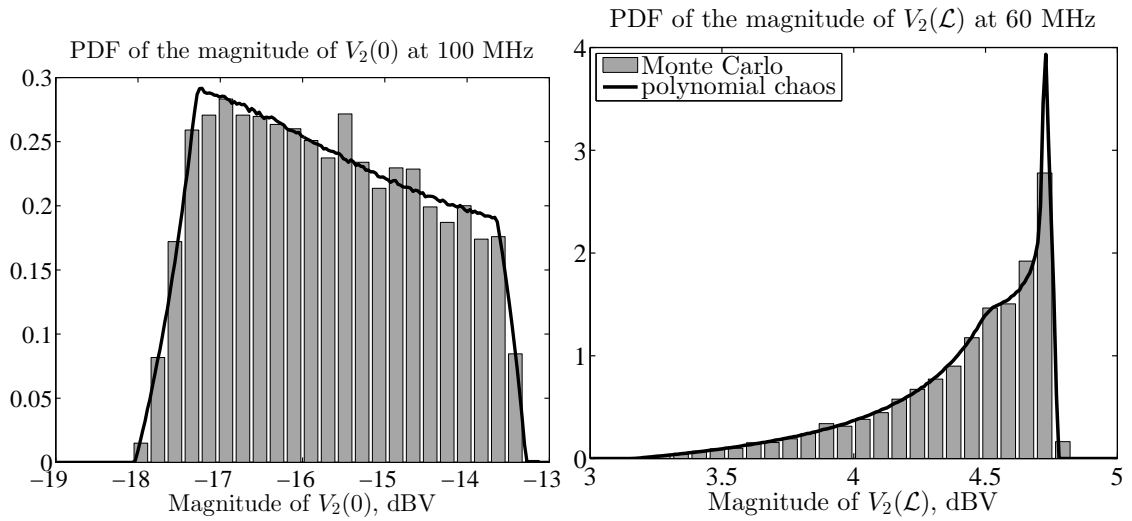


Figure 5.7. Comparison between the probability density functions of the magnitudes of $V_0(0)$ and $V_2(L)$ computed at 100 MHz and 60 MHz, respectively, by means of MC simulations and PC.

near-end termination is diagonal due to the absence of variability in the source resistance.

Fig. 5.8 reports the comparison of the statistical information pertinent to the stochastic response of this line configuration, computed by means of 10000 MC simulations and the PC approach. The left panel shows the average (in black) and standard deviation (in gray) of the magnitude of the far-end voltage. The solid lines are the result of the MC analysis, while the superposed markers indicate the same statistical information obtained from the PC expansions. The right panel compares the PDF computed at 60 MHz instead. The gray bars illustrate the distribution of the samples of the MC simulation, whereas the solid black line is the probability function extracted from the magnitude of the PC expansion of the far-end voltage.

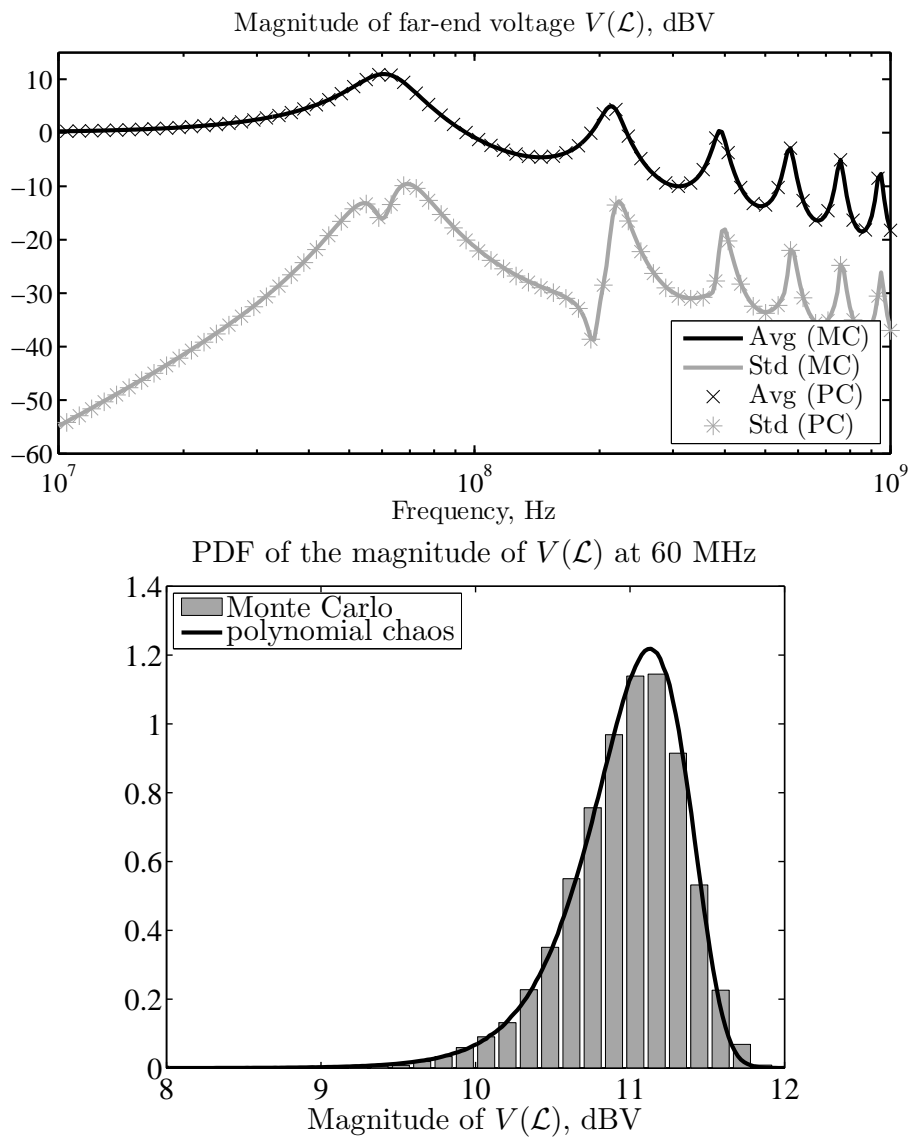


Figure 5.8. Comparison between MC and PC simulations. Top panel: average value (in black) and standard deviation (in gray) of the magnitude of the far-end voltage computed by means of 10000 MC runs (solid lines) and PC (markers). Bottom panel: probability density function of the far-end voltage at 60 MHz, computed via MC analysis (gray bars) and PC (black line).

Chapter 6

Applications

For the sake of a better understanding, the application of PC to the stochastic analysis of MTLs has been introduced by means of basic and tutorial examples. More realistic and meaningful application examples are provided in this chapter, in which the PC technique is applied to the analysis of cable bundles and PCB lines. Also, time-domain computations are presented, based on Fourier analysis. The proposed examples consist of a revised and more comprehensive discussion of published results.

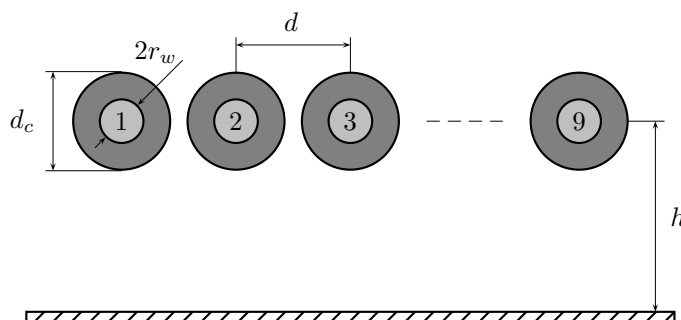


Figure 6.1. Cross-section of a commercial flex cable lying above a ground plane.

6.1 Example #1 — Flex Cable

We consider first the stochastic analysis of the commercial 3MTM .050" High Flex Life Cable (28 AWG stranded), shown in Fig. 6.1 in a standard 9-wire configuration and lying at a height of $h = 8$ cm above a perfectly-conducting ground plane. The wire radius is $r_w = 7.5$ mils and the dielectric coating is made by polyvinyl chloride (PVC), with relative permittivity of 3.5. A cable length of 80 cm is assumed. According to the vendor's datasheet, the tolerances on the wire-to-wire distance and dielectric coating diameter result in the above geometric variables to lie in the ranges $d \in [48, 50]$ mils and $d_c \in [32, 38]$ mils, respectively. Therefore, such parameters are considered as two independent uniform random variables inside those ranges. For the computation of

the p.u.l. parameters of such an inhomogeneous line, there are no closed-form formulas available. A numerical routine, based on the application of the method of moments (MoM) to cylindrical geometries, is then used [54]. As far as the terminal conditions are concerned, conductor #4 is energized by a 1-V voltage source with a 50Ω resistance, whilst the other conductors are kept in a low state by 50Ω resistors. The far-end terminations are loaded with 10 pF capacitors.

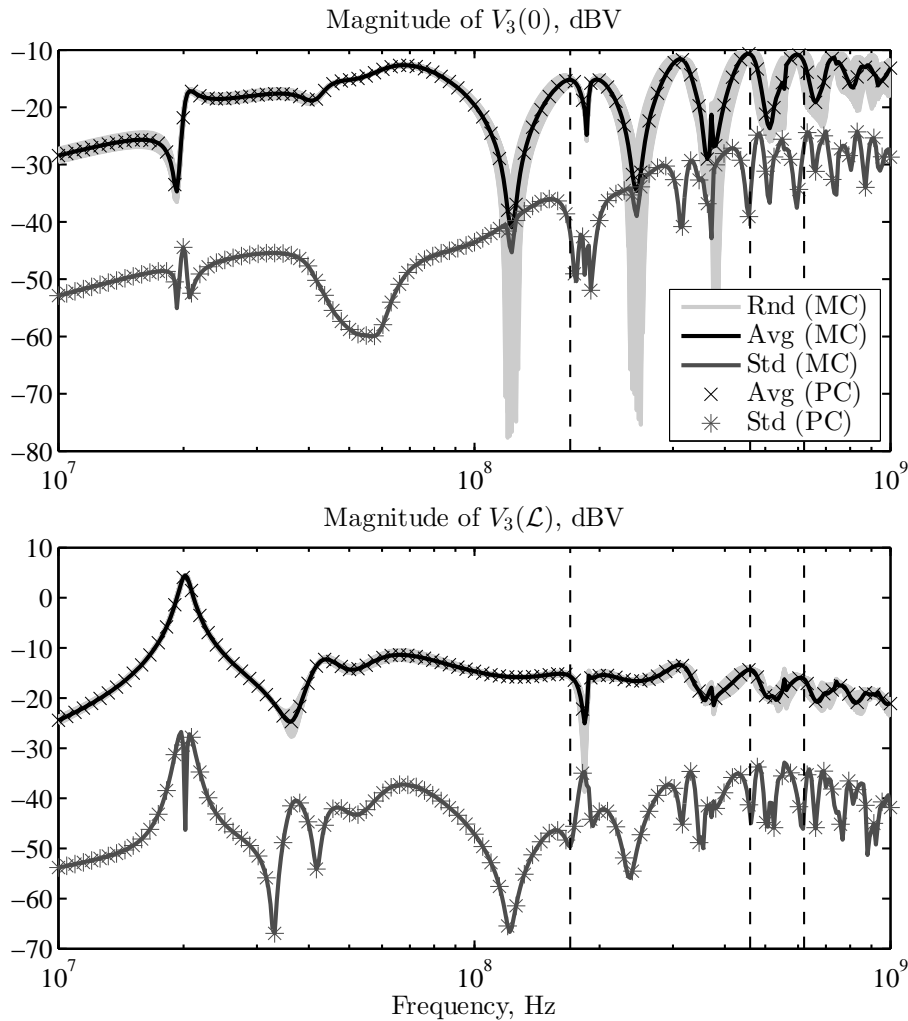


Figure 6.2. Stochastic simulation of the 9-wire flex cable of Fig. 6.1: magnitude of near-end (top panel) and far-end (bottom panel) crosstalk voltages. Light gray lines: samples from MC simulation; black and dark gray lines: average response and standard deviation computed by means of 10000 MC simulations. Markers (crosses \times and asterisks $*$) denote the same statistical information obtained from third-order PC expansions.

Fig. 6.2 shows the stochastic simulation of the near-end (left panel) and far-end (right panel) crosstalk voltages on conductor #3, namely $V_3(0)$ and $V_3(L)$, respectively, from 1 MHz to 1 GHz. The light gray lines are a subset of samples from the MC simulation, whereas the black and dark

gray lines are the average responses and the standard deviations, obtained after 10000 MC runs. Furthermore, the markers (asterisks) indicate the same quantities estimated from a third-order PC simulation and are in very good agreement. Fig. 6.3 displays the PDFs computed at three different frequencies, indicated by the dashed vertical lines in Fig. 6.2, with both the PC and MC methods. In this case, in order to better compare the two approaches, an equal number of 10000 random values is used to sample the PC expansions, and the results are collected into the same bins.

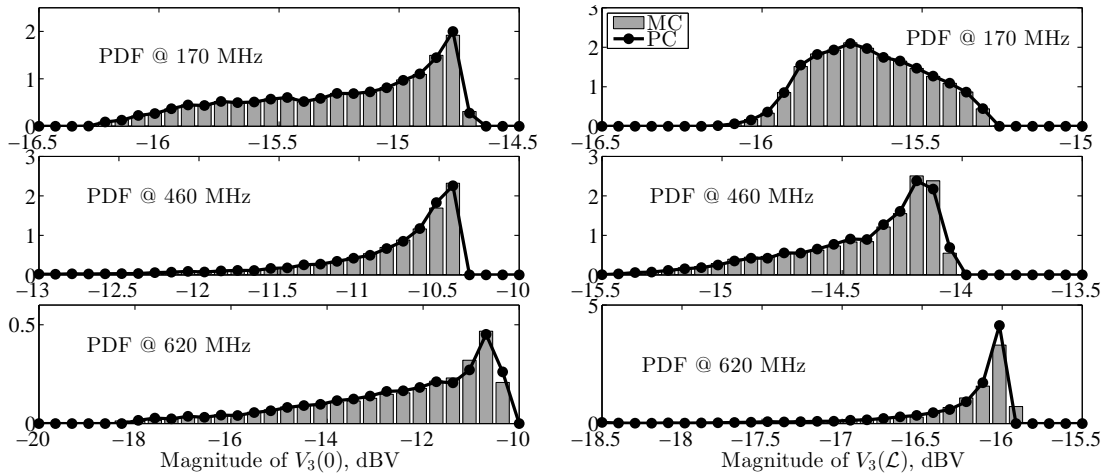


Figure 6.3. Probability density functions of the magnitudes of the near- and far-end crosstalk voltages, computed at three different frequencies by means of both MC simulations (gray bars) and PC expansions (dotted black lines).

As far as the simulation times are concerned, the MC analysis required 27 min 57 s, while the PC solution of the augmented transmission-line equations took 9.6 s. The computation of the PC expansions of the p.u.l. parameters and the creation of the corresponding augmented matrices took only 0.9 s. Finally, the evaluation of the statistical information required 1.7 s. The achieved speed-up is thence about $130\times$. This application example confirms the strength, efficiency and accuracy of the proposed technique.

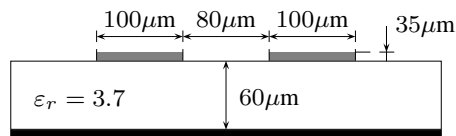


Figure 6.4. Cross-section of the coupled microstrip line.

6.2 Example #2 — Microstrip Line with Temperature Variations

Fig. 6.4 shows the cross-section of a microstrip line with two coupled traces. This is a common configuration for on-board lines. We consider a source resistance of 25Ω , a load capacitance

of 10 pF, and a line length of 5 cm. In this case, such values are referred to a temperature of $T_{\text{ref}} = 25^\circ\text{C}$. In order to analyze the effects of possible fluctuations in the operating temperature, we consider a uniform temperature variation in the range $[0, 125]^\circ\text{C}$. A temperature coefficient of $\alpha_R = \alpha_C = 200 \text{ ppm}/^\circ\text{C}$ is considered for the source resistors and load capacitors, whereas a coefficient of $\alpha_\epsilon = 500 \text{ ppm}/^\circ\text{C}$ is considered for the substrate permittivity. Hence, the above parameters can be expressed in terms of a normalized uniform random variable ξ_1 , which parameterizes temperature variations, as follows

$$\begin{cases} R_S = R_S|_{T_{\text{ref}}}[1 + \alpha_R(\bar{T} + \Delta T\xi_1 - T_{\text{ref}})], \\ C_L = C_L|_{T_{\text{ref}}}[1 + \alpha_C(\bar{T} + \Delta T\xi_1 - T_{\text{ref}})], \\ \epsilon_r = \epsilon_r|_{T_{\text{ref}}}[1 + \alpha_\epsilon(\bar{T} + \Delta T\xi_1 - T_{\text{ref}})], \end{cases} \quad (6.1)$$

where $\bar{T} = \Delta T = 62.5^\circ\text{C}$ are the average temperature and its semi-interval of variation. Moreover, an additional, statistically independent uncertainty, due to the manufacturing process, is ascribed to the nominal permittivity at the reference temperature, which is then supposed to lie in the range $[3.5, 4]$. The complete parametrization of the relative permittivity is thence

$$\epsilon_r = (\bar{\epsilon}_r + \Delta\epsilon_r\xi_2)[1 + \alpha_\epsilon(\bar{T} + \Delta T\xi_1 - T_{\text{ref}})], \quad (6.2)$$

with $\bar{\epsilon}_r = 3.75$, $\Delta\epsilon_r = 0.25$, and where ξ_2 parameterizes the process variations.

Fig. 6.5 collects the results of a stochastic simulation of this structure, in which one conductor is excited by 1-V source whilst the adjacent conductor is kept quiet. The left panel shows the voltage transmitted to the far-end side of the active conductor, $V_1(\mathcal{L})$, whereas the right panel shows the far-end crosstalk on the neighboring line, $V_2(\mathcal{L})$. Again, the statistical information obtained via MC simulations (solid black and dark gray lines) is compared with the approximations given by the PC expansions of the terminal voltages (markers). PC expansions of order four are used in this case. Like in the previous example, the PDFs at different frequencies are computed both with MC and PC and are shown in Fig. 6.6, again revealing excellent agreement. The computational time is here 11 min 34 s for the MC analysis and 5.3 s for the PC simulation, including the time required for the expansion (0.2 s) and augmentation (1.9 s) of the p.u.l. parameters, as well as the post-processing evaluation (0.2 s) of the expansions. The p.u.l. parameters of the coupled microstrip line are computed by means of empirical formulas available in [83]–[85]. The speed-up for this example is thence $130\times$.

6.3 Example #3 — Transient Analysis of a Microstrip Line

We next consider a time-domain, transient analysis of the coupled microstrip line of Fig. 6.4, where now the loads are deterministic and equal to 50Ω (near end) and 10 pF (far end). The voltage generator has a Gaussian waveform with a peak amplitude of 1 V and a width of about 0.35 ns at half amplitude. The variability is here provided by the trace separation and the substrate permittivity, assumed as two independent Gaussian random variables with a 10% relative standard deviation. As anticipated in Chapter 2, it is possible to compute time-domain results via Fourier analysis. The procedure amounts to the following steps:

1. Compute the frequency components of the time-domain waveform via Fourier transform.

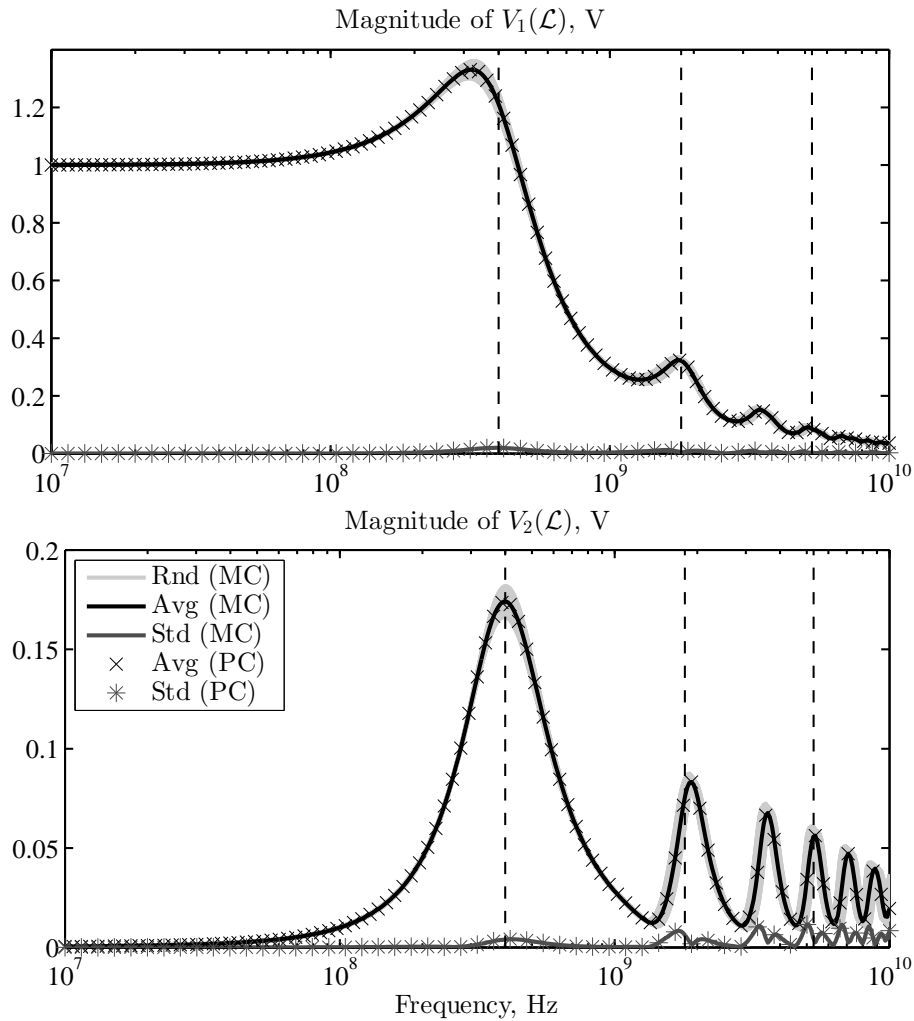


Figure 6.5. Stochastic simulation of the coupled microstrip line of Fig. 6.4 in presence of temperature and process variations: magnitude of transmitted voltage (top panel) and of the crosstalk voltage (bottom panel). Light gray lines: samples from MC simulation; black and dark gray lines: average response and standard deviation computed via 10000 MC simulations. For comparison, the markers (crosses \times and asterisks $*$) denote the same statistical information obtained from fourth-order PC expansions.

2. Use such components as phasor values of the voltage source for a frequency-domain analysis, thus obtaining the frequency components of the output waveform.
3. Retrieve the output time-domain waveform through inverse Fourier transform.

We recall here that the Fourier transform of a waveform $x(t)$ is defined as

$$X(\omega) = \mathcal{F}\{x(t)\} = \int_{-\infty}^{+\infty} x(t)e^{-j\omega t} dt, \quad (6.3)$$

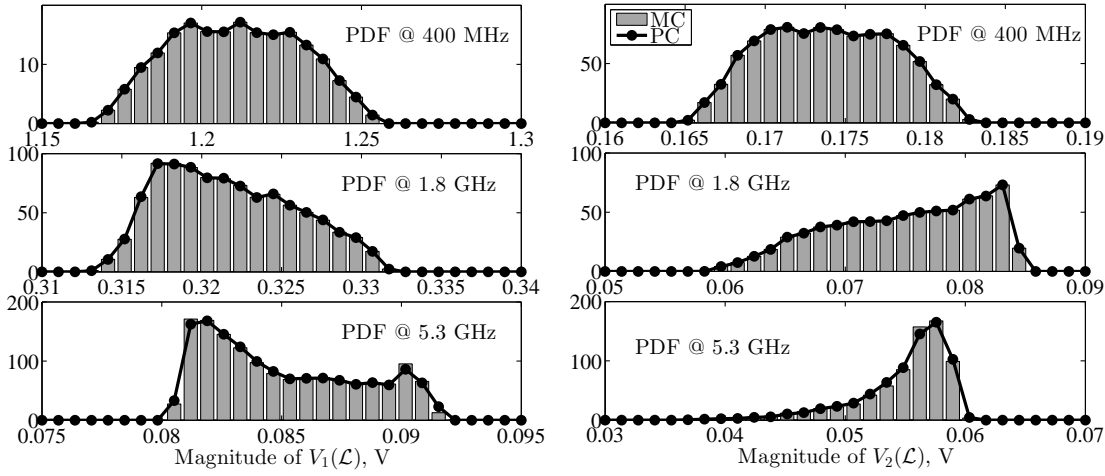


Figure 6.6. Probability density functions of the magnitudes of far-end voltages, computed at three different frequencies by means of both MC simulations (gray bars) and PC expansions (dotted black lines).

whereas the inverse Fourier transform is simply

$$x(t) = \mathcal{F}^{-1}\{X(\omega)\} = \frac{1}{2\pi} \int_{-\infty}^{+\infty} X(\omega) e^{j\omega t} d\omega. \quad (6.4)$$

The quantity $X(\omega)$ is referred to as the spectrum of the signal $x(t)$.

The aforementioned Gaussian voltage waveform can be analytically expressed as

$$x(t) = e^{-\frac{(t-t_0)^2}{2\zeta^2}}, \quad (6.5)$$

where $\zeta = 0.15$ ns plays the role of “standard deviation” and parameterizes the pulse width, whilst t_0 is a delay factor indicating the time at which the pulse reaches its maximum. A delay of $t_0 = 1$ ns is assumed here. The Fourier transform of a Gaussian function is analytically available, and is a Gaussian itself with inverse “variance” $1/\zeta^2$, while the delay factor merely corresponds to a phase shift. More precisely, the spectrum of the voltage source is

$$X(\omega) = \zeta \sqrt{2\pi} e^{-\frac{\omega^2 \zeta^2}{2}} e^{-j\omega t_0}. \quad (6.6)$$

For the practical simulation, waveforms need to be discretized into a finite number of time and frequency points. Suppose we want to observe the line response up to $T_{\max} = 10$ ns, evaluated at $N_t + 1 = 1001$ time points. The Fourier transform then becomes a discrete Fourier transform, and this also implies that the waveform is treated as periodic with period equal to T_{\max} . Therefore, in order to avoid aliasing in the Fourier analysis, the observation time T_{\max} must be large enough to allow all the responses to decay to zero. The number of frequency points to simulate is equal to the

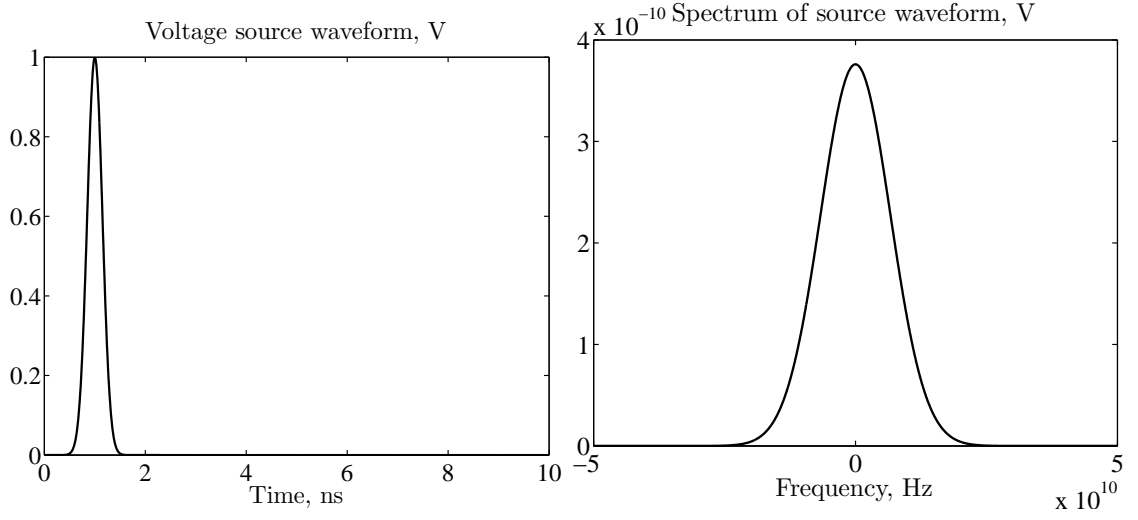


Figure 6.7. Gaussian voltage pulse: Time-domain waveform (left panel) and magnitude of its spectrum (right-panel).

number of time points, i.e. $N_t + 1$. According to the reverse interpretation of the Nyquist-Shannon theorem, the maximum frequency to be considered is

$$f_{\max} = \frac{N_t}{2T_{\max}} = \frac{1}{2\Delta t} \quad (6.7)$$

and is thence 50 GHz, whereas the spacing between the points is

$$\Delta f = \frac{1}{T_{\max}}. \quad (6.8)$$

Fig. 6.7 displays both $x(t)$ (left panel) and the magnitude of its spectrum $X(\omega)$ (right panel). It should be noted that also negative frequencies must be considered in the analysis.

It is now possible to perform a transient simulation of the near- and far-end crosstalk voltages. We need to evaluate the frequency-domain solution at a total of $N_t + 1$ frequency points: N_t negative frequencies down to $-f_{\max}$, N_t positive frequencies up to f_{\max} , plus the DC solution for $f = 0$. Expression (6.6) provides the values of the phasor voltage source at a given frequency, and the spectra of the crosstalk voltages is given by the corresponding frequency-domain solutions. Alternatively, thanks to the properties of linear time-invariant systems, the spectrum of an output waveform is obtainable as

$$X_{\text{out}}(\omega) = H(\omega) \cdot X(\omega), \quad (6.9)$$

where $H(\omega)$ is the frequency-domain response computed by considering a constant 1-V source. This property is useful when different excitation signals are considered. Also, an actual computation of the response for negative frequencies is not needed, thanks to the property

$$H(-\omega) = H^*(\omega), \quad (6.10)$$

where operator $*$ denotes the complex conjugate. Finally, the DC solution for $f = 0$ is not obtainable from the classical solution of the telegrapher's equations. Nonetheless, it is easy to show with an analysis of the DC circuit, where the line conductors are replaced by short circuits and the load capacitors are open circuits, that the DC components of crosstalk voltages are null. Once the spectra of the output crosstalk voltages are known, the time-domain waveforms are calculated with the `IFFT` function, available in MATLAB for the calculation of the inverse Fourier transform.

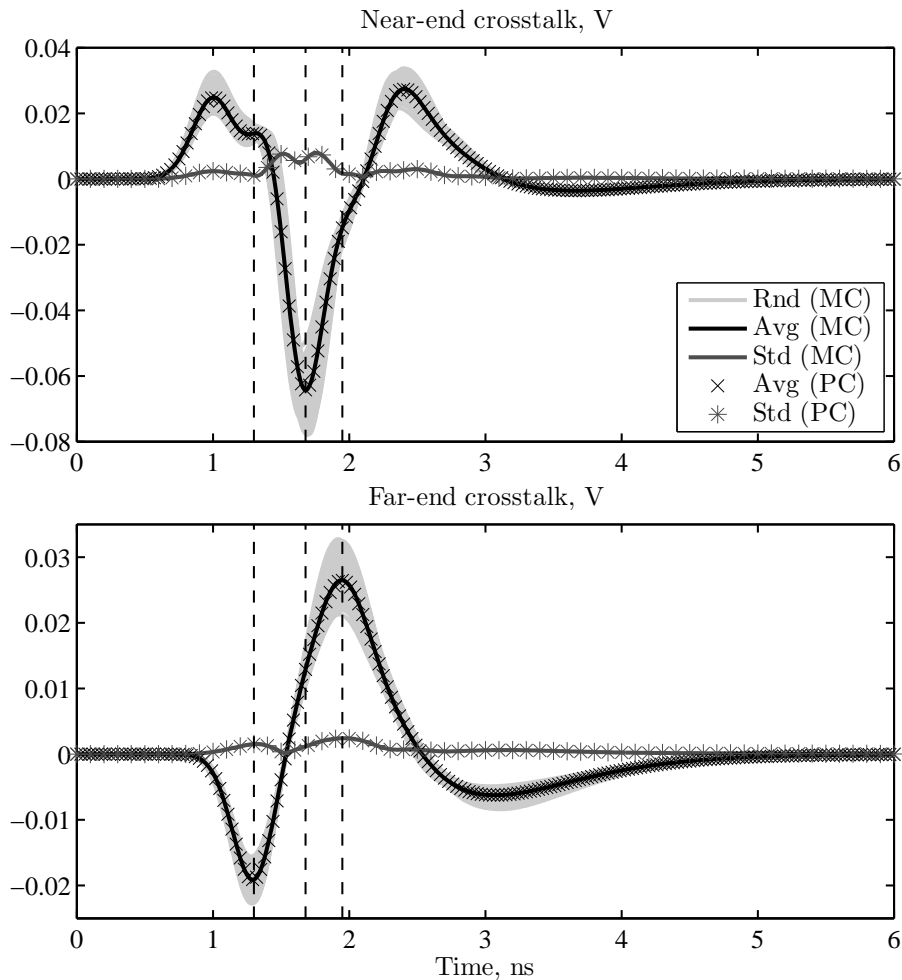


Figure 6.8. Stochastic simulation of the transient near-end (top panel) and far-end (bottom panel) crosstalk voltages on the coupled microstrip line of Fig. 6.4. Light gray lines: spread in the response due to process variability; black and dark gray lines: average responses and standard deviations computed via MC simulations. The markers (crosses \times and asterisks $*$) display the same information obtained via second-order PC expansions.

As to the PC simulation, a single frequency-domain solution of the corresponding augmented line allows to obtain the spectra of the PC-expansion coefficients [86]. The time-domain coeffi-

cients are then computed again via inverse Fourier transform. It is relevant to point out that, thanks to the linearity of the Fourier transform, the structure of the PC expansions is preserved also in time domain:

$$v(t, \boldsymbol{\xi}) = \frac{1}{2\pi} \int_{-\infty}^{\infty} V(\omega, \boldsymbol{\xi}) e^{j\omega t} d\omega \approx \frac{1}{2\pi} \int_{-\infty}^{\infty} \sum_{k=0}^P V_k(\omega) \phi_k(\boldsymbol{\xi}) e^{j\omega t} d\omega = \sum_{k=0}^P \left(\frac{1}{2\pi} \int_{-\infty}^{\infty} V_k(\omega) e^{j\omega t} d\omega \right) \phi_k(\boldsymbol{\xi}) = \sum_{k=0}^P v_k(t) \phi_k(\boldsymbol{\xi}). \quad (6.11)$$

Fig. 6.8 shows the near- and far-end time-domain crosstalk voltages. The light gray lines are once again a subset of samples from the MC simulation. The solid black and dark gray lines are the average response and the standard deviation estimated from 10000 MC runs. For comparison, the asterisks indicate the same quantities provided by the PC simulation. In this case, relations (4.10) and (4.11) can be used to readily obtain this statistical information. The above comparison demonstrates how the accuracy of PC is preserved when considering transient analyses as well. Finally, Fig. 6.9 shows the PDFs computed at different time points with both MC and PC, showing excellent agreement as well. The simulation times are 14 min and 3.3 s for the MC and PC analyses, respectively, thus yielding a speed-up of $250\times$.

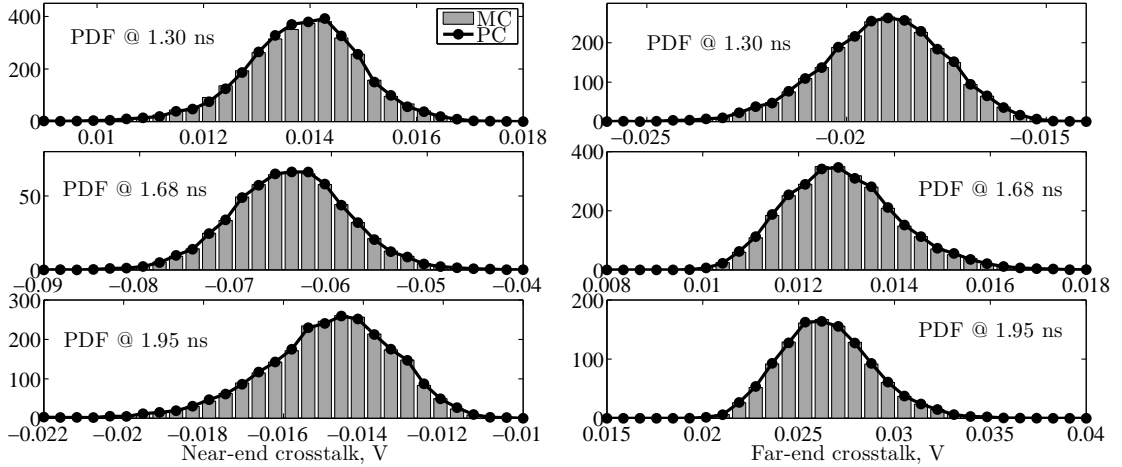


Figure 6.9. Probability density functions of the near-end (left panel) and far-end (right panel) transient crosstalk voltages, computed at three different time points. Gray bars indicate the distribution of the MC samples, whereas the dotted black lines are the distribution obtained from the PC expansions.

6.4 Example #4 — Time-Domain Simulation of a Cascaded Structure

For the sake of implementational simplicity into a MATLAB environment, so far we limited ourselves to consider only basic source-line-load circuits. In this section, we extend the formulation

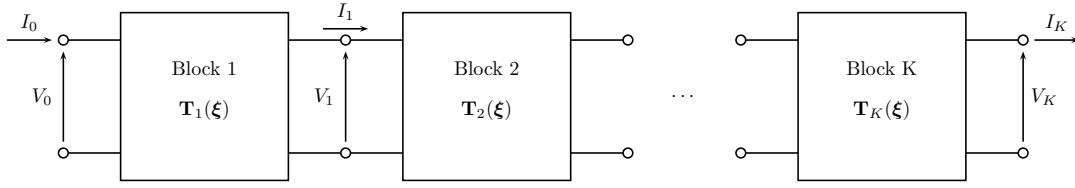


Figure 6.10. Illustration of a cascade connection of stochastic blocks.

to the analysis of a more general situation, in which there is a certain number K of stochastic blocks in a cascade connection, as shown in Fig. 6.10. If each block is described by its own CPM \mathbf{T}_k , $k = 1, \dots, K$, the total CPM relating voltages and currents at the two external terminations is readily given by the product of the single CPMs:

$$\begin{bmatrix} \mathbf{V}_K \\ \mathbf{I}_K \end{bmatrix} = \begin{bmatrix} \mathbf{T}_{K,11} & \mathbf{T}_{K,12} \\ \mathbf{T}_{K,21} & \mathbf{T}_{K,22} \end{bmatrix} \begin{bmatrix} \mathbf{V}_{K-1} \\ \mathbf{I}_{K-1} \end{bmatrix} = \mathbf{T}_K \mathbf{T}_{K-1} \cdots \mathbf{T}_1 \begin{bmatrix} \mathbf{V}_0 \\ \mathbf{I}_0 \end{bmatrix}. \quad (6.12)$$

For transmission-line sections, the CPM is readily given by (2.16), whereas for blocks composed by lumped elements, it can be derived in accordance to its definition and by means of classical circuit laws. The complete solution can be obtained by combining the overall CPM with the terminal constraints defining the source and load configurations, exactly as shown in Section 2.2.3.

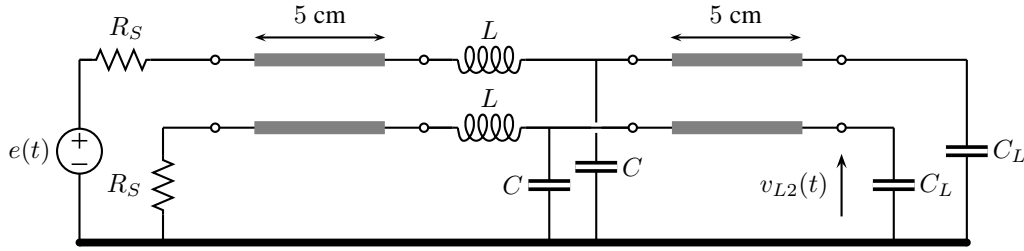


Figure 6.11. Cascaded interconnect structure.

When the blocks are stochastic, the application of the PC approach allows to derive an augmented deterministic counterpart for the CPM of each block [87]. The simulation is then carried out as in the case of single MTLs, i.e. by considering the overall augmented CPM, resulting from the product of the augmented matrices of each block, and combining it with the augmented terminal conditions. For stochastic MTLs, the augmented CPM is readily given by (5.35). For blocks with random lumped elements instead, it is possible to expand the CPM matrix entries as follows

$$\mathbf{T}_{mn}(\boldsymbol{\xi}) \approx \sum_{k=0}^P \mathbf{T}_{mn,k} \phi_k(\boldsymbol{\xi}), \quad (6.13)$$

with $m, n = 1, 2$. The augmented CPM is then

$$\tilde{\mathbf{T}} = \begin{bmatrix} \tilde{\mathbf{T}}_{11} & \tilde{\mathbf{T}}_{12} \\ \tilde{\mathbf{T}}_{21} & \tilde{\mathbf{T}}_{22} \end{bmatrix}, \quad (6.14)$$

with

$$\tilde{\mathbf{T}}_{mn,ij} = \sum_{k=0}^P \mathbf{T}_{mn,k} \langle \phi_k \phi_j, \phi_i \rangle. \quad (6.15)$$

As an illustrative example, we consider the structure of Fig. 6.11, consisting of two coupled microstrip lines, having the same cross-section displayed in Fig. 6.4, connected by means of a simple LC circuit, which represents a short connector. The source resistances are $R_S = 25 \Omega$ and the load capacitors are $C_L = 10$ pF. The connector parameters are $L = 3$ nH and $C = 0.4$ pF instead. The variability is provided by the substrate parameters h and ε_r , which are shared by both the transmission-line segments, and by the connector parameters L and C . Every parameter is considered as an independent Gaussian random variable with 10% relative standard deviation from its nominal value. It is easily shown that the CPM of the intermediate, lumped section is

$$\mathbf{T}_C = \left[\begin{array}{cc|cc} 1 & 0 & -j\omega L & 0 \\ 0 & 1 & 0 & -j\omega L \\ \hline -j\omega C & 0 & 1 - \omega^2 LC & 0 \\ 0 & -j\omega C & 0 & 1 - \omega^2 LC \end{array} \right]. \quad (6.16)$$

Finally, the voltage source is a digital signal: a periodic, trapezoidal wave with peak amplitude of 1 V, rise and fall times of 100 ps, total period of $T = 5$ ns and duty cycle of 50%. The signal being periodic, its spectrum consists of discrete components h_n (harmonics) appearing at frequencies $f_n = n f_0 = n/T$. Therefore, the time-domain waveform can be expressed in terms of a Fourier series, i.e.

$$x(t) = \sum_{n=-\infty}^{\infty} h_n e^{jnt} = h_0 + \sum_{n=1}^{\infty} (h_n e^{jnt} + h_n^* e^{-jnt}) = h_0 + \sum_{n=1}^{\infty} 2|h_n| \cos(\omega_n t + \angle h_n), \quad (6.17)$$

where property $h_{-n} = h_n^*$ has been used. The output waveforms can be expressed in a similar fashion, where the corresponding harmonics are obtained from the frequency-domain solution.

For the analysis, a finite number of 100 harmonics, computed via the FFT MATLAB routine, is considered. For the PC-based simulation, the augmented CPM of the line sections is computed according to (5.35), after the usual augmentation of the p.u.l. parameters. As to the lumped section instead, the PC expansion is readily obtained by replacing L and C in (6.16) with $L + \sigma_L \xi_3$ and $C + \sigma_C \xi_4$, respectively, where $\sigma_L = 0.1 \cdot L$ and $\sigma_C = 0.1 \cdot C$ are the standard deviations of the connector parameters, whilst ξ_3 and ξ_4 are the two standard normal random variables parameterizing their variations.

Fig. 6.12 shows the result of the stochastic simulation of the time-domain crosstalk at the right-end termination, indicated with $v_{L2}(t)$. The left panel shows the spread in the response due to the variability in the circuit parameters (light gray lines) and the resulting average response (black line) and standard deviation (dark gray line). The superposed markers denote the same statistical information obtained from a second-order PC expansion. It is worth mentioning that this time-domain simulation, carried out via frequency-domain analysis by considering a periodic source, provides the steady-state solution, as if the digital wave has been applied for a time long enough for the transients having decayed to zero. Because of this, the response appears not be causal, i.e. non-zero for time $t = 0$. Finally, the right panel compares the PDFs computed at three different

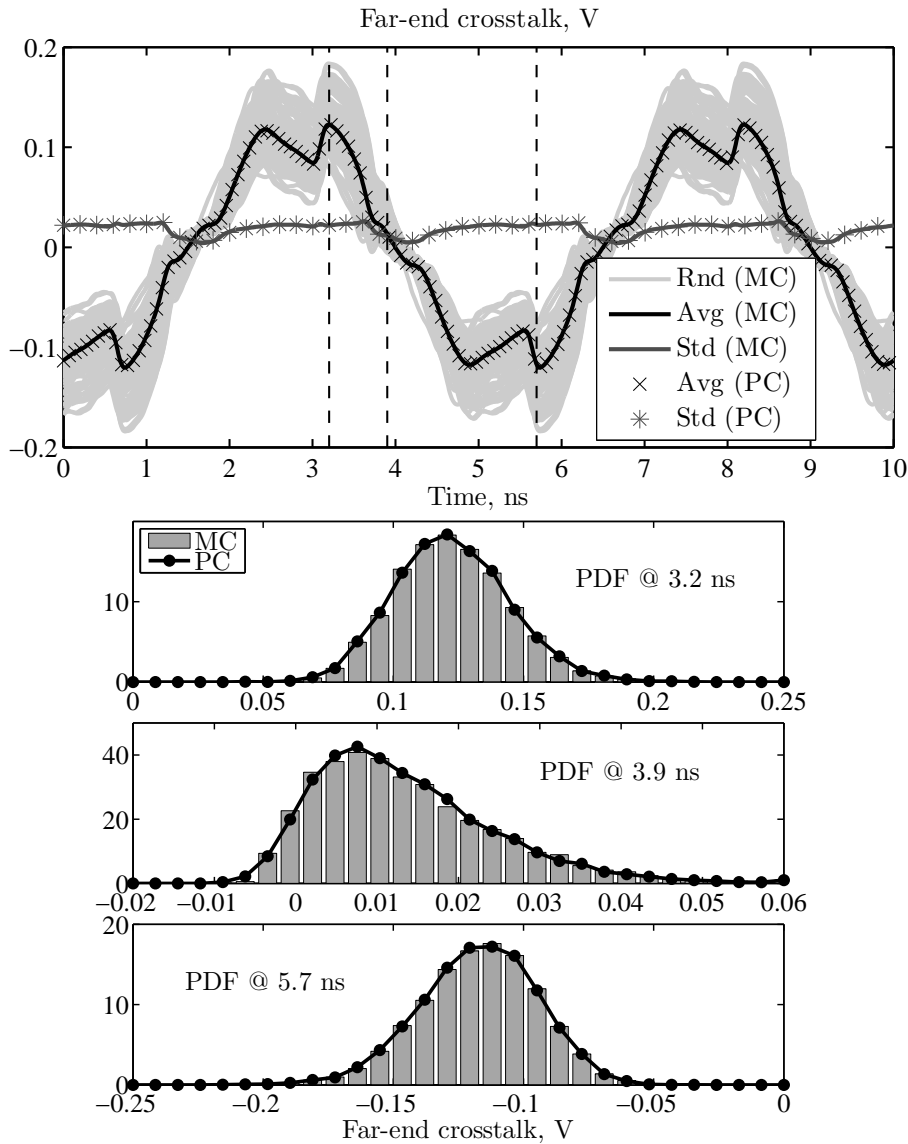


Figure 6.12. Stochastic simulation of the time-domain crosstalk at the far-end termination of the cascaded structure of Fig. 6.11. In the top panel, light gray lines: subset of MC samples showing the fluctuation of the response; solid black and dark gray lines: average response and its standard deviation obtain after running 10000 MC simulations. The crosses (×) and asterisks (*) denote the average and standard deviation given by third-order PC expansions. In the bottom panel, three probability density functions, computed at different time points from both MC simulations (gray bars) and PC expansions (dotted black lines).

time points. As far as the computational times are concerned, the MC analysis took 6 min 23 s, whereas the PC simulation required 3.3 s, thus leading to a 110× speed-up. This example once again shows the strength of the proposed technique both in terms of accuracy and efficiency gain.

Chapter 7

SPICE Implementation

The previous chapter showed how the proposed technique is general and can be applied to arbitrary transmission-line geometries. Moreover, the methodology confirmed to be very efficient in terms of both accuracy and computational time with respect to the standard MC method. However, there are two considerable limitations in the present formulation:

1. The approach is in essence a frequency-domain method. Although time-domain result can be obtained via Fourier analysis, the correct choice of the frequency points may be critical. Moreover, this precludes any possibility of including non-linear circuit elements.
2. Only source-line-load configurations, or slightly more general cascaded structures, can be easily analyzed. The simulation of more complex interconnect topologies (e.g., interconnect trees) requires cumbersome and ad hoc implementations.

In this context, we identify as a “complex topology” a circuit which contains many nodes and a combination of several distributed and lumped elements. A clear example is the transmission-line network illustrated in Fig. 1.1. When at least one of the network elements is stochastic, the voltage and current waveforms in the circuit become random variables and require a statistical description. Therefore, the methodology would benefit of the integration into standard and well-consolidated circuit analysis tools, such as SPICE. To this end, a SPICE-compatible formulation and implementation is presented in this chapter.

7.1 A Topological Rule for the Integration of Transmission Lines

The engine of SPICE-type tools for circuit analysis is based on the solution of the corresponding MNA equations, where the unknowns are the node voltages (defined with respect to a reference node) and the branch currents of voltage-defined components [88]. The MNA equations are created by considering the specific branch constitutive equations of each element in the network. As described in Chapter 4, the application of PC and SGM to the governing equations of MTLs leads to an augmented set of equations, which relate the voltage and current PC coefficients and can be interpreted as the constitutive equations pertaining to a MTL of larger dimension. Upon this interpretation, it is reasonable to associate a node to each additional terminal of this augmented

MTL. The corresponding node voltages are then the expansion coefficients of the stochastic terminal voltages of the original line. This procedure, already illustrated in Fig. 5.1, is repeated in Fig. 7.1 with emphasis on the modification of the circuit nodes. On the left is a stochastic line with two signal conductors ($N = 2$), described by random p.u.l. parameters \mathbf{R} , \mathbf{L} , \mathbf{G} , \mathbf{C} , and connecting four nodes denoted with letters A, B, C, D. After application of the SGM with $P = 2$ terms, the original line is expanded into a line with six conductors, which is described by deterministic p.u.l. parameters $\tilde{\mathbf{R}}$, $\tilde{\mathbf{L}}$, $\tilde{\mathbf{G}}$, $\tilde{\mathbf{C}}$, and connecting twelve nodes. These new nodes are denoted using the previous letters, and numbers indicating the expansion coefficient. In fact, each of the four original node voltages is now associated to three nodes, whose voltages are the corresponding PC-expansion coefficients.

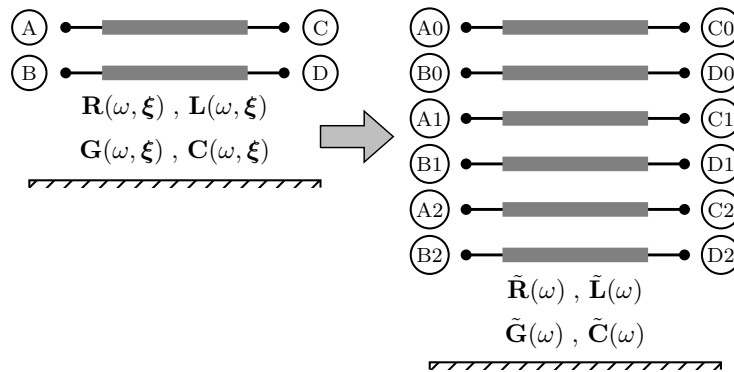


Figure 7.1. Illustration of the conversion of stochastic transmission lines into the augmented circuit instance.

The above illustration suggests a topological rule for the creation of a deterministic, augmented instance of a circuit containing several stochastic MTLs:

1. Expand the stochastic node voltages and currents in the original circuit into PC series.¹
2. Associate each voltage coefficient to a node of the augmented circuit instance.
3. Connect the resulting nodes by means of augmented MTLs, whose pertinent p.u.l. parameters are obtained via the application of the SGM as described in Chapter 4.

More practical details about the inclusion of the augmented line models into standard SPICE-type circuit solvers are given in Section 7.3. For the determination of the PC coefficients of the unknown, stochastic waveforms, the problem then amounts to performing a single circuit simulation of this deterministic, augmented circuit network, rather than running a large number of MC simulations of the original, stochastic network. However, a realistic network, like the one in Fig. 1.1, unavoidably includes also non-distributed components. The information about how to treat these lumped elements is still missing and is given in the next section.

¹It is important to remark that all the expansions must consider every random variable in the circuit, as in principle every node voltage and branch current may be affected by it.

7.2 Inclusion of Linear Lumped Elements

Concerning the inclusion in the simulation procedure of lumped circuit components, in this thesis we limit ourselves to consider deterministic linear elements. This means that the variability in the network is exclusively provided by the distributed parts, as this is the main topic of the work. A preliminary assessment for the inclusion of stochastic linear lumped elements in SPICE-type PC-based simulations is provided in [89]. Yet, a more general simulation framework, with the additional inclusion of nonlinear circuit elements, is still under development at the time this text is being written.

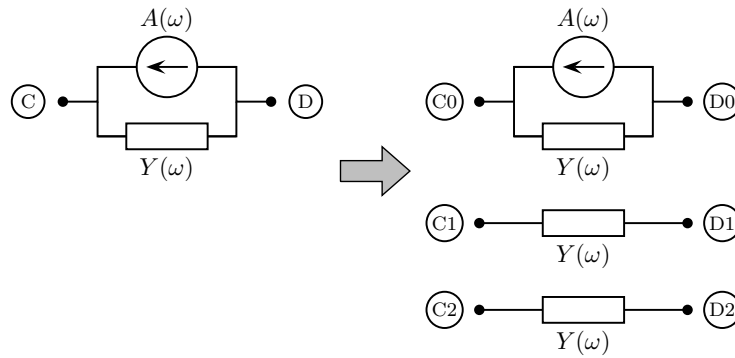


Figure 7.2. Illustration of the conversion of deterministic lumped elements into the augmented circuit instance.

For the discussion, we consider a linear lumped element connecting two nodes indicated as C and D (see Fig. 7.2, left side), and whose constitutive equation is expressed in the frequency domain in the form of a Norton equivalent:

$$I(\omega, \xi) = Y(\omega)[V_C(\omega, \xi) - V_D(\omega, \xi)] - A(\omega). \quad (7.1)$$

The above definition equivalently applies for any of the classical linear lumped circuit elements, i.e. resistors (with $Y(\omega) = 1/R$), capacitors ($Y(\omega) = j\omega C$), and inductors ($Y(\omega) = 1/j\omega L$). Moreover, it can be readily converted to time domain by replacing the admittance Y with the corresponding time-domain operator, obtained via inverse Fourier transform. It should be noted that the element characteristics, defined by the equivalent admittance Y and the equivalent current source A , are deterministic and therefore do not depend on the usual random vector ξ . Nevertheless, the node voltages and the branch current are still to be regarded as stochastic, because of the presence in the network of other random circuit components.

Substitution of PC expansions for the voltage and current variables in (7.1), yields

$$\sum_{k=0}^P I_k(\omega) \phi_k(\xi) = Y(\omega) \sum_{k=0}^P V_{C,k}(\omega) \phi_k(\xi) - Y(\omega) \sum_{k=0}^P V_{D,k}(\omega) \phi_k(\xi) - A(\omega). \quad (7.2)$$

Once again, the application of the SGM, i.e.

$$\sum_{k=0}^P I_k(\omega) \underbrace{\langle \phi_k, \phi_i \rangle}_{=0 \ \forall k \neq i} = Y(\omega) \sum_{k=0}^P V_{C,k}(\omega) \underbrace{\langle \phi_k, \phi_i \rangle}_{=0 \ \forall k \neq i} - Y(\omega) \sum_{k=0}^P V_{D,k}(\omega) \underbrace{\langle \phi_k, \phi_i \rangle}_{=0 \ \forall k \neq i} - \underbrace{\langle A(\omega), \phi_i \rangle}_{=0 \ \forall k \neq 0} \quad (7.3)$$

$\forall i = 0, \dots, P$ allows to derive the following deterministic equations relating the PC coefficients:

$$\begin{aligned} I_0(\omega) &= Y(\omega) [V_{C,0}(\omega) - V_{D,0}(\omega)] - A(\omega), \\ I_1(\omega) &= Y(\omega) [V_{C,1}(\omega) - V_{D,1}(\omega)], \\ &\vdots \\ I_P(\omega) &= Y(\omega) [V_{C,P}(\omega) - V_{D,P}(\omega)]. \end{aligned} \quad (7.4)$$

The above equations are decoupled and define the behavior of the elements connecting the $2(P+1)$ nodes associated to the expansion coefficients of node voltages V_C and V_D , as illustrated in the right side of Fig. 7.2 for the case $P = 2$. The circuit interpretation simply implies the replication of the deterministic elements on the additional branches. On the other hand, no replication is required for the source. For elements shunted to ground, only one node voltage appears in (7.1). The corresponding replicas are therefore all shunted to ground as well.

The overall augmented circuit is then obtained by direct construction and connection of the new elements consistently with the original circuit topology. Stochastic lines are replaced by their augmented counterparts, whereas deterministic lumped elements are replicated, as shown in Figs. 7.1 and 7.2, respectively. For the PC simulation, a single solution of the resulting network provides the PC coefficients for the stochastic circuit variables.

7.3 Description of the Augmented Transmission Lines

As far as the practical implementation is concerned, advanced SPICE-type circuit analysis tools, such as HSPICE or Agilent's ADS, include the "W-element" for the modeling of lossy and dispersive MTLs [90]. The W-element is a circuit component which provides a numerical solution of the telegrapher's equations. It generally accepts as inputs static p.u.l. parameter matrices or, for dispersive lines, tabulated frequency data. This, in principle, allows to readily specify the augmented line parameters as pertaining to a transmission line of larger dimension. However, due to the symmetry of the p.u.l. parameters of physical (reciprocal) lines, only the lower triangular part of the matrices is usually specified. This inherently implies that the augmented line is realizable with a W-element only when orthonormal basis functions are used, as this guarantees the symmetry of the augmented p.u.l. matrices. This is a crucial step for the SPICE-type implementation of the PC-SGM methodology, since classical applications (see, e.g., [51], [52]) typically use standard polynomials, which are only orthogonal.

In addition, HSPICE provides an internal field solver, which is capable of computing lossy and dispersive p.u.l. parameters and simulating a transmission line upon the description of its cross-section. The field solver can be combined with the available feature for MC simulations, thus allowing to perform a statistical analysis of circuits containing transmission lines with stochastic cross-sectional parameters entirely in the HSPICE environment. The field solver basically

computes six frequency independent p.u.l. matrices: the DC inductance \mathbf{L}_0 [H/m], capacitance \mathbf{C}_0 [F/m], resistance \mathbf{R}_0 [Ω /m], and conductance \mathbf{G}_0 [S/m] matrices, as well as the skin effect resistance matrix \mathbf{R}_s [$\Omega/(m\sqrt{\text{Hz}})$] and the dielectric loss conductance matrix \mathbf{G}_d [S/(m · Hz)]. These six matrices are combined in a frequency-dependent way to obtain the dispersive behavior. Also, they are obtainable as an output or supplied as an input to a W-element (the “RLGC model”). For the specification of the augmented transmission-line models, it is alternatively possible to supply the augmented counterpart of this RLGC model, defined by augmented matrices $\tilde{\mathbf{L}}_0$, $\tilde{\mathbf{C}}_0$, $\tilde{\mathbf{R}}_0$, $\tilde{\mathbf{G}}_0$, $\tilde{\mathbf{R}}_s$ and $\tilde{\mathbf{G}}_d$. These are obtainable according to the usual augmentation procedure (5.13). Furthermore, a PC-based model which is consistent with the HSPICE field solver, and therefore with the built-in MC analysis, can be created by projecting the RLGC-model matrices outputted by parametric calls to the field solver.

7.4 Application Examples

In this section, the outlined SPICE-compatible PC formulation is implemented into HSPICE for the statistical analysis of transmission-line networks. The results of the PC-based simulations are compared with those from MC analyses, which are carried out by means of the available feature in HSPICE. However, before continuing, a tutorial example of a HSPICE netlist for the PC-based simulation of a simpler circuit is given.

7.4.1 Example of HSPICE Netlist for the Polynomial Chaos-Based Simulation

We consider the source-line-load configuration of Fig. 2.4. We denote the node of the voltage generator as A, the near-end line terminations as nodes M and N, whilst the far-end terminations as nodes P and Q. Of course, the reference node 0 corresponds to the ground plane. Therefore, the HSPICE netlist for the circuit becomes:

```
Vsource A 0 E
Rsource1 A M RS
Rsource2 N 0 RS
Wt1 M N 0 P Q 0 RLGCMODEL=two_wires N=2 l=80cm
Cload1 P 0 CL
Cload2 Q 0 CL

.MODEL two_wires W MODELTYPE=RLGC, N=2
+ Lo =
+ L11
+ L21 L22
+ Co =
+ C11
+ C21 C22
```

For this lossless line, only the DC p.u.l. inductance matrices need to be supplied. The augmented p.u.l. inductance and capacitance matrices, for a PC-based simulation in presence of variations in

the height above ground and wire-to-wire distance, are given in (5.33) and (5.34), respectively. With the rules outlined above, the HSPICE netlist for the corresponding deterministic simulation is readily given:

```
Vsource A0 0 E

Rsource1_0 A0 M0 RS
Rsource1_1 M1 0 RS
Rsource1_2 M2 0 RS
Rsource1_3 M3 0 RS
Rsource1_4 M4 0 RS
Rsource1_5 M5 0 RS

Rsource2_0 N0 0 RS
Rsource2_1 N1 0 RS
Rsource2_2 N2 0 RS
Rsource2_3 N3 0 RS
Rsource2_4 N4 0 RS
Rsource2_5 N5 0 RS

Waugm_t1 M0 N0 M1 N1 M2 N2 M3 N3 M4 N4 M5 N5 0
+ P0 Q0 P1 Q1 P2 Q2 P3 Q3 P4 Q4 P5 Q5 0
+ RLGCMODEL=augmented_line N=12 l=80cm

Cload1_0 P0 0 CL
Cload1_1 P1 0 CL
Cload1_2 P2 0 CL
Cload1_3 P3 0 CL
Cload1_4 P4 0 CL
Cload1_5 P5 0 CL

Cload2_0 Q0 0 CL
Cload2_1 Q1 0 CL
Cload2_2 Q2 0 CL
Cload2_3 Q3 0 CL
Cload2_4 Q4 0 CL
Cload2_5 Q5 0 CL

.MODEL augmented_line W MODELTYPE=RLGC, N=12
+ Lo =
+ Ltilde00
+ Ltilde10 Ltilde11
+ Ltilde20 Ltilde21 Ltilde22
...
```

```

+ Co =
+ Ctilde00
+ Ctilde10 Ctilde11
+ Ctilde20 Ctilde21 Ctilde22
...

```

It is worth noting that nodes M1...M5 are shunted to ground, because no replication of the voltage source is required.

7.4.2 Transmission-Line Network with Single Microstrip Lines

The first example deals with the interconnect network illustrated in Fig. 1.1. In this case, the voltage source is a 1-V pulse with rise/fall times of 200 ps and width of 2.6 ns. The lines have a microstrip cross-section (cfr. Fig. 6.4) with copper traces (conductivity of 58 MS/m), having a thickness of 20 μm and a width of 150 μm . The board substrate has a thickness of 100 μm , permittivity of 4.1 and loss tangent of 0.02. These substrate parameters, which are shared by all the lines, assume independent random Gaussian variations of 10%. The HSPICE field solver is used for the characterization of the transmission-line segments, which are then implemented as W-elements characterized by the description of their cross-section.

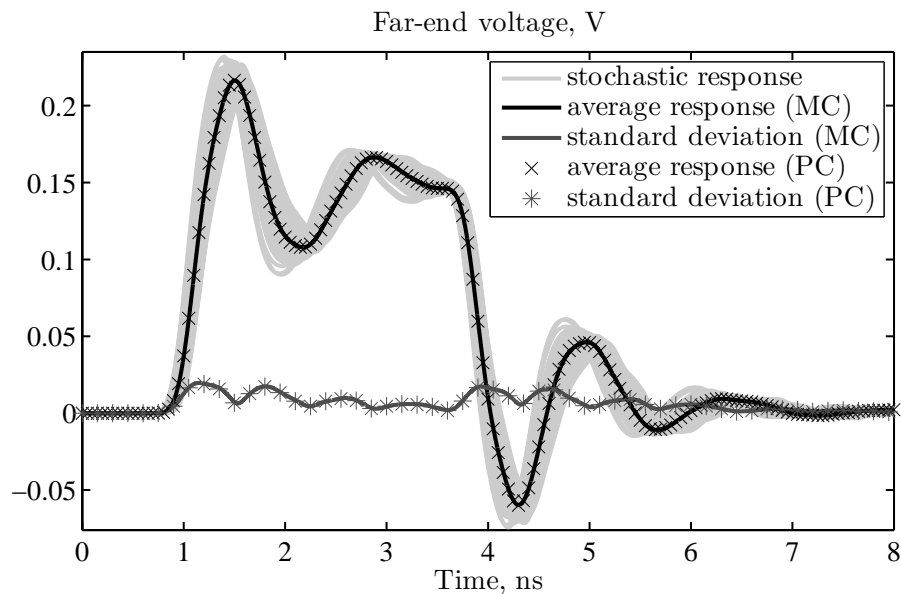


Figure 7.3. Stochastic transient analysis of the voltage $v_{\text{out}}(t)$. Light gray lines: samples of the random response; black and dark gray lines: average response and standard deviation obtained via 1000 MC simulations; markers: average response (crosses \times) and standard deviation (asterisks $*$) obtained from the PC expansions.

A MC simulation with 1000 samples is run using the available HSPICE feature. The plot in Fig. 7.3 shows the stochastic transient response (ligh gray lines) of the voltage transmitted to

the far-end side of the network, indicated as $v_{\text{out}}(t)$ in Fig. 1.1, together with its average (black line) and standard deviation (dark gray line). These statistical parameters are also obtained from a second-order PC-based simulation (cfr. the markers), which reveals perfect agreement. The circuit simulation of the augmented network required 7.5 s instead, whereas the MC simulation took 38 min 25 s. For this first example, the speed-up in circuit simulation is then $310\times$, even though a very small number of samples is considered for the MC analysis. For the PC simulation, a RLGC model, described by augmented matrices $\tilde{\mathbf{L}}_0$, $\tilde{\mathbf{C}}_0$, $\tilde{\mathbf{R}}_0$, $\tilde{\mathbf{R}}_s$, $\tilde{\mathbf{G}}_0$ and $\tilde{\mathbf{G}}_d$, is computed. This step took 22.2 s. It is relevant to remark that the created model can be stored and re-used for other circuit simulations involving the same stochastic line structure. Hence, the time required by its computation is not considered for the speed-up.

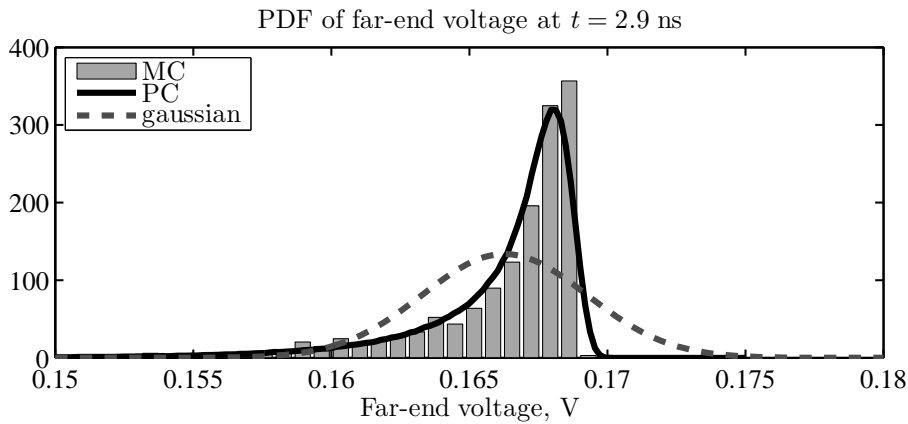


Figure 7.4. Probability distribution of $v_{\text{out}}(t)$, computed at $t = 2.9$ ns from the MC samples (bars) and PC expansions (solid black line). Dashed gray line: corresponding Gaussian distribution.

As we already know, despite the normal distribution of the random input parameters, the distribution of the response is in general not Gaussian, and therefore average value and standard deviation are not sufficient for a complete statistical characterization. For instance, Fig. 7.4 displays the PDF at $t = 2.9$ ns, computed from the MC samples (bars) and from the PC expansion (solid black line). For comparison, the dashed gray line is the Gaussian distribution corresponding to the estimated mean value and standard deviation.

7.4.3 Transmission-Line Network with Coupled Microstrip Lines

We now consider the transmission-line network displayed in Fig. 7.5. The coupled lines again have a microstrip cross-section, with random geometrical parameters. The copper trace width, trace-to-trace separation, trace thickness, and substrate thickness have 10% independent relative standard deviations with respect to the nominal values indicated in the figure. Furthermore, the substrate has a permittivity of 3.7 and a loss tangent of 0.02. The voltage source is a Gaussian pulse of peak amplitude of 1 V and a width of about 0.177 ns at half amplitude.

Fig. 7.6 shows the results obtained with the HSPICE MC analysis (1000 samples) of the far-end crosstalk voltage $v_{\text{FX}}(t)$, which required 14 min 15 s. The comparison with a PC simulation,

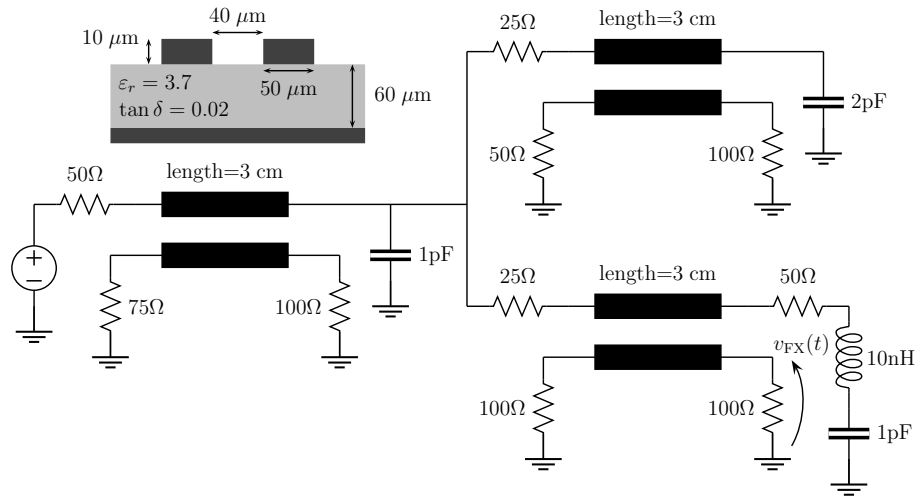


Figure 7.5. Transmission-line network with coupled microstrip traces and corresponding line cross-section.

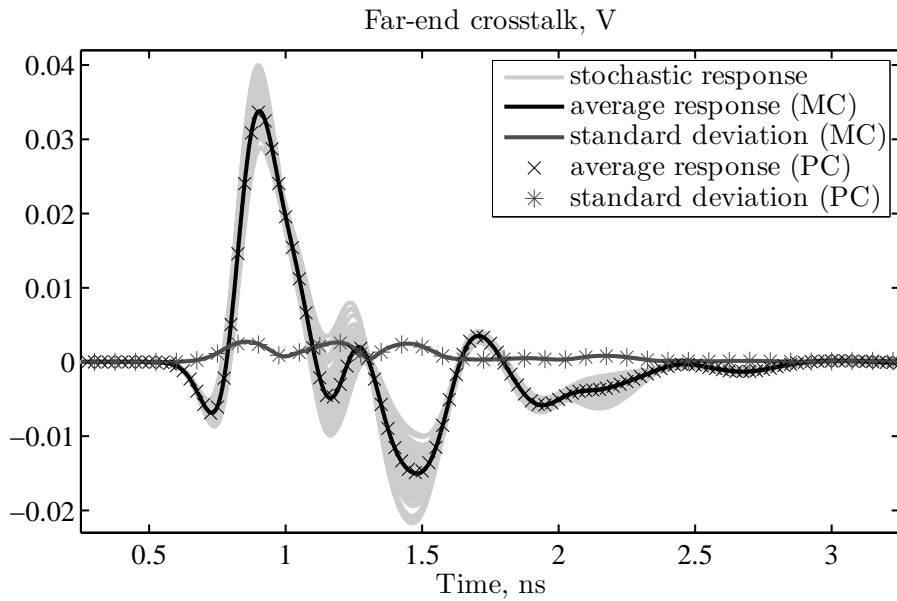


Figure 7.6. Stochastic transient analysis of the far-end crosstalk voltage $v_{FX}(t)$. Curves identification as in the inset of Fig. 7.3.

taking 14.2 s and based on a second-order augmented RLGC model, confirms the accuracy of the proposed technique and shows a $60\times$ speed-up. The generation of the augmented model required 55 s. Finally, Fig. 7.7 displays the PDF for the crosstalk peak, occurring at $t = 0.9$ ns. Again, it is possible to appreciate the better reproduction of the distribution provided by the PC result.

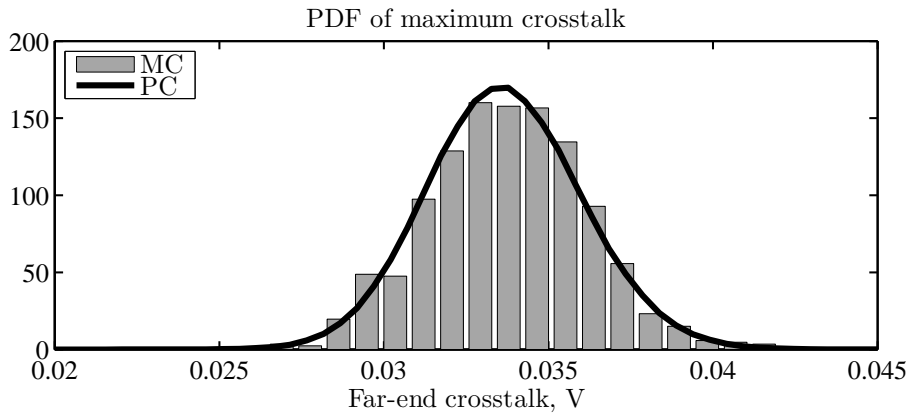


Figure 7.7. Probability distribution of the maximum crosstalk at $t = 0.9$ ns, computed from the MC samples (bars) and PC expansions (solid black line).

This chapter concludes the illustration of the proposed framework for the stochastic circuit simulation of high-speed interconnects. The strength and accuracy of the proposed PC technique is preserved for SPICE-based simulations, whereas the efficiency turns out to be even better, with speed-ups of about two orders of magnitude even when considering a smaller number of MC samples. It is relevant to point out that this time-domain analysis, achieved via the transient simulation of an augmented circuit instance, raises the critical question as to whether the passivity of the circuit is preserved [91]. This issue has been addressed in [92], leading to the conclusion that the passivity depends on the accuracy of the PC expansions of the p.u.l. parameters and that, for practical applications, the answer is always positive. The next chapter concludes this thesis with the illustration of a further application of PC in the transmission-line analysis: the assessment of the effects of a random electromagnetic wave incidence. This means that the response variability is not due to variations in the transmission-line properties or terminations, but to an external stochastic field.

Chapter 8

Random Field Incidence

Another relevant and possible source of variability is the incidence on a transmission line of random electromagnetic fields [93]. A typical example of a random field is a plane wave with arbitrary parameters like amplitude, polarization or direction of incidence. This kind of study is of great importance, for instance in the modeling of the fields coupling to transmission lines inside reverberation chambers [94], [95]. In [50], closed-form probabilistic models for the random plane-wave field coupling to a single transmission line were developed. However, these simplified results are still based on low-frequency approximations and pre-defined structures, in this case a single lossless wire above a perfect ground. Moreover, only certain kinds of random field parameters can be accounted for, and the generalization of the approach is highly non-trivial. The work in [96] extends the results to high frequencies, but retains all the other limitations. A more general approach to tackle this issue can be again formulated based on the PC theory.

8.1 Transmission-Line Equations for Incident Field Excitation

In presence of an impinging electromagnetic field, equivalent source terms add to the telegrapher's equations (2.14) [54]:

$$\frac{d}{dz}\mathbf{V}(z, \omega) = -\mathbf{Z}(\omega)\mathbf{I}(z, \omega) + \mathbf{V}_F(\omega, z), \quad (8.1a)$$

$$\frac{d}{dz}\mathbf{I}(z, \omega) = -\mathbf{Y}(\omega)\mathbf{V}(z, \omega) + \mathbf{I}_F(\omega, z). \quad (8.1b)$$

The distributed source terms \mathbf{V}_F and \mathbf{I}_F can be conveniently expressed as functions of the sole incident electric field:

$$\mathbf{V}_F(\omega, z) = \begin{bmatrix} \vdots \\ -\frac{\partial}{\partial z} \int_{C_i} \vec{E}_t(\omega) \cdot d\vec{l} + E_{z,i}(\omega, z) - E_{z,0}(\omega, z) \\ \vdots \end{bmatrix}, \quad (8.2a)$$

$$\mathbf{I}_{F,i}(\omega, z) = -\mathbf{Y}(\omega) \begin{bmatrix} \vdots \\ \int_{C_i} \vec{E}_t(\omega) \cdot d\vec{l} \\ \vdots \end{bmatrix}, \quad (8.2b)$$

where $\int_{C_i} \vec{E}_t \cdot d\vec{l}$ is the line integral of the transverse electric field on the circuit between conductor i and the reference, whereas $E_{z,i}$ is the longitudinal field parallel to the i th conductor. From now on and for notational convenience, we neglect the dependence on the angular frequency ω .

8.1.1 Solution of the Forced Transmission-Line Equations

The general solution of (8.1) is

$$\begin{bmatrix} \mathbf{V}(z = \mathcal{L}) \\ \mathbf{I}(z = \mathcal{L}) \end{bmatrix} = \begin{bmatrix} \Phi_{11}(\mathcal{L}) & \Phi_{12}(\mathcal{L}) \\ \Phi_{21}(\mathcal{L}) & \Phi_{22}(\mathcal{L}) \end{bmatrix} \begin{bmatrix} \mathbf{V}(z = 0) \\ \mathbf{I}(z = 0) \end{bmatrix} + \begin{bmatrix} \mathbf{V}_{FT}(z = \mathcal{L}) \\ \mathbf{I}_{FT}(z = \mathcal{L}) \end{bmatrix}, \quad (8.3)$$

where forcing terms \mathbf{V}_{FT} and \mathbf{I}_{FT} appear, with respect to (2.17), because of the field excitation. These are *convolutions* between the source terms and the CPM:

$$\mathbf{V}_{FT}(\mathcal{L}) = \int_0^{\mathcal{L}} [\Phi_{11}(\mathcal{L} - \tau) \mathbf{V}_F(\tau) + \Phi_{12}(\mathcal{L} - \tau) \mathbf{I}_F(\tau)] d\tau, \quad (8.4a)$$

$$\mathbf{I}_{FT}(\mathcal{L}) = \int_0^{\mathcal{L}} [\Phi_{21}(\mathcal{L} - \tau) \mathbf{V}_F(\tau) + \Phi_{22}(\mathcal{L} - \tau) \mathbf{I}_F(\tau)] d\tau. \quad (8.4b)$$

The new general solution can still be combined with terminal relations defining the source and load configurations. We limit ourselves to mention the case in which both the source and load constraints are expressed as Thévenin equivalents. The currents at the line extremities are obtainable as

$$\begin{aligned} \mathbf{I}(z = 0) = & [\Phi_{12} - \Phi_{11} \mathbf{Z}_S - \mathbf{Z}_L \Phi_{22} + \mathbf{Z}_L \Phi_{21} \mathbf{Z}_S]^{-1} [\mathbf{V}_L + \\ & -(\Phi_{11} - \mathbf{Z}_L \Phi_{21}) \mathbf{V}_S] - \mathbf{V}_{FT}(\mathcal{L}) + \mathbf{Z}_L \mathbf{I}_{FT}(\mathcal{L}), \end{aligned} \quad (8.5a)$$

$$\mathbf{I}(z = \mathcal{L}) = \mathbf{I}_{FT}(\mathcal{L} + \Phi_{21} \mathbf{V}_S + (\Phi_{22} - \Phi_{21} \mathbf{Z}_S) \mathbf{I}(z = 0), \quad (8.5b)$$

whilst the voltages are still computed according to (2.20). This solution procedure provides the terminal voltages and currents at a given frequency, and is iterated for every frequency point of interest.

8.1.2 Uniform Plane-Wave Incidence

When the incident field is a uniform plane wave, the situation greatly simplifies. Nonetheless, the case is still relevant, because for example the field radiated by a distant source is a spherical wave which can locally be considered as a plane wave. Furthermore, in reverberation chambers, the total electric field can be represented as a superposition of (random) plane waves [97], [98].

Fig. 8.1 illustrates a plane-wave field impinging on a MTL. The field is characterized by its polarization η and direction of incidence, which is in turn expressed by polar coordinates via the

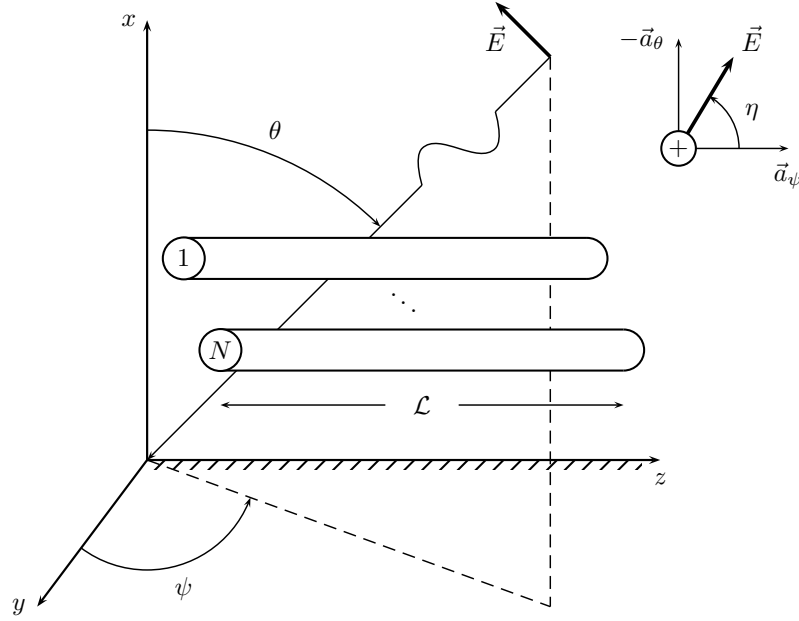


Figure 8.1. Illustration of a plane-wave field incising on a transmission line.

colatitude θ (the complimentary angle of the elevation) and azimuth ψ . With the above definitions, the explicit expression of the electric field in a point with Cartesian coordinates (x, y, z) is

$$\vec{E} = E_0(e_x \vec{a}_x + e_y \vec{a}_y + e_z \vec{a}_z)e^{-j\beta_x x} e^{-j\beta_y y} e^{-j\beta_z z}, \quad (8.6)$$

where $\vec{a}_{x,y,z}$ are the axis versors, E_0 is the field amplitude,

$$\begin{cases} e_x = \sin \eta \sin \theta \\ e_y = -\sin \eta \cos \theta \cos \psi - \cos \eta \sin \psi \\ e_z = -\sin \eta \cos \theta \sin \psi + \cos \eta \cos \psi \end{cases} \quad (8.7)$$

and

$$\begin{cases} \beta_x = -\beta \cos \theta \\ \beta_y = -\beta \sin \theta \cos \psi \\ \beta_z = -\beta \sin \theta \sin \psi, \end{cases} \quad (8.8)$$

with $\beta = \omega/c_0$ being the phase constant for the incident wave ($c_0 = 299792458$ m/s is the speed of light in vacuum). In this case, the convolution terms take closed forms [54]:

$$\mathbf{V}_{FT}(\mathcal{L}) = \frac{1}{2} \mathbf{Y}^{-1} \mathbf{T} \mathbf{M}^+ - \begin{bmatrix} \vdots \\ E_{Tm}(\mathcal{L}) \\ \vdots \end{bmatrix} + \frac{1}{2} \mathbf{Y}^{-1} \mathbf{T} \mathbf{N}^+, \quad (8.9a)$$

$$\mathbf{I}_{FT}(\mathcal{L}) = -\frac{1}{2} \mathbf{T} \boldsymbol{\gamma}^{-1} \mathbf{M}^- - \frac{1}{2} \mathbf{T} \boldsymbol{\gamma}^{-1} \mathbf{N}^-, \quad (8.9b)$$

with \mathbf{T} and γ defined in (2.19). The entries of the remaining vector terms are related to the incident electric field. In the specific case of a line lying above a perfect ground plane, and by denoting the cross-sectional coordinates of the center of conductor m as (x_m, y_m) , they are as follows:

$$M_i^\pm = -2jE_0e_z \left[e^{\gamma_i\mathcal{L}} \frac{1 - e^{-(\gamma_i + j\beta_z)\mathcal{L}}}{\gamma_i + j\beta_z} \pm e^{-\gamma_i\mathcal{L}} \frac{e^{(\gamma_i - j\beta_z)\mathcal{L}} - 1}{\gamma_i - j\beta_z} \right] \times \sum_{m=1}^N \left[\beta_x x_m \frac{\sin(\beta_x x_m)}{\beta_x x_m} e^{-j\beta_y y_m} \right] [\mathbf{T}^{-1}\mathbf{Y}]_{im}, \quad (8.10)$$

$$N_i^\pm = E_0 [e^{\gamma_i\mathcal{L}} \pm e^{-\gamma_i\mathcal{L}}] \times \sum_{m=1}^N \left[(e_x x_m + e_y y_m) \frac{\sin(\psi_m^+)}{\psi_m^+} e^{-j\psi_m^+} + (e_x x_m + e_y y_m) \frac{\sin(\psi_m^-)}{\psi_m^-} e^{-j\psi_m^-} \right] [\mathbf{T}^{-1}\mathbf{Y}]_{im}, \quad (8.11)$$

with

$$\psi_m^\pm = \beta_x x_m \pm \beta_y y_m, \quad (8.12)$$

and finally

$$E_{Tm}(\mathcal{L}) = E_0 (e_x x_m + e_y y_m) \frac{\sin(\psi_m^+)}{\psi_m^+} e^{-j\psi_m^+} e^{-j\beta_z \mathcal{L}} + E_0 (e_x x_m - e_y y_m) \frac{\sin(\psi_m^-)}{\psi_m^-} e^{-j\psi_m^-} e^{-j\beta_z \mathcal{L}}. \quad (8.13)$$

8.2 Application of Polynomial Chaos

When the impinging field is random, the distributed source terms \mathbf{V}_F and \mathbf{I}_F in (8.1) become stochastic and can be in principle expanded into a PC representation. However, in this thesis we limit ourselves to consider the case in which the incident field is a plane wave and it is the sole source of variability (i.e., the inherent, cross-sectional line properties and its terminations are deterministic). The availability of closed-form relations for the forcing terms in this situation suggests to expand \mathbf{V}_{FT} and \mathbf{I}_{FT} in (8.3), rather than \mathbf{V}_F and \mathbf{I}_F in (8.1). In this way, the solution procedure will not involve further integrations like those in (8.2) or (8.4).

The randomness of the field implies that the wave parameters E_0 , η , θ , ψ are possibly stochastic and parameterizable by pertinent normalized variables collected into a random vector $\boldsymbol{\xi}$. This variability of the wave parameters leads to a variability of the terms $e_{x,y,z}$ and $\beta_{x,y,z}$ in (8.10)–(8.13). As a result, the forcing terms in (8.9) in turn depend on the random vector $\boldsymbol{\xi}$ and can therefore be expressed as PC expansions:

$$\mathbf{V}_{FT}(\boldsymbol{\xi}) \approx \sum_{k=0}^P \mathbf{V}_{FT,k} \phi_k(\boldsymbol{\xi}), \quad (8.14a)$$

$$\mathbf{I}_{FT}(\boldsymbol{\xi}) \approx \sum_{k=0}^P \mathbf{I}_{FT,k} \phi_k(\boldsymbol{\xi}), \quad (8.14b)$$

where the coefficients $\mathbf{V}_{FT,k}$ and $\mathbf{I}_{FT,k}$ are computed according to (4.12) via the numerical integration of relations (8.9). Substitution of (8.14) and of the corresponding expansions of the voltage and current variables (5.6) into (8.3) produces

$$\sum_{k=0}^P \begin{bmatrix} \mathbf{V}_k(\mathcal{L}) \\ \mathbf{I}_k(\mathcal{L}) \end{bmatrix} \phi_k(\boldsymbol{\xi}) = \begin{bmatrix} \Phi_{11}(\mathcal{L}) & \Phi_{12}(\mathcal{L}) \\ \Phi_{21}(\mathcal{L}) & \Phi_{22}(\mathcal{L}) \end{bmatrix} \sum_{k=0}^P \begin{bmatrix} \mathbf{V}_k(0) \\ \mathbf{I}_k(0) \end{bmatrix} \phi_k(\boldsymbol{\xi}) + \sum_{k=0}^P \begin{bmatrix} \mathbf{V}_{FT,k}(\mathcal{L}) \\ \mathbf{I}_{FT,k}(\mathcal{L}) \end{bmatrix} \phi_k(\boldsymbol{\xi}). \quad (8.15)$$

It is worth noting that the deterministic nature of the line characteristics does not require any modification in the CPM. Application of Galerkin weighting $\forall \phi_i, i = 0, \dots, P$, to the left- and right-hand sides of (8.15), leads to the following set of $P + 1$ *uncoupled* equations [99]:

$$\begin{bmatrix} \mathbf{V}_i(\mathcal{L}) \\ \mathbf{I}_i(\mathcal{L}) \end{bmatrix} = \begin{bmatrix} \Phi_{11}(\mathcal{L}) & \Phi_{12}(\mathcal{L}) \\ \Phi_{21}(\mathcal{L}) & \Phi_{22}(\mathcal{L}) \end{bmatrix} \begin{bmatrix} \mathbf{V}_i(0) \\ \mathbf{I}_i(0) \end{bmatrix} + \begin{bmatrix} \mathbf{V}_{FT,i}(\mathcal{L}) \\ \mathbf{I}_{FT,i}(\mathcal{L}) \end{bmatrix} \quad (8.16)$$

$\forall i = 0, \dots, P$. The above equations imply that the expansion coefficients \mathbf{V}_k and \mathbf{I}_k , for the voltages and currents at the line terminations, are merely related by the general solution of the *original*, deterministic line configuration, and are affected by the k th coefficient of the forcing functions only. This is due to the assumption that the variability is solely provided by the incident field and does not affect the line parameters. If the terminations are also deterministic, the problem is totally decoupled, and the sought-for expansion coefficients are readily obtained via the iterative solution of (8.16), $\forall k = 0, \dots, P$, by means of (8.5) and (2.20). In contrast to the case of variations in the line properties, the PC coefficients of the stochastic voltages and currents at the line terminations are not given by the solution of a $(P + 1)$ -time larger system of equations, but by the iterative solution of $P + 1$ uncoupled problems, having the original size and where the excitation is provided by the sequence of the coefficients $\mathbf{V}_{FT,k}$ and $\mathbf{I}_{FT,k}$. This results in a faster computational time, although for this kind of analysis a larger number of expansion terms is usually also required (see the application example below).

It is worth noting that the PC-based simulation can be interpreted in this case as a superposition of analyses, carried out by considering the expansion coefficients of \mathbf{V}_{FT} and \mathbf{I}_{FT} as excitations, thus being completely analogous to a Fourier analysis. The stochastic problem is then determined by a collection of deterministic simulations of the original problem. However, contrary to the MC analysis, for each iteration the forcing functions are not chosen at random, but are given by the sequence of the PC-expansion coefficients of the forcing terms.

8.3 Application Example

A thorough comparison between the PC approach and the available closed-form probabilistic models [50] for the study of the excitation of a single lossless line by a random plane-wave field is provided in [100]. In this section, we propose a more general and realistic application example, which cannot be analyzed with the previous methods.

We consider again the flex cable in Fig. 6.1. The geometric parameters were $r_w = 7.5$ mils, $d_c = 35$ mils, $d = 50$ mils, $h = 8$ cm, and are now all regarded as deterministic. The terminations

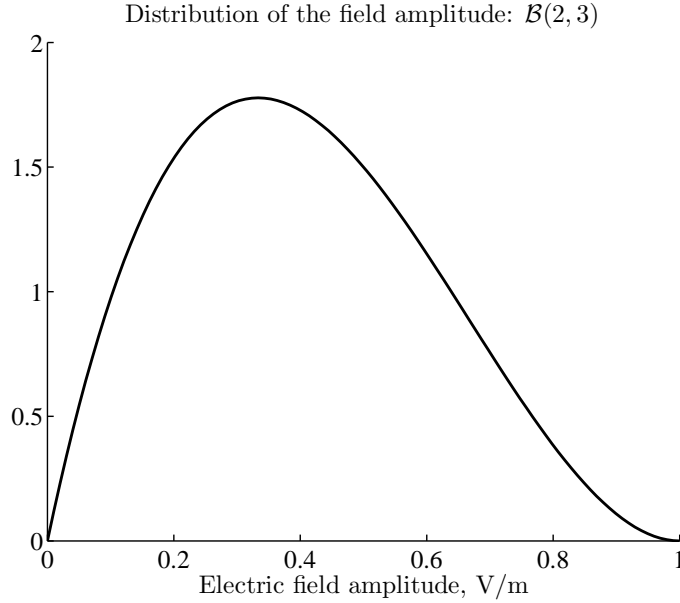


Figure 8.2. Probability distribution of the amplitude of the incident electric field.

were $R_S = 25 \Omega$ and $C_L = 10$ pF. A cable length of 1 m is considered here. We analyze two different situations: 1) field incidence with random amplitude and polarization; 2) field incidence with random colatitude and azimuth. The second situation is of particular interest, as it refers to the case of completely random direction of incidence in the whole solid angle, and because no closed-form results are available in [50], even for single transmission lines.

8.3.1 Random Field Amplitude and Polarization

In this first example, the wave amplitude E_0 has a beta distribution with parameters $\nu_1 = 2$ and $\nu_2 = 3$ in the range $[0, 1]$ V/m (see Fig. 8.2) [50]. The polarization angle η is assumed to be uniform in the range $[-\pi, \pi]$ instead. The remaining wave parameters, i.e. colatitude and azimuth, have fixed values of $\theta = \pi/6$ and $\psi = \pi/4$, respectively.

Fig. 8.3 shows (top plot) the statistical assessment of the current induced at the far-end termination of the third conductor of the cable. The plot displays both the average response (black line) and the standard deviation (dark gray line), computed with the MC method (10000 samples), together with a reduced set of samples of the random response (light gray lines). It is relevant to note that the variability is here indeed high, the standard deviation being on the same order of magnitude as the average response. For comparison, the markers indicate the average response (circles) and standard deviation (asterisks) obtained by means of PC, showing excellent agreement. The PC simulation is based on the six-order expansion of the forcing terms into 28 Legendre polynomials. It should be remarked that, the field amplitude having a beta distribution, the converge of the Legendre-type PC expansions is here non-optimal. Nevertheless, there is no limitation concerning the effective use of this class of basis functions for the expansions (8.14) [20].

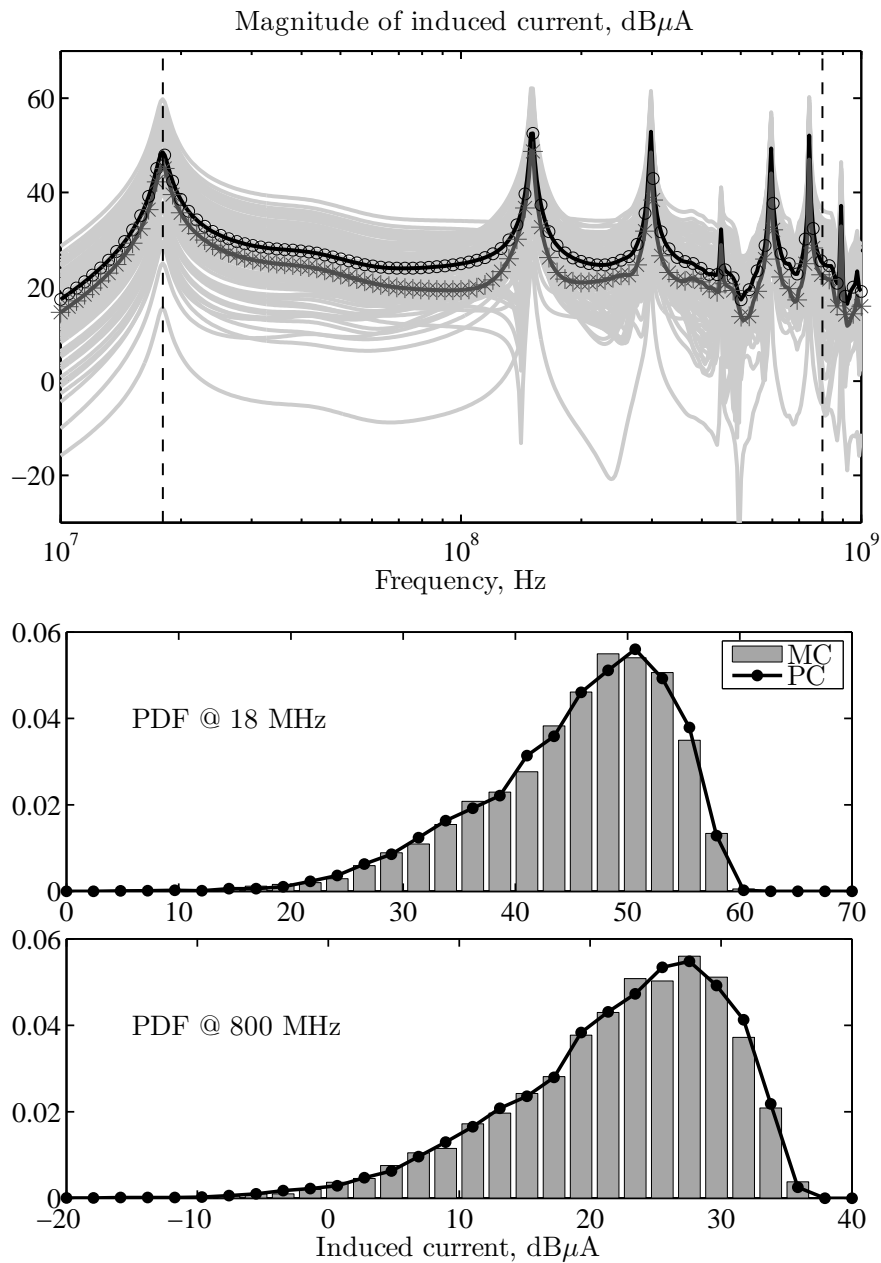


Figure 8.3. Stochastic simulation of the current induced on a flex cable illuminated by a plane wave with random field amplitude and polarization. Top plot: average response (black line) and standard deviation (dark gray line) obtained after 10000 MC simulations; circles (\circ) and asterisks ($*$) indicate the average response and standard deviation obtained from the PC expansions; the light gray lines are different samples of the induced current. Bottom plot: distributions computed at two different frequencies with both MC (gray bars) and PC (dotted line).

Fig. 8.3 also shows (bottom plot) the probability distribution computed at two different frequencies by means of both the MC and PC methods. These frequencies are indicated by the dashed vertical lines in Fig. 8.3. The comparison reveals excellent agreement also at high frequencies, where approximate solutions are no longer valid even for basic line structures. The computational time for the MC simulation is 1 h and 4 min. The PC simulation required an overall time of 12.1 s instead: 10.4 s for the expansion of the forcing terms, 1.5 s for the iterative solution of the forced transmission-line equations, and 0.2 s for the post-processing extraction of the statistical information. It is worth observing that most of the time is required by the calculation of the forcing terms. In the PC simulation, this step is carried out in the pre-processing projection procedure, thus making the iterative solution of the forced equations faster than in the MC analysis. For this example, the speed-up is over $300\times$.

8.3.2 Random Direction of Incidence (Colatitude and Azimuth)

In the second example, the direction of incidence, which is parameterized by colatitude and azimuth, is completely arbitrary and uniformly distributed in the whole solid angle. The random parameters are thus $\sin \theta \in [0, 1]$ and $\psi \in [0, 2\pi]$. The wave amplitude and polarization angle are instead fixed to $E_0 = 1$ V/m and $\eta = \pi/2$. It should be noted that:

1. In order to obtain a uniform distribution over the spherical surface, the sine of the colatitude is assumed as uniformly distributed, rather than colatitude itself.
2. The cable cross-section being symmetric, the actual range of variation of the azimuth can be halved into the range $\psi \in [0, \pi]$.

Fig. 8.4 shows the results of the statistical analysis of the induced current for this second case, confirming the accuracy of the PC approach when compared to a MC analysis based on 10000 runs. However, for this situation, the convergence of the PC expansions is much slower, and up to 351 expansion terms (order $p = 25$) are required for the higher frequencies!! This is due to the highly non-smooth behavior of the forcing functions, which partially invalidates the fundamental assumption of the PC approach, i.e. that there is a mild impact of the random variables on the response. Since a much smaller number of terms is sufficient at lower frequencies, the expansion order is here increased only for higher frequencies, therefore speeding-up the overall projection procedure.

Although for a given number of expansion terms, as already discussed, the simulation procedure is faster with respect to the case of cross-sectional variations, the above considerations may appear detrimental for the PC technique. In fact, a fine and apparently unpredictable tuning of the expansion order seems to be necessary, thus limiting the practical applicability of the approach to the analysis of random field incidences. Nevertheless, it should be observed that the variability is here related to the external field, whose parameters are not affected by the line structure which is illuminated, and the amount of randomness is thence nearly independent from the specific configuration being considered, although the coupling effects of course change from one case to another. Experimental verifications led to the conclusion that the optimal number of expansion terms to be included does not actually change when different line geometries are considered.

For the this second example, the MC simulation still required 1 h and 4 min, since it is independent from the kind of random variable being considered. The PC-based analysis required

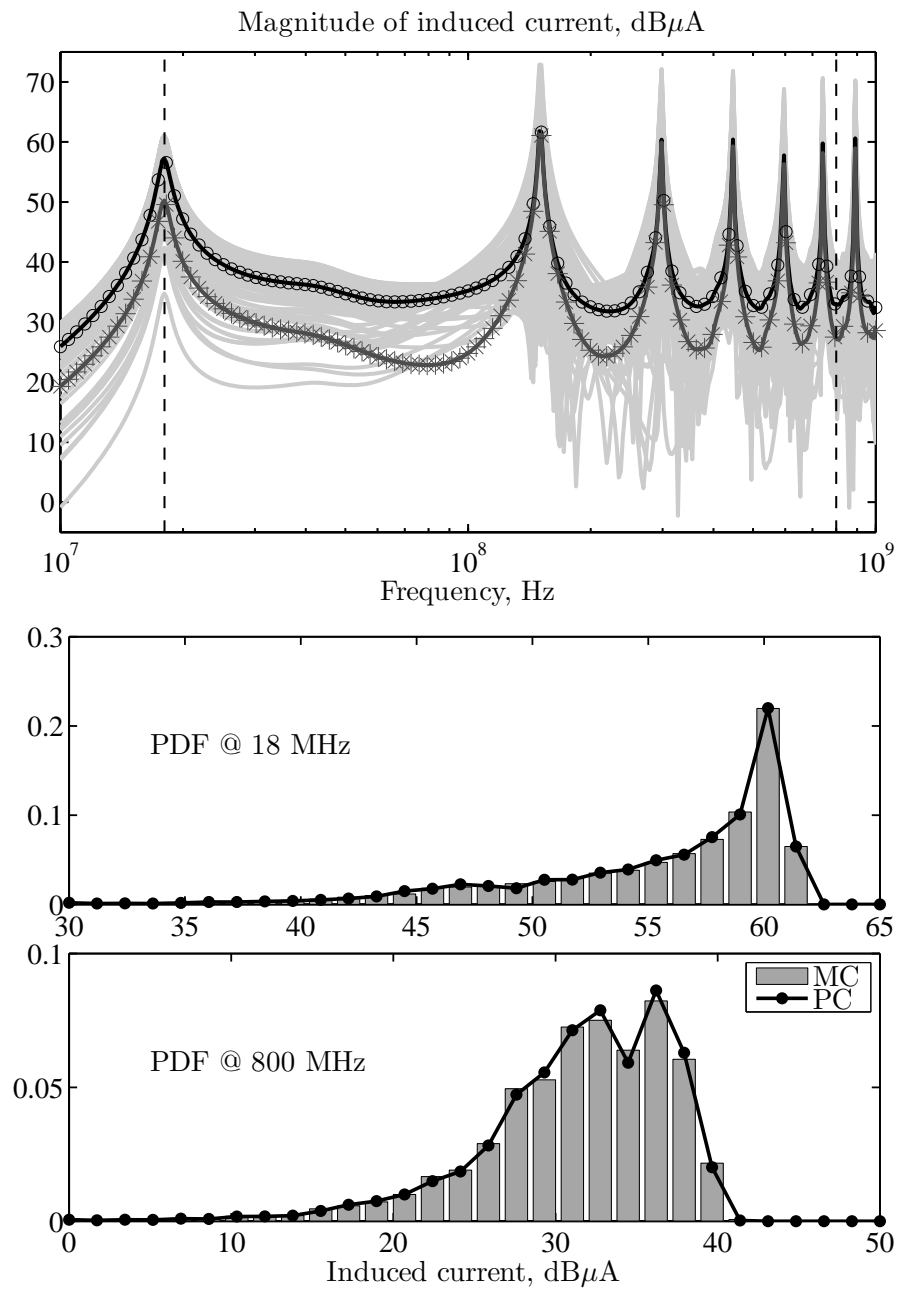


Figure 8.4. Stochastic simulation of the current induced on a flex cable illuminated by a plane wave with random direction of incidence. Curves identification as in the inset of Fig. 8.3.

62.2 s for the expansions, 18.2 s for the solution, and 0.9 s for the estimation of the statistical information. A still impressive speed-up of about $50\times$ is thence obtained.

Conclusions

Due to the increasing miniaturization and large-scale integration, the impact of uncertainties arising from manufacturing tolerances, partially unavailable layout/positioning constraints, operating conditions, or interference, is becoming more and more important for modern electronic devices. This results in system responses which are more suitably described from a statistical, rather than deterministic, viewpoint, i.e. as stochastic processes. Instead of predicting nominal response, a statistical assessment via numerical simulation is then required in the early design phase, in order to estimate the response fluctuation and set realistic design margins. This is traditionally achieved by means of brute-force and time-consuming sampling-based methods such as Monte Carlo, which require a large number of deterministic runs. In this regard, efficient simulation techniques have been investigated and proposed in the recent literature.

Nevertheless, in the framework of circuit simulation, a general and comprehensive approach for the statistical assessment of high-speed interconnects with the inclusion of random transmission lines, was still missing. This thesis presents an efficient stochastic modeling strategy for high-speed links affected by an inherent variability in their physical parameters, such as geometry, material properties, and temperature. The technique is based on the so-called polynomial chaos theory, whose underlying idea is the expansion of stochastic circuit responses in terms of orthogonal polynomial bases. This representation enables a fast extraction of statistical information upon determination of the expansion coefficients, which is carried out by means of a single simulation of a deterministic, though augmented, instance of the original system. Despite the increased system size, the overall simulation time is usually much lower than running a large number of Monte Carlo simulations. The new system equations are obtained through the application of a stochastic Galerkin method to the original (stochastic) governing equations.

The original contribution of this work lies in the extension of existing polynomial chaos-based modeling techniques, which had been previously applied to the analysis of lumped circuits, to distributed interconnects, consisting of transmission-line elements described by telegrapher's equations. The approach is general and applies to arbitrary multiconductor line geometries and is not affected by low-frequency approximations. It has been first applied to the frequency-domain analysis of basic multiconductor transmission-line configurations, i.e. source-line-load circuits or their cascade connection. Time-domain analysis has been then achieved via Fourier analysis.

Afterwards, a SPICE-compatible formulation was proposed, which made possible the convenient description and simulation of the augmented system instance into standard and well-consolidated SPICE-type commercial circuit analysis tools. The formulation is based on an modified (*orthonormalized*) discretization scheme for the stochastic Galerkin method, and allows the circuit interpretation of the augmented constitutive equations by means of standard electrical com-

ponents. This permits to take advantage of available circuit solvers for a more accurate simulation of complex circuit topologies, which previously required cumbersome, ad-hoc implementations or the development of customized software.

Finally, a different application scenario, where the variability of transmission-line responses is induced by random external fields, is successfully addressed via the polynomial chaos approach. In this case, the limitations of existing, closed-form probabilistic models for the field coupling onto basic line structures under low-frequency and weak-coupling assumptions, are by far overcome.

As far as the computational time is concerned, the proposed methodology provides a more efficient alternative with respect to traditional sampling-based methods, like Monte Carlo, with achieved speed-ups of about two orders of magnitude and excellent agreement on the accuracy. A large number of application examples is presented, thus showing the feasibility, flexibility and strength of the advocated approach. The accuracy of the polynomial chaos representation is controlled by the order of the polynomial expansions, which in turn affects the overall number of terms and therefore the size of the augmented problem that has to be solved for the determination of the expansion coefficients. For practical situations, choosing an order between two and four already provides comparable accuracy with respect to the Monte Carlo method. The number of terms also grows with the number of random parameters considered. This suggests that the efficiency is decreased when the number of variables is incremented, and this represents so far one of the main limitations of the proposed method. One of the plans for future work is therefore the investigation of possible alternative formulations, which might mitigate the overhead arising when a large number of random parameters is considered.

Further plans concern the modeling of random cables or cables illuminated by random fields, which is still in its infancy. In this regard, there is an increasing demand for models accounting for the unavoidable random wrapping and twisting of cable bundles. Finally, the SPICE implementation has been so far limited to linear transmission-line networks where the variability is exclusively due to the distributed elements. An enhanced tool, which also includes equivalent circuit descriptions for stochastic linear lumped elements, as well as for nonlinear terminations, is currently under development.

Bibliography

- [1] D. Poljak, *Advanced Modeling in Computational Electromagnetic Compatibility*. Hoboken, NJ: Wiley, 2007.
- [2] C. R. Paul, *Introduction to Electromagnetic Compatibility*. 2nd edition, Hoboken, NJ: Wiley, 2006.
- [3] S. Natarajan, M. A. Breuer, and S. K. Gupta, "Process variations and their impact on circuit operation," in *Proceedings of the 1998 IEEE International Symposium on Defect and Fault Tolerance in VLSI Systems*, Nov. 1998, pp. 73–81.
- [4] S. Nassif, "Design for variability in DSM technologies," in *Proceedings of the 1st IEEE International Symposium on Quality Electronic Design*, San Jose, CA, Mar. 2000, pp. 451–454.
- [5] D. Boning and S. Nassif, "Models of process variations in device and interconnect," in *Design of High Performance Microprocessor Circuits*, A. Chandrakasan, W. J. Bowhill, and F. Fox, Eds. New York: Wiley, 2001.
- [6] S. Borkar, T. Karnik, S. Narendra, J. Tschanz, A. Keshavarzi, and V. De, "Parameter variations and impact on circuits and microarchitecture," in *Proceedings of the 40th Annual Design Automation Conference*, New York, NY, 2003, pp. 338-342.
- [7] Y. Massoud and A. Nieuwoudt, "Modeling and design challenges and solutions for carbon nanotube-based interconnect in future high performance integrated circuits," *ACM Journal on Emerging Technologies in Computing Systems*, vol. 2, no. 3, pp. 155–196, Jul. 2006.
- [8] A. Nieuwoudt and Y. Massoud, "On the impact of process variations for carbon nanotube bundles for VLSI interconnect," *IEEE Transactions on Electron Devices*, vol. 54, no. 3, pp. 446–455, Mar. 2007.
- [9] A. Nieuwoudt and Y. Massoud, "On the optimal design, performance, and reliability of future carbon nanotube-based interconnect solutions," *IEEE Transactions on Electron Devices*, vol. 55, no. 8, pp. 2097–2110, Aug. 2008.
- [10] C. Chiang and J. Kawa, *Design for Manufacturability and Yield for Nano-Scale CMOS*. New York: Springer-Verlag, 2007.
- [11] M. Orshansky, S. Nassif, and D. Boning, *Design for Manufacturability and Statistical Design: A Constructive Approach*. New York: Springer-Verlag, 2010.

- [12] A. H. Zaabab, Q. J. Zhang, and M. Nakhla, "A neural network modeling approach to circuit optimization and statistical design," *IEEE Transactions on Microwave Theory and Techniques*, vol. 43, no. 6, pp. 1349–1358, Jun. 1995.
- [13] Q. Zhang, J. J. Liou, J. McMacken, J. Thomson, and P. Layman, "Development of robust interconnect model based on design of experiments and multiobjective optimization," *IEEE Transactions on Electron Devices*, vol. 48, no. 9, pp. 1885–1891, Sep. 2001.
- [14] M. D. Morris and T. J. Mitchell, "Exploratory designs for computational experiments," *Journal of Statistical Planning and Inference*, vol. 43, pp. 381–402, 1995.
- [15] W. L. Loh, "On Latin hypercube sampling," *The Annals of Statistics*, vol. 24, no. 5, pp. 2058–2080, 1996.
- [16] G. S. Fishman, *Monte Carlo: Concepts, Algorithms, and Applications*. New York: Springer-Verlag, 1996.
- [17] H. Niederreiter, P. Hellekalek, G. Larcher, and P. Zinterhof, *Monte Carlo and Quasi-Monte Carlo Methods*. New-York: Springer-Verlag, 1998.
- [18] W. M. Smith, "Worst case circuit analysis – an overview (electronic parts/circuits tolerance analysis)," in *Proceedings of the Annual Reliability and Maintainability Symposium*, Jan 1996, pp. 326–334.
- [19] R. G. Ghanem and P. D. Spanos, *Stochastic Finite Elements. A Spectral Approach*. New York: Springer-Verlag, 1991.
- [20] D. Xiu and G. E. Karniadakis, "The Wiener-Askey polynomial chaos for stochastic differential equations," *SIAM Journal on Scientific Computing*, vol. 24, no. 2, pp. 619–644, 2002.
- [21] B. J. Debuschere, H. N. Najm, P. P. Pébay, O. M. Knio, R. G. Ghanem, and O. P. Le Maître, "Numerical challenges in the use of polynomial chaos representations for stochastic processes," *SIAM Journal on Scientific Computing*, vol. 26, no. 2, pp. 698–719, 2005.
- [22] R. Ghanem, "A stochastic Galerkin expansion for nonlinear random vibration analysis," *Probabilistic Engineering Mechanics*, vol. 8, no. 3-4, pp. 255–264, 1993.
- [23] R. Ghanem and W. Brzakala, "Stochastic finite-element analysis of soil layers with random interface," *Journal of Engineering Mechanics*, vol. 122, no. 4, pp. 361–369, Apr. 1996.
- [24] D. Xiu and G. E. Karniadakis, "Modeling uncertainty in steady state diffusion problems via generalized polynomial chaos," *Computer Methods in Applied Mechanics and Engineering*, vol. 191, no. 43, pp. 4927–4948, Sep. 2002.
- [25] D. Xiu, D. Lucor, C.-H. Su, and G. E. Karniadakis, "Stochastic modeling of flow-structure interactions using generalized polynomial chaos," *Transactions of the ASME Journal of Fluids Engineering*, vol. 124, no. 1, pp. 51–59, 2002.

- [26] D. Xiu and G. E. Karniadakis, "Modeling uncertainty in flow simulations via generalized polynomial chaos," *Journal of Computational Physics*, vol. 187, no. 1, pp. 137–167, May 2003.
- [27] J. A. S. Witteveen, S. Sarkar, and H. Bijl, "Modeling physical uncertainties in dynamic stall induced fluidstructure interaction of turbine blades using arbitrary polynomial chaos," *Computers & Structures*, vol. 85, no. 11–14, pp. 866–878, Jun.–Jul. 2007.
- [28] S. Finette, "Embedding uncertainty into ocean acoustic propagation models (L)," *The Journal of the Acoustical Society of America*, vol. 117, no. 3, pp. 997–1000, 2005.
- [29] D. B. Creamer, "On using polynomial chaos for modeling uncertainty in acoustic propagation," *The Journal of the Acoustical Society of America*, vol. 119, no. 4, pp. 1979–1994, 2006.
- [30] S. Finette, "A stochastic representation of environmental uncertainty and its coupling to acoustic wave propagation in ocean waveguides," *The Journal of the Acoustical Society of America*, vol. 120, no. 5, pp. 2567–2579, 2006.
- [31] F. S. Hover and M. S. Triantafyllou, "Application of polynomial chaos in stability and control," *Automatica*, vol. 42, no. 5, pp. 789–795, May 2006.
- [32] J. Silly-Carette, D. Lautru, M.-F. Wong, A. Gati, J. Wiart, and V. Fouad Hanna, "Variability on the propagation of a plane wave using stochastic collocation methods in a bio electromagnetic application," *IEEE Microwave and Wireless Components Letters*, vol. 19, no. 4, pp. 185–187, Apr. 2009.
- [33] O. Aiouaz, D. Lautru, M.-F. Wong, E. Conil, A. Gati, J. Wiart, and V. Fouad Hanna, "Uncertainty analysis of the specific absorption rate induced in a phantom using a stochastic spectral collocation method," *Annals of Telecommunications*, vol. 66, no. 7-8, pp. 409–418, Aug. 2011.
- [34] C. Chauvière, J. S. Hesthaven, and L. Lurati, "Computational modeling of uncertainty in time-domain electromagnetics," *SIAM Journal on Scientific Computing*, vol. 28, no. 2, pp. 751–775, 2006.
- [35] R. Gaignaire, S. Clénet, B. Sudret, and O. Moreau, "3-D spectral stochastic finite element method in electromagnetism," *IEEE Transactions on Magnetics*, vol. 43, no. 4, pp. 1209–1212, Apr. 2007.
- [36] R. S. Edwards, A. C. Marvin, and S. J. Porter, "Uncertainty analyses in the finite-difference time-domain method," *IEEE Transactions on Electromagnetic Compatibility*, vol. 52, no. 1, pp. 155–163, Feb. 2010.
- [37] R. Shen, S. X.-D. Tan, J. Cui, W. Yu, Y. Cai, and G.-S. Chen, "Variational capacitance extraction and modeling based on orthogonal polynomial method," *IEEE Transactions on Very Large Scale Integration (VLSI) Systems*, vol. 18, no. 11, pp. 1556–1566, Nov. 2010.

- [38] K. Beddek, Y. Le Menach, S. Clénet, and O. Moreau, “3-D stochastic spectral finite-element method in static electromagnetism using vector potential formulation,” *IEEE Transactions on Magnetics*, vol. 47, no. 5, pp. 1250–1253, May 2011.
- [39] F. Gong, H. Yu, L. Wang, and L. He, “A parallel and incremental extraction of variational capacitance with stochastic geometric moments,” *IEEE Transactions on Very Large Scale Integration (VLSI) Systems*, vol. 20, no. 9, pp. 1729–1737, Sep. 2012.
- [40] Q. Su and K. Strunz, “Stochastic circuit modelling with Hermite polynomial chaos,” *IET Electronics Letters*, vol. 41, no. 21, pp. 1163–1165, Oct. 2005.
- [41] W. Schoutens, *Stochastic Processes and Orthogonal Polynomials*. New York: Springer-Verlag, 2000.
- [42] T. K. Tang and M. S. Nakhla, “Analysis of high-speed VLSI interconnects using the asymptotic waveform evaluation technique,” *IEEE Transactions on Computer-Aided Design*, vol. 11, no. 3, pp. 341–352, Mar. 1992.
- [43] V. Venkatraman and W. Burlison, “Impact of process variations on multi-level signaling for on-chip interconnects,” in *Proceedings of the 18th IEEE International Conference on VLSI Design*, 2005, pp. 362–367.
- [44] Q. J. Zhang and M. Nakhla, “Yield analysis and optimization of VLSI interconnects in multichip modules,” in *Proceedings of the IEEE Multi-Chip Module Conference*, 1993, pp. 160–163.
- [45] T. Mikazuki and N. Matsui, “Statistical design techniques for high-speed circuit boards with correlated structure distributions,” *IEEE Transactions on Components, Packaging and Manufacturing Technology – Part A*, vol. 17, no. 1, pp. 159–165, Mar. 1994.
- [46] A. Ciccolella and F. G. Canavero, “Stochastic prediction of wire coupling interference,” in *Proceedings of the 1995 IEEE International Symposium on Electromagnetic Compatibility*, Atlanta, GA, Aug. 1995, pp. 51–56.
- [47] Y. Cao, P. Gupta, A. B. Kahng, D. Sylvester, and J. Yang, “Design sensitivities to variability: extrapolations and assessments in nanometer VLSI,” in *Proceedings of the 15th Annual IEEE International ASIC/SOC Conference*, Rochester, NY, Sep. 2002, pp. 411–415.
- [48] S. Shiran, B. Reiser, and H. Cory, “A probabilistic model for the evaluation of coupling between transmission lines,” *IEEE Transactions on Electromagnetic Compatibility*, vol. 35, no. 3, pp. 387–393, Aug. 1993.
- [49] D. Bellan, S. A. Pignari, and G. Spadacini, “Characterisation of crosstalk in terms of mean value and standard deviation,” in *IEE Proceedings of Science, Measurement and Technology*, vol. 150, no. 6, pp. 289–295, Nov. 2003.
- [50] D. Bellan and S. Pignari, “A probabilistic model for the response of an electrically short two-conductor transmission line driven by a random plane wave field,” *IEEE Transactions on Electromagnetic Compatibility*, vol. 43, no. 2, pp. 130–139, May 2001.

- [51] S. Vruthula, J. M. Wang, and P. Ghanta, "Hermite polynomial based interconnect analysis in the presence of process variations," *IEEE Transactions on Computer-Aided Design of Integrated Circuits and Systems*, vol. 25, no. 10, pp. 2001–2011, Oct. 2006.
- [52] N. Mi, S. X.-D. Tan, Y. Cai, and X. Hong, "Fast variational analysis of on-chip power grids by stochastic extended Krylov subspace method," *IEEE Transactions on Computer-Aided Design of Integrated Circuits and Systems*, vol. 27, no. 11, pp. 1996–2006, Nov. 2008.
- [53] K. Strunz and Q. Su, "Stochastic formulation of SPICE-type electronic circuit simulation using polynomial chaos," *ACM Transactions on Modeling and Computer Simulation*, vol. 18, no. 4, pp. 15:1–15:23, Sep. 2008.
- [54] C. R. Paul, *Analysis of Multiconductor Transmission Lines*. New York: Wiley, 1994.
- [55] X. Li, J. M. Wang, W. Tang, and H. Wu, "Stochastic analysis for crosstalk noise of coupled interconnects with process variations," in *Proceedings of the IEEE International Conference on Integrated Circuit Design and Technology and Tutorial*, 2008, pp. 289–292.
- [56] I. S. Stievano and F. G. Canavero, "Response variability of high-speed interconnects via Hermite polynomial chaos," in *Proceedings of the 14th IEEE Workshop on Signal Propagation on Interconnects*, Hildesheim, Germany, May 2010, pp. 3–6.
- [57] W. Delbare and D. De Zutter, "Space-domain Green's function approach to the capacitance calculation of multiconductor lines in multilayered dielectrics with improved surface charge modeling," *IEEE Transactions on Microwave Theory and Techniques*, vol. 37, no. 10, pp. 1562–1568, Oct. 1989.
- [58] T. Demeester and D. De Zutter, "Quasi-TM transmission line parameters of coupled lossy lines based on the Dirichlet to Neumann boundary operator," *IEEE Transactions on Microwave Theory and Techniques*, vol. 56, no. 7, pp. 1649–1660, Jul. 2008.
- [59] C. A. Desoer and E. S. Kuh, *Basic Circuit Theory*. Auckland: McGraw-Hill, 1969.
- [60] F.-L. Lin and R.-B. Wu, "Analysis of coplanar-waveguide discontinuities with finite-metallization thickness and nonrectangular edge profile," *IEEE Transactions on Microwave Theory and Techniques*, vol. 45, no. 12, pp. 2131–2137, Dec. 1997.
- [61] M. Loève, *Probability Theory*. 4th edition, New York: Springer-Verlag, 1977.
- [62] D. Lucor, C.-H. Su, and G. E. Karniadakis, "Karhunen-Loeve representation of periodic second-order autoregressive processes," *Lecture Notes in Computer Science*, vol. 3038, pp. 827–834, 2004.
- [63] A. Papoulis, *Probability, Random Variables and Stochastic Processes*. 3rd edition, New York: McGraw-Hill, 1991.
- [64] M. H. Kalos and P. A. Whitlock, *The Monte Carlo Methods*. 2nd edition, Hoboken, NJ: Wiley, 2008.

- [65] W. Kim and M. Swaminathan, "Characterization of co-planar silicon transmission lines with and without slow-wave effect," *IEEE Transactions on Advanced Packaging*, vol. 30, no. 3, pp. 526–532, Aug. 2007.
- [66] N. Wiener, "The homogeneous chaos," *American Journal of Mathematics*, vol. 60, pp. 897–936, 1938.
- [67] R. Cameron and W. Martin, "The orthogonal development of nonlinear functionals in series of Fourier-Hermite functionals," *The Annals of Mathematics*, vol. 48, no. 2, pp. 385–392, 1947.
- [68] R. Askey and J. Wilson, "Some basic hypergeometric polynomials that generalize Jacobi polynomials," *Memoirs of the American Mathematical Society*, vol. 54, no. 319, Mar. 1985.
- [69] X. Wan, G. E. Karniadakis, "Multi-element generalized polynomial chaos for arbitrary probability measures," *SIAM Journal on Scientific Computing*, vol. 28, no. 3, pp. 901–928, 2006.
- [70] D. Xiu, "Fast numerical methods for stochastic computations: a review," *Communications in Computational Physics*, vol. 5, no. 2–4, pp. 242–272, Feb. 2009.
- [71] J. Bäck, F. Nobile, L. Tamellini, and R. Tempone, "Stochastic spectral Galerkin and collocation methods for PDEs with random coefficients: A numerical comparison," in *Spectral and High Order Methods for Partial Differential Equations*, J. S. Hesthaven and E. M. Rønquist, Eds. New York: Springer-Verlag, 2011.
- [72] O. G. Ernsta, A. Muglera, H.-J. Starkloffa, and E. Ullmanna, "On the convergence of generalized polynomial chaos expansions," *ESAIM: Mathematical Modelling and Numerical Analysis*, vol. 46, no. 2, pp. 317–339, Mar. 2012.
- [73] I. Babuška, F. Nobile, and R. Tempone, "A stochastic collocation method for elliptic partial differential equations with random input data," *SIAM Journal on Numerical Analysis*, vol. 45, no. 3, pp. 1005–1034, May 2007.
- [74] M. Abramowitz and I. A. Stegun, *Handbook of Mathematical Functions*. New York: Dover, 1972.
- [75] I. S. Gradshteyn and I. M. Ryzhik, *Table of Integrals, Series, and Products*. 7th edition, San Diego: Academic Press, 2007.
- [76] J. A. Gaunt, "The triplets of Helium," *Philosophical Transactions of the Royal Society of London*, vol. 228, pp. 151–196, Feb. 1929.
- [77] W. H. Press, S. A. Teukolsky, W. T. Vetterling, and B. P. Flannery, *Numerical Recipes: The Art of Scientific Computing*. 3rd edition, New York: Cambridge University Press, 2007.
- [78] G. H. Golub and J. H. Welsch, "Calculation of Gauss quadrature rules," *Mathematics of Computation*, vol. 23, pp. 221–230, 1969.

- [79] I. S. Stievano, P. Manfredi, and F. G. Canavero, "Stochastic analysis of multiconductor cables and interconnects," *IEEE Transactions on Electromagnetic Compatibility*, vol. 53, no. 2, pp. 501–507, May 2011.
- [80] I. S. Stievano, P. Manfredi, and F. G. Canavero, "Parameters variability effects on multiconductor interconnects via Hermite polynomial chaos," *IEEE Transactions on Components, Packaging and Manufacturing Technology*, vol. 1, no. 8, pp. 1234–1239, Aug. 2011.
- [81] D. Vande Ginste, D. De Zutter, D. Deschrijver, T. Dhaene, P. Manfredi, and F. Canavero, "Stochastic modeling-based variability analysis of on-chip interconnects," *IEEE Transactions on Components, Packaging and Manufacturing Technology*, vol. 2, no. 7, pp. 1182–1192, Jul. 2012.
- [82] P. Manfredi, D. Vande Ginste, D. De Zutter, and F. G. Canavero, "Improved polynomial chaos discretization schemes to integrate interconnects into design environments," *accepted for publication in IEEE Microwave and Wireless Components Letters*.
- [83] M. Kirschning and R. H. Jansen, "Accurate wide-range design equations for the frequency-dependent characteristic of parallel coupled microstrip lines," *IEEE Transactions on Microwave Theory and Technoques*, vol. 32, no. 1, pp. 83–90, Jan. 1984.
- [84] M. Kirschning and R. H. Jansen, "Accurate wide-range design equations for the frequency-dependent characteristics of parallel coupled microstrip lines (corrections)," *IEEE Transactions on Microwave Theory and Technoques*, vol. 33, no. 3, p. 288, Mar. 1985.
- [85] B. C. Wadell, *Transmission Line Design Handbook*. Boston: Artech House, 1991.
- [86] P. Manfredi, I. S. Stievano, and F. G. Canavero, "Transient analysis of PCB lines with the inclusion of parameters uncertainties," in *Proceedings of the 2011 IEEE Symposium on Electromagnetic Compatibility*, Long Beach, CA, Aug. 2011, pp. 146–149.
- [87] P. Manfredi, I. S. Stievano, and F. G. Canavero, "Stochastic evaluation of parameters variability on a terminated signal bus," in *Proceedings of the 10th International Symposium on Electromagnetic Compatibility*, York, UK, Sep. 2011, pp. 362–367.
- [88] W. J. McCalla, *Fundamentals of Computer-Aided Circuit Simulation*. Boston: Kluwer Academic Publishers, 1988.
- [89] P. Manfredi, I. S. Stievano, and F. G. Canavero, "Alternative SPICE implementation of circuit uncertainties based on orthogonal polynomials," in *Proceedings of the 20th IEEE Conference on the Electrical Performance of Electronic Packages and Systems*, San Jose, CA, Oct. 2011, pp. 41–44.
- [90] "HSPICE® User Guide: Signal Integrity". Version B-2008.09, September 2008.
- [91] P. Triverio, S. Grivet-Talocia, M. S. Nakhla, F. G. Canavero, and R. Achar, "Stability, causality, and passivity in electrical interconnect models," *IEEE Transactions on Advanced Packaging*, vol. 30, no. 4, pp. 795–808, Nov. 2007.

- [92] P. Manfredi, D. Vande Ginste, D. De Zutter, and F. G. Canavero, "On the passivity of polynomial chaos-based augmented models for stochastic circuits," *submitted to IEEE Transactions on Circuits and Systems – Part I*.
- [93] G. T. Capraro and C. R. Paul, "A probabilistic approach to wire coupling interference prediction," in *Proceedings of the 4th International Zurich Symposium on Electromagnetic Compatibility*, Zurich, Switzerland, 1981, pp. 267–272.
- [94] R. Holland and R. H. St. John, "Statistical response of EM-driven cables inside an overmoded enclosure," *IEEE Transactions on Electromagnetic Compatibility*, vol. 40, no. 1 – part 1, pp. 311–324, Nov. 1998.
- [95] M. Magdowski, S. V. Tkachenko, and R. Vick, "Coupling of stochastic electromagnetic fields to a transmission line in a reverberation chamber," *IEEE Transactions on Electromagnetic Compatibility*, vol. 53, no. 2, pp. 308–317, May 2011.
- [96] M. Magdowski and R. Vick, "Closed-form formulas for the stochastic electromagnetic field coupling to a transmission line with arbitrary loads," *IEEE Transactions on Electromagnetic Compatibility*, vol. 54, no. 5, pp. 1147–1152, Oct. 2012.
- [97] D. A. Hill, "Plane wave integral representation for fields in reverberation chambers," *IEEE Transactions on Electromagnetic Compatibility*, vol. 40, no. 3, pp. 209–217, Aug. 1998.
- [98] D. A. Hill, *Electromagnetic Fields in Cavities. Deterministic and Statistical Theories*. Hoboken, NJ: Wiley, 2009.
- [99] P. Manfredi and F. G. Canavero, "Polynomial chaos for random field coupling to transmission lines," *IEEE Transactions on Electromagnetic Compatibility*, vol. 54, no. 3, pp. 677–680, Jun. 2012.
- [100] P. Manfredi and F. G. Canavero, "Polynomial chaos representation of transmission-line response to random plane waves," in *Proceedings of the 11th International Symposium on Electromagnetic Compatibility*, Rome, Italy, Sep. 2012.

List of Publications

Journal Publications

- I. S. Stievano, P. Manfredi, and F. G. Canavero, “Stochastic analysis of multiconductor cables and interconnects,” *IEEE Transactions on Electromagnetic Compatibility*, vol. 53, no. 2, pp. 501–507, May 2011.
- I. S. Stievano, P. Manfredi, and F. G. Canavero, “Parameters variability effects on multiconductor interconnects via Hermite polynomial chaos,” *IEEE Transactions on Components, Packaging and Manufacturing Technology*, vol. 1, no. 8, pp. 1234–1239, Aug. 2011.
- P. Manfredi, M. Fontana, I. S. Stievano, and F. G. Canavero, “Comparison of stochastic methods for the variability assessment of technology parameters,” *Radio Science*, vol. 47, RS0N03, pp. 1–8, Feb. 2012.
- I. S. Stievano, P. Manfredi, and F. G. Canavero, “Carbon nanotube interconnects: process variation via polynomial chaos,” *IEEE Transactions on Electromagnetic Compatibility*, vol. 54, no. 1, pp. 140–148, Feb. 2012.
- P. Manfredi and F. G. Canavero, “Polynomial chaos for random field coupling to transmission lines,” *IEEE Transactions on Electromagnetic Compatibility*, vol. 54, no. 3, pp. 677–680, Jun. 2012.
- D. Vande Ginste, D. De Zutter, D. Deschrijver, T. Dhaene, P. Manfredi, and F. G. Canavero, “Stochastic modeling-based variability analysis of on-chip interconnects,” *IEEE Transactions on Components, Packaging and Manufacturing Technology*, vol. 2, no. 7, pp. 1182–1192, Jul. 2012.
- P. Manfredi, I. S. Stievano, and F. G. Canavero, “Time and frequency-domain evaluation of stochastic parameters on signal lines,” *Advanced Electromagnetics*, vol. 1, no. 3, pp. 85–93, Dec. 2012.
- P. Manfredi, D. Vande Ginste, D. De Zutter, and F. G. Canavero, “Improved polynomial chaos discretization schemes to integrate interconnects into design environments,” accepted for publication in *IEEE Microwave and Wireless Components Letters*.

- P. Manfredi, D. Vande Ginste, D. De Zutter, and F. G. Canavero, “Uncertainty assessment of lossy and dispersive lines in SPICE-type environments,” accepted for publication in *IEEE Transactions on Components, Packaging and Manufacturing Technology*.

Conference Publications

- P. Manfredi, I. S. Stievano, and F. G. Canavero, “Parameters variability effects on microstrip interconnects via Hermite polynomial chaos,” in *Proceedings of the 19th Conference on Electrical Performance of Electronic Packaging and Systems*, Austin, TX, Oct. 2010, pp. 149–152.¹
- I. S. Stievano, P. Manfredi, and F. G. Canavero, “Impact of parameters variability on the electrical performance of carbon nanotube interconnects,” in *Proceedings of the 15th IEEE Workshop on Signal Propagation on Interconnects*, Naples, Italy, May 2011, pp. 83–86.
- P. Manfredi, M. H. Azarian, and F. G. Canavero, “Numerical simulation of impedance discontinuities resulting from degradation of interconnections on printed circuit boards,” in *Proceedings of the 15th IEEE Workshop on Signal Propagation on Interconnects*, Naples, Italy, May 2011, pp. 93–96.
- P. Manfredi and F. G. Canavero, “Polynomial chaos-based tolerance analysis of microwave planar guiding structures,” in *Digest of the 2011 IEEE MTT-S International Microwave Symposium*, Baltimore, MD, Jun. 2011, pp. 1–4.²
- P. Manfredi, I. S. Stievano, and F. G. Canavero, “Transient analysis of PCB lines with the inclusion of parameters uncertainties,” in *Proceedings of the 2011 IEEE Symposium on Electromagnetic Compatibility*, Long Beach, CA, Aug. 2011, pp. 146–149.
- P. Manfredi, I. S. Stievano, and F. G. Canavero, “Crosstalk transient analysis of PCB interconnects including process variability,” in *Proceedings of the XXX General Assembly and Scientific Symposium of the International Union of Radio Science*, Istanbul, Turkey, Aug. 2011, pp. 1–4.
- P. Manfredi, M. Fontana, I. S. Stievano, and F. G. Canavero, “Comparison of stochastic methods for the variability assessment of technology parameters,” in *Proceedings of the XXX General Assembly and Scientific Symposium of the International Union of Radio Science*, Istanbul, Turkey, Aug. 2011, pp. 1–4.³
- P. Manfredi, I. S. Stievano, and F. G. Canavero, “Stochastic evaluation of parameters variability on a terminated signal bus,” in *Proceedings of the 10th International Symposium on Electromagnetic Compatibility*, York, UK, Sep. 2011, pp. 362–367.

¹Awarded as best student paper.

²Awarded with an honorable mention.

³Recognized with a Young Scientist award.

- P. Manfredi, I. S. Stievano, and F. G. Canavero, “Alternative SPICE implementation of circuit uncertainties based on orthogonal polynomials,” in *Proceedings of the 20th Conference on Electrical Performance of Electronic Packaging and Systems*, San Jose, CA, Oct. 2011, pp. 41–44.
- P. Manfredi, I. S. Stievano, and F. G. Canavero, “Polynomial chaos helps assessing parameters variations of PCB lines,” in *Proceedings of the 2011 IEEE Electrical Design of Advanced Packaging and Systems Symposium*, Hangzhou, China, Dec. 2011, pp. 1–4.
- P. Manfredi, I. S. Stievano, and F. G. Canavero, “Time- and frequency-domain evaluation of stochastic parameters on signal lines,” in *Proceedings of the 1st Advanced Electromagnetics Symposium*, Paris, France, Apr. 2012, pp. 498–506.
- P. Manfredi, I. S. Stievano, and F. G. Canavero, “Expedite stochastic SPICE simulations by means of polynomial chaos,” in *Proceedings of the 16ème Colloque International sur la Compatibilité Electromagnétique*, Rouen, France, Apr. 2012, pp. 1–4.
- P. Manfredi, I. S. Stievano, and F. G. Canavero, “Performance of modal signaling vs. medium dielectric variability,” in *Proceedings of the 16th IEEE Workshop on Signal and Power Integrity*, Sorrento, Italy, May 2011, pp. 81–84.
- D. Vande Ginste, D. De Zutter, D. Deschrijver, T. Dhaene, P. Manfredi, and F. G. Canavero, “Frequency and time domain variability analysis of an on-chip inverted embedded microstrip line using a macromodeling-based stochastic Galerkin method,” in *Proceedings of the 16th IEEE Workshop on Signal and Power Integrity*, Sorrento, Italy, May 2011, pp. 85–88.
- P. Manfredi and F. G. Canavero, “Impact of dielectric variability on modal signaling over cable bundles,” in *Proceedings of the 2012 ESA Workshop on Aerospace EMC*, Venice, Italy, May 2011, pp. 1–4.
- P. Manfredi and F. G. Canavero, “Statistical prediction of temperature effects inside through-silicon vias by means of orthogonal polynomials,” in *Digest of the 2012 IEEE MTT-S International Microwave Symposium*, Montréal, Canada, Jun. 2012, pp. 1–4.
- D. Vande Ginste, D. De Zutter, D. Deschrijver, T. Dhaene, P. Manfredi, and F. G. Canavero, “Analysis of common-mode noise on on-chip differential lines through stochastic modeling of parameter variability,” in *Proceedings of the 2012 IEEE Symposium on Electromagnetic Compatibility*, Pittsburgh, PA, Aug. 2012, pp. 144–149.
- P. Manfredi and F. G. Canavero, “Polynomial chaos representation of transmission-line response to random plane waves,” in *Proceedings of the 11th International Symposium on EMC*, Rome, Italy, Sep. 2012.
- P. Manfredi, I. S. Stievano, G. Perrone, P. Bardella, and F. G. Canavero, “A statistical assessment of opto-electronic links,” in *Proceedings of the 21th Conference on Electrical Performance of Electronic Packaging and Systems*, Tempe, AZ, Oct. 2012, pp. 61–64.

- P. Manfredi, D. Vande Ginste, D. De Zutter, and F. G. Canavero, “Frequency- and time-domain stochastic analysis of lossy and dispersive interconnects in a SPICE-like environment,” in *Proceedings of the 21th Conference on Electrical Performance of Electronic Packaging and Systems*, Tempe, AZ, Oct. 2012, pp. 65–68.
- P. Manfredi and F. G. Canavero, “Statistical analysis of multiconductor cables and interconnects with internal variability and field coupling,” in *Proceedings of the 42nd European Microwave Conference*, Amsterdam, Netherlands, Oct. 2012.

Submitted Manuscripts

- P. Manfredi, D. Vande Ginste, D. De Zutter, and F. G. Canavero, “On the passivity of polynomial chaos-based augmented models for stochastic circuits,” *submitted to the IEEE Transactions on Circuits and Systems – Part I*.
- A. Biondi, D. Vande Ginste, D. De Zutter, P. Manfredi, and F. G. Canavero, “Variability analysis of interconnects terminated by general nonlinear loads,” *submitted to the IEEE Transactions on Components, Packaging and Manufacturing Technology*.

Biography

Paolo Manfredi was born in Borgomanero, Italy, in 1985. He received the Bachelor and Master degrees in Electronic Engineering from the Politecnico di Torino in 2008 and 2009, respectively. In both the Bachelor and Master theses he focused on issues related to the modeling of interconnection structures. Since January 2010, he joined the EMC Group as a PhD student. His research topic concerns extended models for signal propagation and field coupling on interconnects, with a particular focus on stochastic models for the inclusion of uncertainties. Mr. Manfredi was selected for the IBM Best Student Recognition Event in 2009 and for the Optime award from the Unione Industriali di Torino in 2010. He won the Best Student Paper Award at the 19th IEEE Conference on Electrical Performance of Electronic Packaging and Systems (EPEPS 2010). Moreover, in 2011 he received an honorable mention at the IEEE MTT-S International Microwave Symposium (IMS 2011) and was a Young Scientist awardee at the XXX General Assembly and Scientific Symposium of International Union of Radio Science (URSI GASS 2011). He was a visiting scientist at the Center for Advanced Life Cycle Engineering (CALCE) at the University of Maryland – College Park in June 2011 and from February to March 2012. He was also a visiting scientist at the Department of Information Technology (INTEC) at Ghent University from April to July 2012.